– Ph.D Thesis –

Electric Power Generation from Deep Sea Hydrothermal Vent Using Thermoelectric Generators

熱電発電素子を用いた深海噴出熱水からの発電について

LUAN MING
(47-117625)

Department of Ocean Technology, Policy and Environment
Graduate School of Frontier Sciences
The University of Tokyo

Supervisor: Prof. Shinichi Takagawa
Prof. Toshihiro Maki

東京大学
THE UNIVERSITY OF TOKYO

List of Figures

List of Tables

Nomenclature

a	Number of TEMs which have maximum output power
b	Number of TEMs which have minimum output power
d_1	Diameter of inner aluminum pipe
d_2	Diameter of inner TEMs layer
d_3	Diameter of outer TEMs layer
d_4	Diameter of outer aluminum pipe
d_s	Thickness of TEM
$\bar{f}$	Body forces acting on the fluid
h	Heat transfer coefficient
k	Turbulent kinematic energy
k_f	Thermal conductivity of fluid
k_s	Thermal conductivity of semiconductor
k_i	Voltage conversion ratio of TEM through MPPT converter
k_a	Voltage conversion ratio of a type TEM through MPPT converter
k_b	Voltage conversion ratio of b type TEM through MPPT converter
r	Internal resistance of TEM
A	Surface area of generator
A_s	Surface area of TEM
C	Perimeter of generator
C_P	Thermal capacity
$C_{1\varepsilon}$	Model constant number
$C_{2\varepsilon}$	Model constant number
E	Induced voltage of TEM
I_{mpp}	Maximum output current of TEM
I_{mppi}	Output current of single TEM in series connected string
L	Length of generator

N	Number of TEMs in series connected string
P	Output power
P_{mppi}	Output power of single TEM in series connected string
Q_i	Inlet heat flux rate from hydrothermal vent
Q_u	Thermal conduction flux through TEM layer
Q_{elec}	Electrical power produced by TEM
Q_{hot}	Thermal conduction flux input to the hot side of TEM
R	External resistance
R_f	Thermal resistance of TEM
S	Seebeck coefficient
T_f	Temperature of fluid
T_s	Temperature of solid
V	Voltage across the terminals of external resistance
V_{sum}	Output voltage of distributed MPPT architecture
V_{mpp}	Maximum output voltage of single TEM
V_{mppi}	Output voltage of single TEM in series connected string
$V_{sum\_\max}$	Maximum output voltage of distributed MPPT architecture
$V_{sum\_\min}$	Minimum output voltage of distributed MPPT architecture
$\vec{V}$	Velocity of fluid
Z	Figure of merit
α_a	Ratio of output voltage of a type TEM and maximum output voltage
α_b	Ratio of output voltage of b type TEM and maximum output voltage
α_i	Ratio of the output voltage and maximum output voltage
σ_k	Model constant number
σ_ε	Model constant number
η	Efficiency of TEM
η_1	Efficiency of generator
η_2	Efficiency of power converted from inlet thermal energy
ε	Dissipation rate
ρ	Density of fluid

ρ_s	Electrical resistivity of semiconductor
μ	Dynamic viscosity
μ_t	Turbulent viscosity
δ_{in_Al}	Thickness of the inner aluminum wall
δ_{TEM}	Thickness of TEMs layer
δ_{ou_Al}	Thickness of the outer aluminum wall
ΔT	Temperature difference on both sides of TEM
∇	Del operator

Abbreviations

ROV: Remotely Operated Vehicle

AUV: Autonomous Underwater Vehicle

IIS: Institute of Industrial Science

NBC: North Big Chimney

LED: Luminous Emission Diode

TEM: Thermo-Electric Module

CFD: Computer Fluid Dynamics

SIMPLE: Semi-Implicit Method for Pressure-Linked Equations

RSTM: Reynolds Stress Transport Modeling

MPPT: Maximum Power Point Tracking

MPP: Maximum Power Point

Contents

Chapter 1 Introduction

1.1 Motivation and aims

Since 1977, the first hydrothermal vent was discovered while exploring an oceanic spreading ridge near the Galapagos Islands, approximately 13000 km ridges have been surveyed representing 20% of the global ridges of the world [1]. So far, about 280 vent sites along the ridges have been reported, and most of them exist at a depth of 2000 to 2500 meters [2].

Hydrothermal vents are formed by the movement of tectonic plates and always are found at volcanically active places. According to the local pressure and activities of neighborhood active basins, they mainly exist as two types of configurations: a zone of diffuse fluids venting and a cluster of distinct spring venting through the seabed. In published literatures, it is recorded that most of the hot fluids flow out at velocities of 1~5 m/s and at temperature ranging from 60°C to as high as 464°C, hot enough to melt lead [3][4].

Although the temperature is extremely hot, the high ambient pressure keeps the hot fluids from boiling. When they contact with 10°C or near freezing surrounding seawater, a fantastic heat exchange will be caused. Within this process, many kinds of metals and

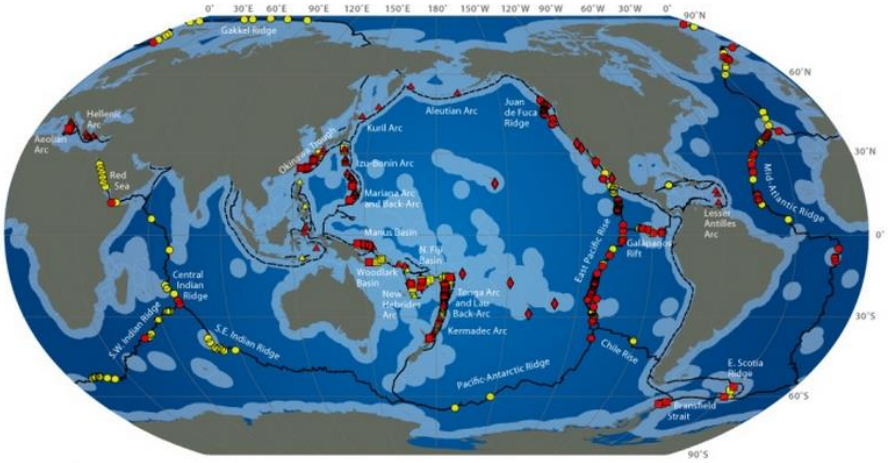

Fig. 1.1 Global distribution of hydrothermal vent fields.

Active vent sites and unconfirmed vent sites are represented by red and yellow points respectively [5].

Fig. 1.2 Configuration of vent.

ROV equipped with manipulator is sampling rocks from vent [6].

Fig. 1.3 Species distribution [7]

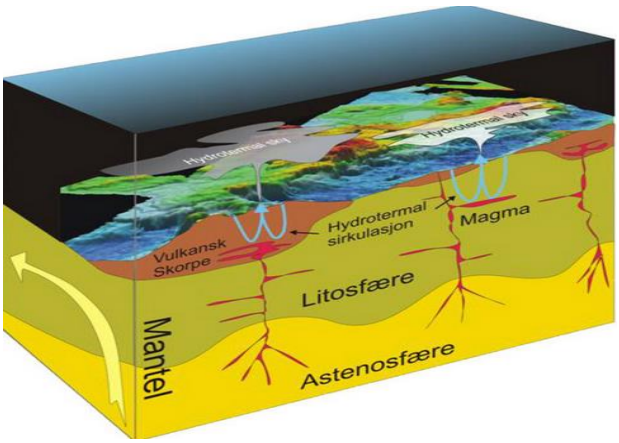

Fig. 1.4 Deep seafloor dynamics [8]

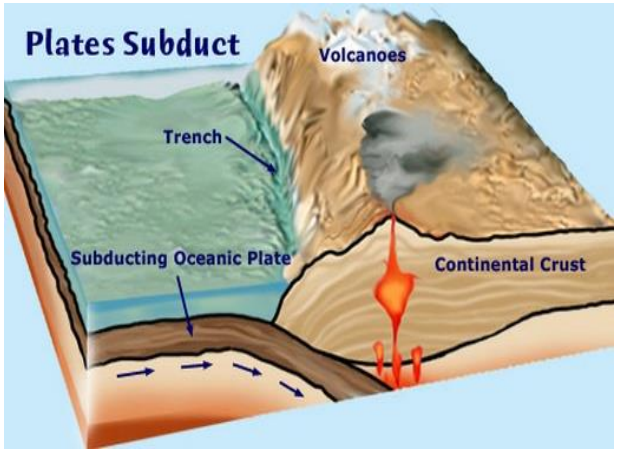

Fig. 1.5 Tectonic movement [9]

Fig. 1.6 Chemistry sampling [10]

minerals are precipitated out of the fluids and the sedimentary accretion of minerals are always found near vent places, including copper, nickel, cobalt and rare minerals. The concentration of these minerals are far rich than in any surface mine and has already been given great intention. Hydrothermal vent also acts as natural systems to help regulate global ocean chemistry, which are based on heat and chemicals that transported from the interior of the Earth.

With the development of underwater technology and profound understanding of hydrothermal vent influences, more extensive researches have been conducted, including the study of relationship between vent sites and species distribution [7], deep sea dynamics [8], tectonic movement analysis [9] and chemistry resource [10], which might be much more complex than geologists had thought before, and help human understand

ocean in new and exciting ways. In these activities, ROV and AUV are indispensable in observing and exploring hydrothermal vent areas, and seabed stations with deep sea sensors also play a very important role in long term data collection.

However, the utilization of these appliances is greatly restricted by the power supply problems. The operation of present AUVs is limited by their onboard energy storage capability. Most AUVs in service today conduct operations on the order of a few hours in duration, and then have to return to the surface station to get recharged. The application of the seabed stations is also heavily limited on the power supply difficulties. In some deep sea areas, it is hard to lay submarine cables from land safely. All of those make it hard to do the survey and exploration in long term continuously.

The purpose of this research is to attempt to generate, store and supply electrical power near hydrothermal vent sites locally, so that the observing AUVs can recharge from the power generation station without returning to the surface in a certain time, the sensors and environment monitoring system can get power locally without laying electric cables from land, which will greatly reduce the unexpected risks.

So far, there are various power generation systems in the sea, such as ocean thermal conversion technology, wave, wind, current power generation. But all of them need big offshore platforms, and long cables are required if transmit power from the big platforms to deep sea appliances. The power generation of these methods is also greatly influenced by the inconstant environment, thus they are not suitable to be used as the power source of AUVs or other seabed stations.

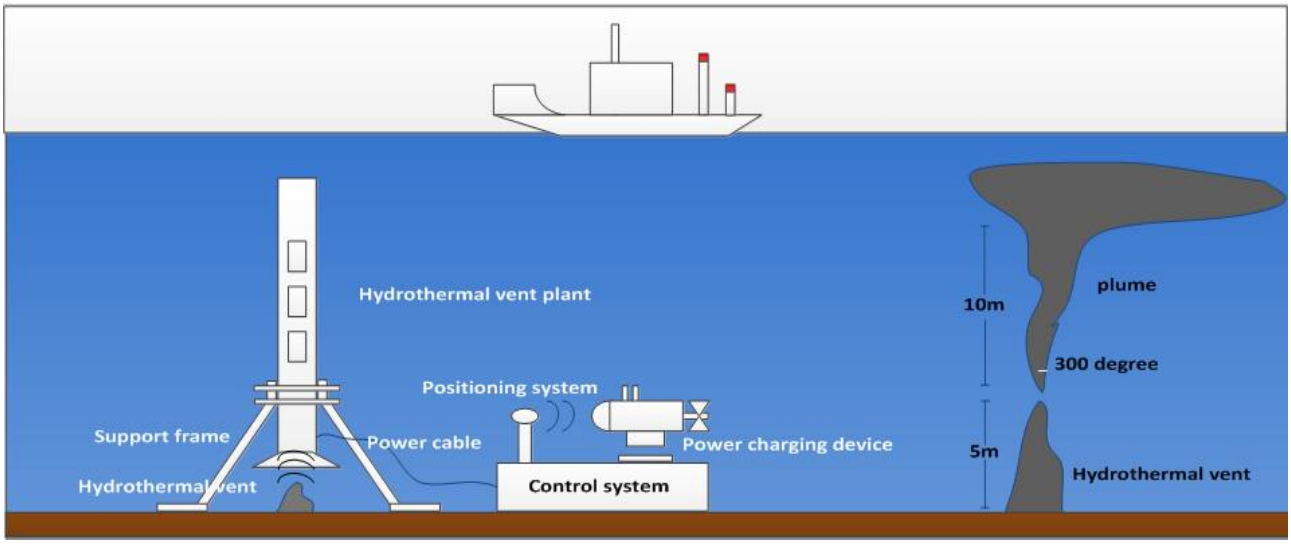

Fig. 1.7 The concept of deep sea power generation system

The superhot fluids released from hydrothermal vent play a very important role in maintaining the energy flow and matter cycling in deep sea. Meanwhile, noticed the enormous thermal energy contained in the hot fluids, this research presents a proposal of exploiting the thermal energy for electricity production. Once the hot water is delivered into the plant, the energy will be converted into electricity, and then the electric power will be stored or supplied to the appliances directly, as shown in Fig. 1.7.

1.2 Research background

1.2.1 The available energy contained in single hydrothermal vent

In southern Japanese sea areas, hydrothermal vent sites have been mainly found and investigated in Kagoshima Bay and Okinawa Trough over several years. Since 2007, the first distinct chimney was found in Wakamiko caldera area, three vent sites have been found successively in Kagoshima Bay [11]. Among these, a distinct chimney named Yamanaka has been observed for a long time, of which the average orifice diameter is 12 cm, and hot fluids flow out with the velocity of 0.3~0.5 m/s over 100°C. When the temperature of the surrounding water is 20°C, the discharging thermal energy can be calculated as 1.52 MW.

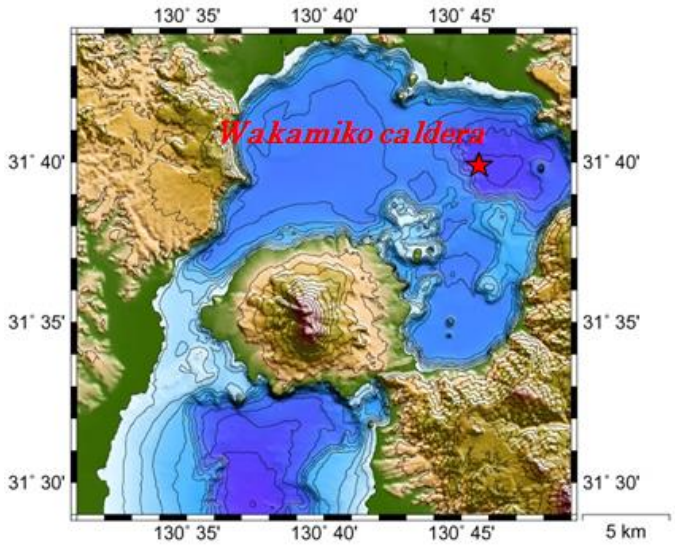

Fig. 1.8 The Hydrothermal Field in Kagoshima Bay [12]

Nearly 20 hydrothermal vent sites located in Okinawa Trough have been discovered and investigated in the published literatures. Okinawa Though which is the extension of Eurasia and Philippine Sea tectonic plates, is considered as the most active region in the west Pacific Ocean. Until now, two major vent clusters have been studied that are

Table 1.1 Three well-known hot fluid sites in the middle part in Okinawa Trough [13]

Name	Location	Depth	Temperature
Minami-Ensei	28°23'N, 127°38'E	about 770 m	270°C
Izena-cauldron	JADE Site, 27°16'N 127°05'E	1300-1600 m	320°C
Iheya-ridge	CLAM Site, 27°33'N	about 1400 m	220°C

Yonaguni Knoll IV area [14] in southern part and three well-known hot fluid sites in the middle part, as listed in Table 1.1.

In those places, the temperatures are nearly as high as the local saturation temperature. For scientific research, some artificial vent sites have been drilled that are close to Iheya-North field. The orifice diameter of these artificial vents is 9 cm, and the hot fluids were observed flowing out with the velocity of 1 m/s over 300°C [15]. When the temperature of the surrounding water is 20°C, the discharging thermal energy can be calculated as 7.48 MW.

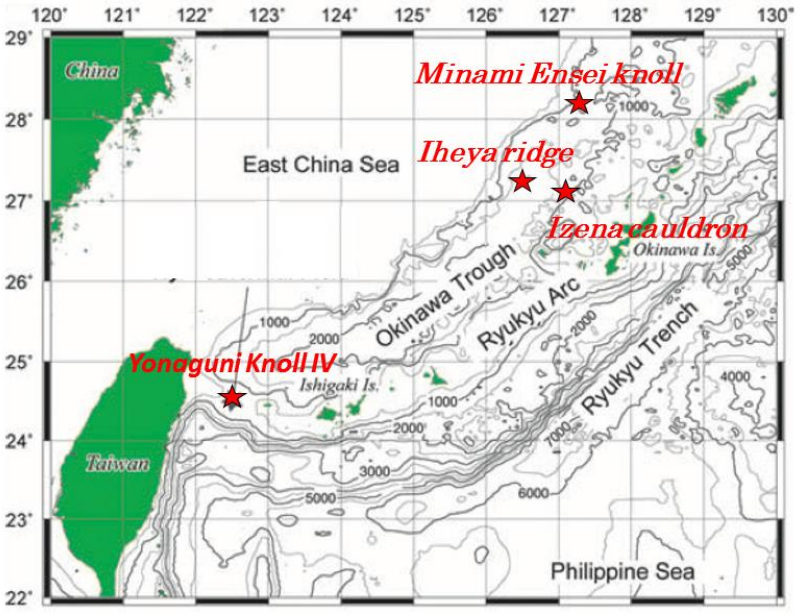

Fig. 1.9 The Hydrothermal Field in Okinawa Trough [16]

According to the calculations mentioned above, it can be known that enormous thermal energy is released from hydrothermal vent continuously. If 1% of thermal energy can be trapped, with an electrical power conversion efficiency of 1%, about 152 W and 748 W can be produced by Yamanaka vent and artificial vent, respectively. The power storage capacity and power consumption of AUVs and seabed stations depends on their characteristics and missions. Taking AUV Tri-ton developed by IIS, U-Tokyo as an

example, the power storage capacity of one battery of it is 25 V, 26 Ah, so the power produced by hydrothermal vent is possible to recharge Tri-ton over a few hours in practical applications.

1.2.2 Estimation of the heat energy discharged from hydrothermal vents

The National Geographic has estimated the energy escaping from the vents will be in an order of magnitude of GW from tens of thousands of kilometers of active ridge system [17]. According to long term investigation, two methods are proposed to calculate the energy contained in vents based on collected data and assumptions.

Baker and German proposed a method by using an indicator to calculate the heat discharge on the large-scale hydrothermal distribution along oceanic spreading ridges [17]. They defined a parameter called Fs (Site frequency) which is the number of sites per 100 km, and presented a table with Fs for different regions based on their exploration. One can get 280 sites located along the studied 13000 km ridges with $Fs = 2.2$.

If apply Baker and German's supposition and assume 2 sites exist in the 100 km long area, there will be at least 20 hydrothermal sites located along the 1000 km long Okinawa Trough region. According to the investigation of nine hydrothermal vents in Iheya-North hydrothermal field, it has been observed the highest temperature was 311°C at North Big Chimney (NBC), and the lowest temperature was 180°C at "180°C vent". The flow rate of hydrothermal emission of NBC has been measured as high as 1 m/s for more than ten years [15]. Though the dimensions of the hydrothermal vents are changing over time, based on the pictures taken from these places [18~20], the average orifice diameter of 5 cm can be considered as a reasonable assumption. Supposing the hot fluids flow out with the velocity of 1 m/s at 250°C, and the temperature of ambient seawater is 20°C, approximately 7.6 MW per site, 152 MW total heat energy is being brought out continuously.

Besides the distinct vents, there are many other configurations of hydrothermal vents, including fissures, flanges and pervasive percolation. A single measurement has been made at a fissure area located in Juan de Fuca ridge. It has a width in the order of decimeters and a length in the order of meters, and yielded a temperature of 330 °C with venting velocity of 0.9 m/s. The temperature and velocity of this fissure area are comparable to a weaker distinct hydrothermal vent. Length, width and the spatial variety of venting from these fissures are not measured completely, but it is conceivable the wide spread distribution of these vents contains gigantic heat energy which maybe

several orders magnitude than distinct vents [21].

From the calculation, it can be known the huge thermal energy is released from the heat exchange of hot fluids and cold seawater continuously. And this energy is possible to be a new power source of AUV, deep sea sensors and seabed stations if they can be captured and utilized properly.

1.2.3 Methods to generate electricity from hydrothermal vent

Ever since the hydrothermal vents were first confirmed, every observer has understood the vast energy contained in the superhot fluids, but no one has realized to produce power from this amazing natural phenomenon. The problems of harsh, inaccessible environment, frequently changes field conditions, make it difficult to place any equipment around hydrothermal vents, leaving this immense untouchable energy in the deep sea water. Recently, two typical concepts were proposed by Hiriart [22] and Bruce C. Marshall [23] to generate power from hydrothermal vent by utilizing its thermal energy and another concept was presented by Yamamoto to produce power by utilizing the electrons contained in hot fluids [24].

(1) Power generation from mechanical process by utilizing the thermal energy.

Hiriart and Espindola described a submersible generator in which a turbine system is encapsulated. As shown in Fig. 1.10, in the external part of one extreme of the submarine, a heat exchanger in the form of conic coil is installed on top of the vent; it works as an evaporator when the hot fluids flow naturally through it. Inside the submarine, turbine, generator, pump and control system are mounted. The stream is produced from liquid which is heated by hydrothermal fluids, then expanded in a high speed turbine, at last the turbine will drive a generator to produce power. The authors declared this working cycle has an efficiency of 80%. But as the system is composed of at least four major parts, such as heat exchanger, turbine, pumps and generator, the efficiency gains at the system level should be checked but now has yet to be demonstrated. Also, many moving parts will directly address reliability problems and maintenance difficulties.

Bruce C. Marshall has patented a Marshall Hydrothermal Recovery System as shown in Fig. 1.11. It starts with a simple system of insulated pipes and a funnel. The hot water will be trapped and move through the pipe until reaching the surface platform which is similar to those used for oil drilling. The superhot fluids would either be used directly or it would heat a clean working fluid within a heat exchanger to drive turbines. But for

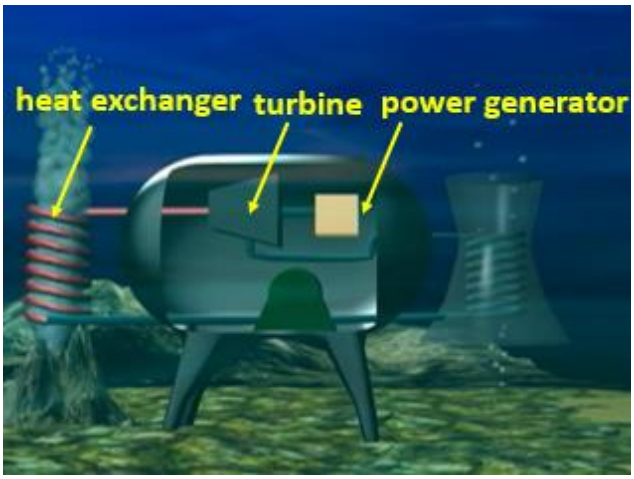

Fig. 1.10 Submersible generator [22]

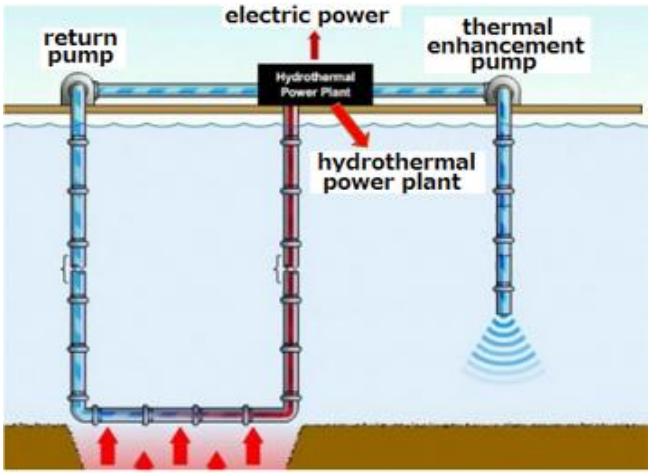

Fig. 1.11 Surface power generator [23]

the pipe system, it might be over thousand meters long to lead the hot water to surface platform, the weight of the system is considerable, and the vertical stability will become a big concern. Another problem is the flow velocity will decrease during the ascending process, and the temperature might drop significantly when hot water arrives at the surface plant.

(2) Power generation by utilizing the electrons contained in hot fluids.

In the recent news, a team from Japan Agency for Marine Earth Science and Technology, and Riken Centre for sustainable Resource Science used the ROV *Hyper-Dolphin* to suspend a fuel cell made by platinum cathode and iridium anode at hydrothermal vent located in Okinawa Trough in Dec. 2012. Three tiny LED was lighted on by the produced power. The hot fluids are highly acid compared with the slight alkalinity of seawater, and contain high concentration of hydrogen and hydrogen sulfide. The fuel cell was designed that the iridium in the anode speeds up the oxidation of hydrogen sulfide which produce the necessary amount of electrons in electrical currents [24]. The authors declared this method is very efficient, if the fuel cell is scaled up enormously, it may become as a new mean of power generation from hydrothermal vent.

(3) A new power generation method by utilizing the temperature difference of hot fluids and cold seawater

As stated before, the fluids are flowing out from the vents over 300°C while the surrounding seawater temperature is around 20°C, creating a very high thermal gradient. The power can be generated from this large temperature difference if

thermoelectric module (TEM) is mounted in hot fluids-cold seawater interface. TEM is a solid state device based on the principle of the Seebeck effect that can convert thermal energy to electric power. The temperature differences drive the mobile carriers to move in the semiconductor and lead to the inhomogeneous charger distribution, thus the electrical current is produced. TEM has been applied in many fields like night vision systems, energy recovery from automobile exhaust gas for its robustness. If TEM performs well in the high pressure environment, then it will probably become a new way of renewable power generation from hydrothermal vents and a stable energy producing way to provide power to AUV and seabed sensors.

1.3 Objective and challenges

Though the hydrothermal vent is discharging superhot fluids continuously, the heat is dissipated into surrounding cold seawater very quickly, and the temperature of hot fluids in several centimeters away from the vent orifice is nearly equal to that of surrounding seawater. Therefore it is very important to capture the thermal energy properly as soon as the hot fluids flow out. Many hydrothermal vents have an irregular orifice and their shapes are changing over time. If the inlet of generator is bigger than the orifice of vent, the cold seawater will enter from the bottom of generator, and mixed with hot fluids as soon as they flow out, thus the thermal energy that can be utilized will decrease greatly. Though the fissure and flanges hydrothermal vents are also discharging enormous heat flux, their configurations decide it is difficult to capture the thermal energy properly.

The high acidity of the hot fluids, which the pH can be as low as 2.8, implies strong corrosive influence to metals [25]. For its high thermal conductivity which is about 200 W/m-K, Aluminum alloy is used to transfer and dissipate heat in many fields. But the poor corrosion resistance makes it difficult to be used here directly. Titanium has been used as the materials for thermoelectric generator to prevent the corrosion from acid exhaust gas, but the low thermal conductivity results in a poor heat transfer and low efficiency of the system. Ceramic like SiC, is strong to corrosion and the thermal conductivity is as high as 200 W/m-K, is a good choice for simple structural generator. However, its fabrication technics make them hard to meet the demand of a complex design.

In our verification experiment, it is found that the metallic sulfide particles adhered to the surface of generator very soon as long as the hot water flowed into the generator. At some hydrothermal vents sites, chimneys grow in equilibrium with the force of the exiting water. Going with the high temperature and high velocity, the growth of the vents

will be in a rapid speed [26]. It has been observed that a chimney located in Guaymas Trough has grown 10~15 centimeters in two days. If the power generator is set on top of the hydrothermal vent directly, it is possible that the metallic sulfide particles and the growing chimney will cover the inner surface of generator even clog the outlet orifice of vent. On the other hand, hydrothermal vent is also the home to variety of creatures, like tubeworm, and it is necessary to consider the potential influences from them. Though there is no record that the creatures which live on the chemicals diffused from hydrothermal vent also like to live at the outside surface of generator, the heat dissipation will be weakened if this happens. Both of these will result in the poor heat transfer, and thus reduce the efficiency. Especially when the generator set on a "smoke" vent, this may shorten its life span and the generator also have to be removed to a new site soon.

For the installation of generator, the porous structures of hydrothermal vents imply they are very easy to be destroyed. The spreading caps of most vents are many times wider than their bases. Peter Lonsdale and Keir Becker have sampled a vent in southern trough of Guaymas Basin [26]. They found with a 1 m diameter cap, it is supported by 1 cm thick walls around a 5 cm wide conduit. Though half the wall thickness is built of rigid recrystallized sulfides, the structures are inherently unstable. Through the proved data, vents have several types according to the temperature, like open orifices, capped vents, hollow mounds, porous spires and etc. Penetrated by hot fluids for a long time, most of them of are very fragile. The hydrothermal vent will be destroyed once the generator is set directly on top of it, and the collapse of a top heavy chimney will recreate a short and openly venting area which is composed by many small holes emanating from mud. So it is necessary to set the generator without contacting with vent directly or drill a deep hole where the structure is relatively hard and can support the generator stably.

Our ultimate objective is to make a power generation system that can be installed in the seabed and transmit power to AUV and seabed station. Four major problems are faced: (1) the configuration of venting orifice can't be determined; (2) high corrosive influences on generator from the hot fluids; (3) adhesion of ejected substances that will result in the poor heat transfer; (4) difficulties of installation and hot thermal energy acquisition in long term continuously. These will be discussed and analyzed in the following chapters.

1.4 Organization of thesis

The thesis is organized into six chapters. The contents include the theoretical development and practical experiments of this research work.

In Chapter 1, the problems faced and the motivations of this research work are presented firstly. The characteristic and availability of the thermal energy discharged from hydrothermal vents are summarized and calculated. Different concepts of power generation from hydrothermal vents are introduced and compared. Considering the efficiency and durability of power generation system, a new way to produce power from vent sites is proposed and the corresponding challenges are analyzed and discussed.

In Chapter 2, TEM is employed as a medium to produce power by utilizing the temperature difference between the hot fluids and cold seawater. The physical properties and working principles of thermoelectric module (TEM) are introduced. Different from the general land use environment, the high pressure and high acidic field environment should be considered in deep sea application. A system is developed to test its performance in various thermal and pressure conditions.

In chapter 3, a compact power generator model is developed in order to confirm whether the heat is still hot enough to drive TEM to produce power after ejection. According to the irregular orifice of hydrothermal vent, compact plate housing is designed and constructed. The field feasibility experiment are presented and discussed.

In Chapter 4, a novel hexagonal shape prototype is proposed which can mount cuboid TEMs and related circuits properly. The differences in temperature distribution of concentric double-pipe prototype and hexagonal shape prototype in various conditions are compared. The influences from solidified sulfide particles which will partially clog the vent or adhere to the inner surface of generator are considered and discussed based on the CFD FLUENT.

Chapter 5 follows the development of a power generation system which is composed of a power generator and power management system. A comprehensive study of power generator on stress intensity, corrosion resistance, heat transfer and flexibility in mechanical design is done. In large power generation system, the output power not only depends on the temperature difference on single TEM, but also the topology of TEMs connection methods. According to the thermal distribution, centralized architecture and distributed architecture are compared and the limitations of both methods are analyzed. Combining with the simulation results, the power mismatch problem caused by the non-uniform temperature distribution on TEMs is studied, and the solutions for distributed architecture are proposed. The field experiment and results are presented and discussed.

Chapter 6 summaries the whole work and the contribution of this research. It is the first deep sea power generation system by utilizing the thermal energy discharged from

hydrothermal vent sites. The methods for long term and large scale power generation are discussed.

Chapter 2 TEM performance testing in various operating conditions

2.1 Introduction

Thermoelectric module (TEM) is a solid state device which can convert thermal energy to electricity power by utilizing the temperature differences known as Seebeck effect. Reversely, if current passes through the TEM, either heating or cooling effect can occur on the surface of it. No moving parts, stable performance and the durability allows TEMs to be used as a power generator in long term.

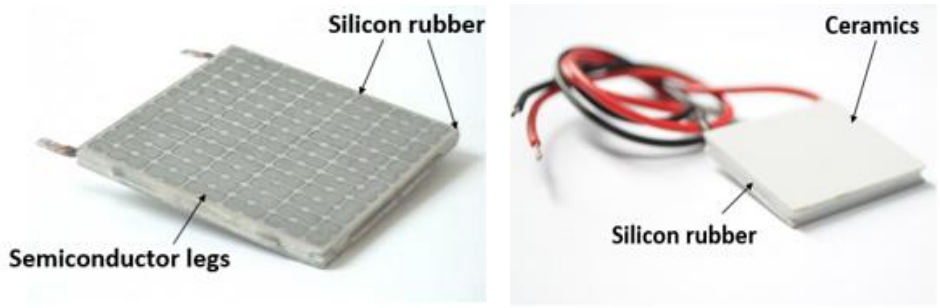

Fig. 2.1 The configuration of thermoelectric module [27] [28]

TEMs have already been used across a variety of industries for both power generations and heating/cooling applications. Not only being utilized in daily life, like power generation by using the thermal energy from hot spring and exhaust gas, it has also been applied to many innovative technologies to offer new functionality gradually. In space, beyond a certain distance the solar radiant flux is not adequate to power spacecraft through solar cells, so all power sources for U.S and former-USSR deep-space probes have used TEMs to convert heat generated by nuclear fissile material to electricity that can operate in the absence of sunlight [29]. TEMs have also been used to produce -80°C in infrared imaging systems for heat seeking missiles and night vision systems [30].

In this research, TEMs are expected to be used as an electrical power generator by converting the temperature difference between hot fluids discharged from hydrothermal vent sites and cold seawater into electrical power. Different from other application environment, when the TEMs are supposed to be used in deep seawater,

two problems have to be considered:

(1) Corrosion resistance problem.

As shown in Fig. 2.1, TEM is composed of many semiconductor legs, and sealed by silicone or epoxy to prevent corrosion from moisture. It has been verified that silicone can offer great moisture resistance for direct seawater application [31]. But for the hot fluids discharged from hydrothermal vent, besides being superhot, it is also extremely acidic. In some hydrothermal vent sites, the pH value of hot fluids can be as low as 2.8 [25]. Most of the silicone can't work exceeding the temperature range of −100°C to 250°C, and the strength of epoxy adhesives degrades when the temperature is above 177°C [32], so the sealant materials will lose sealing capability when the temperature of hot fluids is higher than 250°C.

(2) Pressure influence on power generation ability.

TEM will be mounted in the hot fluids-cold seawater interface. And the water pressure will be imposed on it in the direction that is vertical to its hot and cold sides all the time. The pressure influence on cooling effect of TEM has been tested, and verified it performed well up to 70 MPa [31]. In this chapter, a system was developed for testing its power generation performance in various thermal and pressure conditions to explore the possibility of deep sea application.

2.2 Working principle

Thermoelectric materials are capable of converting heat into electrical power which is known as Seebeck effect, discovered by Thomas Johann Seebeck in 1821. If a heat source is supplied and temperature difference exists across both sides of thermoelectric materials, then a voltage difference will appear across the electrical terminals of materials. Reversely, if a current is supplied across the terminals of TEM, either heating or cooling can occur at the surface, which is known as Peltier effect.

As illustrated in Fig. 2.2 , TEM consists of a large number of thermocouples that are connected electrically in series and thermally in parallel. The thermocouples are junctions of heavily doped semiconductors. During operation, heat is applied to one side and removed from the other side. On the hot side, the kinetic energy of the mobile charge carriers (electrons in the n-type thermocouple and holes in the p-type thermocouple) increases and then they gradually start to diffuse across the energy

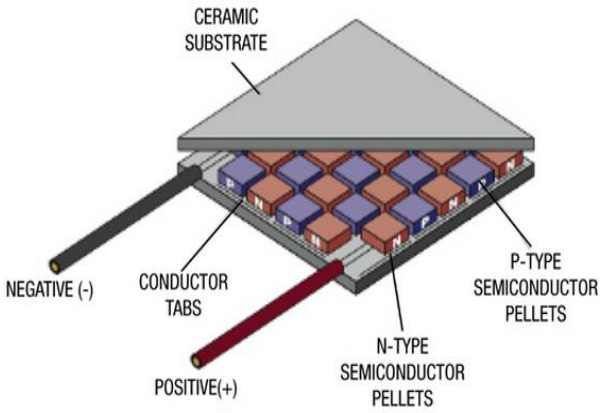

Fig. 2.2 Thermoelectric module construction [33]

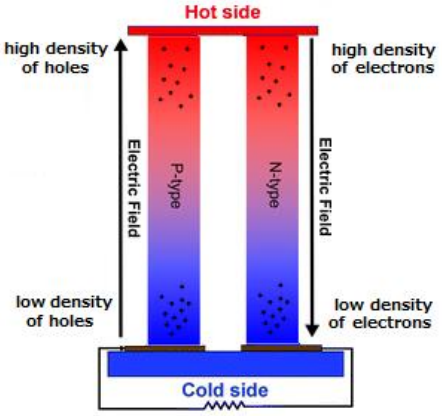

Fig. 2.3 Working principle of thermoelectric module [34]

gradient to the cold side. Since there are more mobile charge carriers at the cold side, the inhomogeneous charger distribution forms an electrical field which opposes the diffusion. If the material is in an open circuit, the equilibrium will be reached when the rate at which carriers move from hot side to cold side due to diffusion is balanced with the rate at which carriers move from cold side to hot side due to electric field. Thus, in balanced state, a voltage will be produced in response to the temperature difference. As shown in Fig. 2.3, the electric field due to a temperature difference across a material results in a positive voltage for a P-type material and negative voltage for N-type material with respect to the hot side. This voltage is known as Seebeck voltage, and the ratio of an induced voltage with E per unit temperature difference ΔT is called Seebeck coefficient [35] [36]:

$$S = -\frac{E}{\Delta T} \tag{2.1}$$

In order for this process to be efficient, it is necessary to find materials to have good electric conductivity that electrons can easily pass through. Also, the material must be poor thermal conductors that temperature difference can maintain on hot and cold sides. Similarly, the Seebeck coefficient should be maximized. Based on these, the performance of thermoelectric materials is always evaluated by the figure of merit Z , which is a measure of a material's relative effectiveness of transporting electrical energy compared to thermal energy:

$$Z = \frac{S^2}{\rho_s k_s} \tag{2.2}$$

where ρ_s is the electrical resistivity and k_s is the thermal conductivity.

On the other hand, the efficiency η of a TEM is the ratio of the electrical power

produced Q_{elec} and the thermal power input to the hot side of the TEM Q_{hot} :

$$\eta = \frac{Q_{elec}}{Q_{hot}} \tag{2.3}$$

Q_{hot} is also the heat flux that transfer through the module and is given by Fourier's law of conduction:

$$Q_{hot} = \frac{k_s A_s}{d_s} \Delta T \tag{2.4}$$

where A_s is the surface area, and d_s is the thickness of TEM.

Q_{elec} is the electric power, determined by the resistive heating relation:

$$Q_{elec} = \frac{E^2}{r} \tag{2.5}$$

where r is the internal resistance of TEM.

Based on (2.1) ~ (2.5), and if the resistivity of the module is irrespective of temperature, the efficiency η of the TEM can be written as:

$$\eta = Z\Delta T \tag{2.6}$$

To maximize power generation efficiency, the temperature difference ΔT between the hot and cold sides should be as large as possible. In today's best commercial heating/cooling TEM, $Z\Delta T$ is about 1.0. Heremans at Ohio State University and an internal team claimed reaching $Z\Delta T$ of 1.5 at 50°C in 2008 [37]. Despite of these results, many kinds of new materials are still in the developing stage and have yet to be used in application.

2.3 Fabricated materials

The thermoelectric semiconductor material most often used today is an alloy of Bismuth Telluride, the performance of which peaks within a temperature range (T~ 300°C) that is best suited for most general applications. Most of the thermoelectric materials are fabricated by either directional crystallization from a melt or pressed powder metallurgy [38]. However, the Bismuth Telluride is not very attractive when the temperature is higher than 350°C because decomposition, vaporization, or melting of the constituents can easily occur when the temperature is above 350°C.

In addition to Bismuth Telluride (Bi_2Te_3), there are other thermoelectric materials, including Lead Telluride (PbTe), Silicon Germanium (SiGe), and Bismuth Antimony (BiSb) alloys that may be used in specific temperature range as shown in Fig. 2.4.

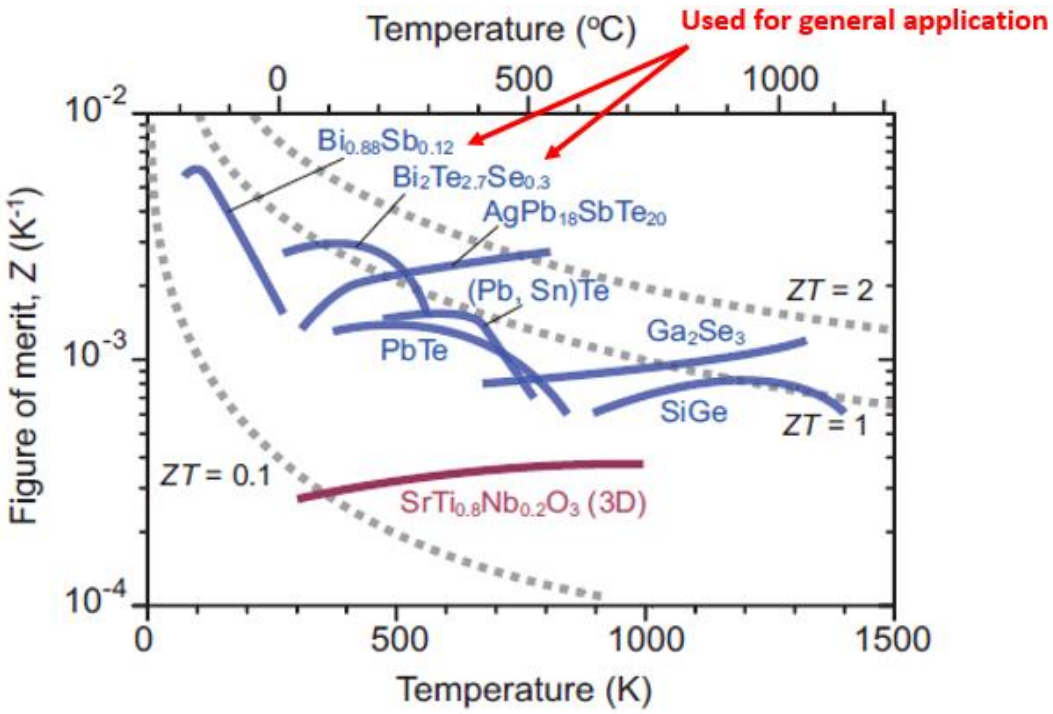

Fig. 2.4 Figure of merit Z vs. temperature for conventional heavy-metal-based materials [39]

The heavy metals contained in these materials, like gallium, germanium are mostly toxic and low in natural abundance, thus they are always used in specific environment [40].

In this research, as the temperature of hydrothermal vent distributed in Japanese Sea area is ~300°C, the TEM which is made by Bismuth Telluride is employed here. There are two important ways to improve the performance of the module's performance. One is to improve the intrinsic efficiencies of thermoelectric materials, and many efforts are underway to do this. Another is to improve the way in which existing TEMs are currently used. In this research work, the major work will be concentrated on the latter one.

2.4 Review of typical thermoelectric generator application

Over the years, the range of power generation systems by utilizing TEMs have been expanded from micro watt system to experimental large scale 1 kW [41]. In the medium scale generation, which is generally defined from 100 W to 1 kW, geothermal energy and vehicle exhaust power generation have made progress by utilizing TEMs. Toshiba Corporation has conducted a geothermal generation system by utilizing thermal energy from hot spring and already operated for more than 20000 hours

continuously [42]. As shown in Fig. 2.5, four sets of hot water channels and five sets of river water channels are alternately arranged, then TEMs are installed in the space of two contiguous channels. The hot water channels are made by Titanium in order to resist the corrosion from hot springs of which the pH is as low as 2. It was reported that 150 W was produced by 320 pieces of TEMs when the temperature of hot spring is 94°C. In Fig. 2.6, the output of TEMs and a commercial 4 kW photovoltaic power generation system per unit area are compared, and found that the thermoelectric power generation is obviously superior to a photovoltaic cell.

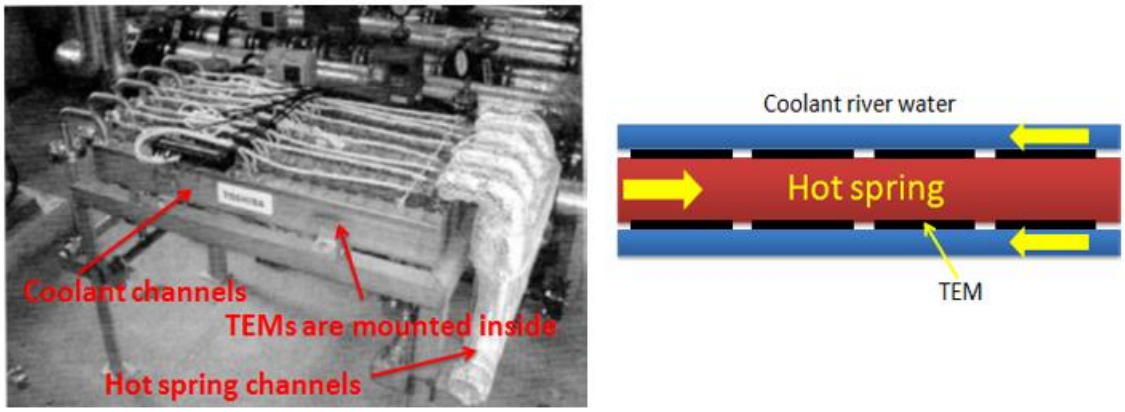

Fig. 2.5 Thermoelectric power generation system utilizing hot springs [42]

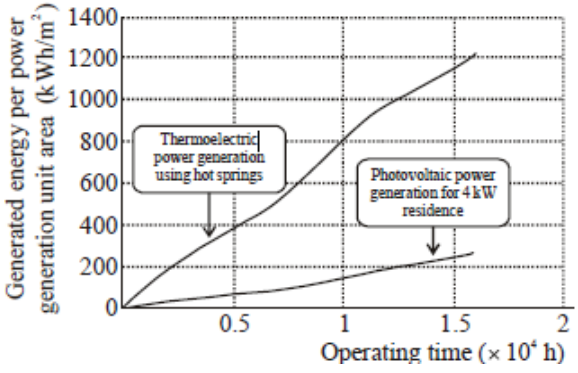

Fig. 2.6 Comparison of generated power with photovoltaic system per unit area [42]

Many groups have researched on the thermoelectric waste heat recovery system for vehicles. It has typically reported that about 255 W was produced in vehicle test done by Clarkson University [43], and over 600 W was generated in BMW X6 and Lincoln MKT vehicles test in 2012 [44]. Fig. 2.7 shows the configuration of the generator tested by BMW X6, a cylindrical structure was designed and the TEMs were arranged along its surface.

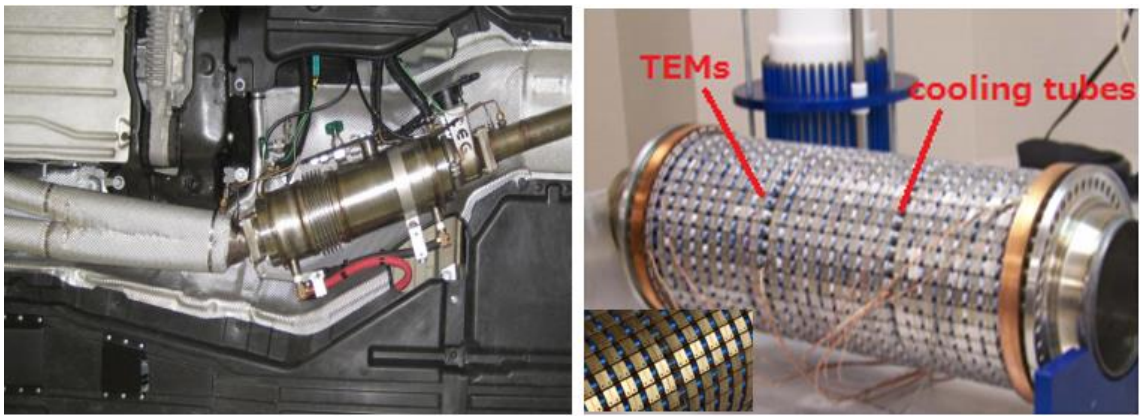

Fig. 2.7 TEM integration into the exhaust line of BMW X6 prototype vehicle [44]

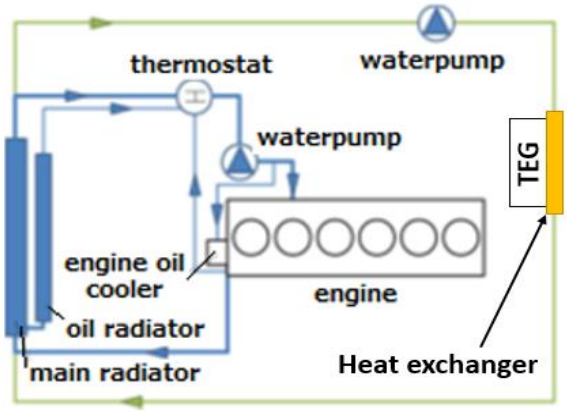

Fig. 2.8 TEM cooling circulation system

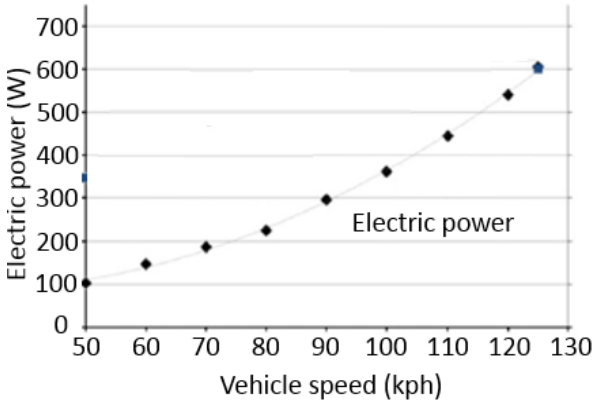

Fig. 2.9 Output power vs. vehicle speed

The fast speed causes the waste gas leaves the tail pipe at a high temperature, which brings high temperature heat distribution on the hot side of TEMs. While in the same time, it is necessary to dissipate heat efficiently from the cold side of TEMs to maintain a high temperature difference on both sides of them. In order to realize this, water coolant circulation system is always applied as shown in Fig. 2.8.

Water is tapped just at the outlet of engine radiator, and then pumped to pass through the cold side heat exchanger, lastly goes back to the radiator. The variation of generated power with vehicle speed is shown in Fig. 2.9 that was tested on the generator installed in BMW X6. Over 360°C of the temperature of waste gas was reached when the speed was 130 km/h and the temperature difference on both sides of TEM was measured as 280°C. Under this condition, 605 W was produced.

In these designs, some potential problems exist. In the structure design of thermoelectric power generators for vehicles, many fins are attached in the exhaust gas sides to increase the heat transfer area as shown in Fig. 2.10. But the exhaust gas velocity will decrease because of the high density fin arrangement which may

produce thick thermal boundary layer, thus results in the decrease in power generation. As reported from the experiment done on a diesel trucks, the excessive fins caused poor heat transfer, and only half of the target power was obtained [45]. According to the different flow velocity and cross sectional area, the number of fins should be optimized.

As shown in Fig. 5.7, a preload pressure is commonly imposed on the TEMs to make sure good heat transfer with heat exchanger surfaces, which will make the configuration of generator much more complex and the added structures also bring an additional thermal resistance to the system.

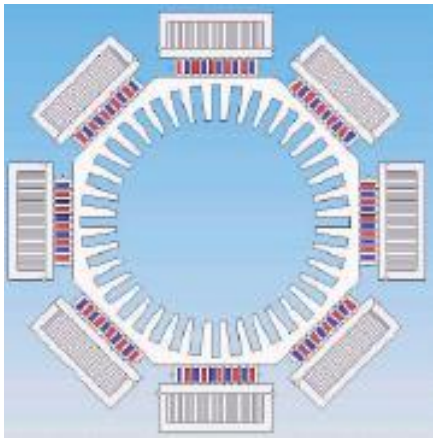

Fig. 2.10 Fin arrangement

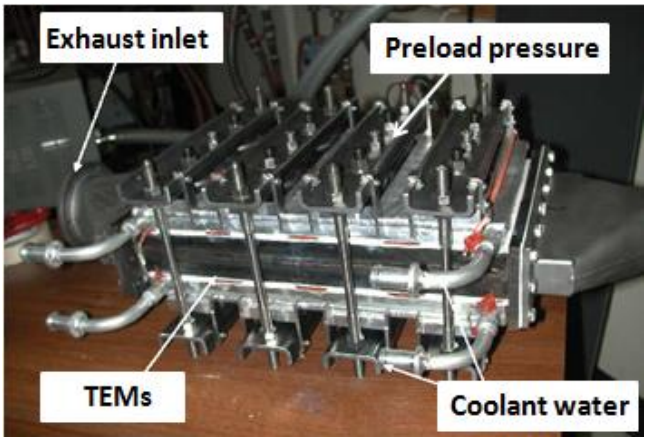

Fig. 2.11 Vehicle power generator with preload pressure

In power management system of these applications, the generated power has not been utilized efficiently in most TEM power generation systems. In the present land used generator, many TEMs are always connected in series to achieve an applicable voltage. However, for an efficient integration, the internal resistance of TEMs should be close to the load's resistance for maximum power extraction. But this is not always feasible; the non-uniform thermal conditions will result in the power mismatch problem if the TEMs are simply connected in series or parallel. This weakness will be studied later.

2.5 Performance of TEM in various thermal conditions

The TEM used at the first stage in this experiment was made of Bismuth Telluride and manufactured by Hi-Z, Technology Inc. The specification are listed in

Table 2.1. A system was developed for testing the performance of TEM under various thermal and pressure conditions. The system consisted of a TEM sandwiched in two copper blocks as

Table 2.1 The specification of TEM Hi-Z 14

properties	Value
Dimensions (cm)	6.3(L)×6.3(W)×0.5(H)
Thermal conductivity (W/m-K)	2.4
Internal resistance (Ω)	0.28
Matched load output voltage (V)	0.71 (Th = 100°C Tc = 35°C)
Matched load output power (W)	2.6

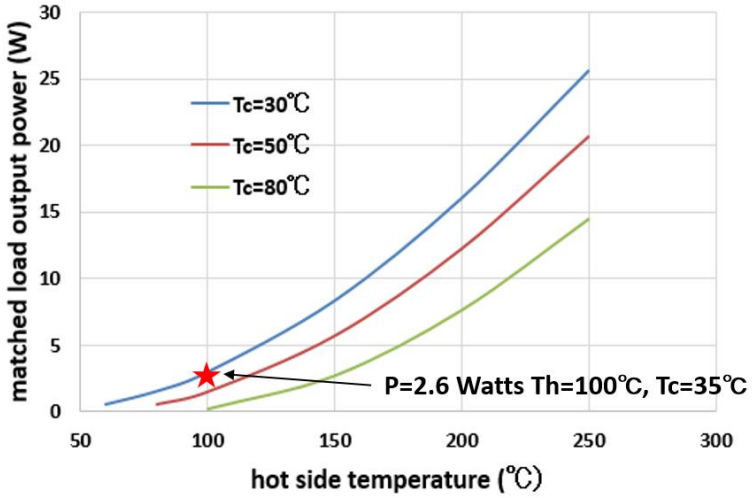

Fig. 2.12 The power output of Hi-Z 14 in various thermal conditions

shown in Fig. 2.13. Two platinum surface temperature sensors (CHINO R060) were embedded into the center pocket fabricated on each block and were in contact with the hot and cold sides of TEM, respectively. A super rapid heater (500 W, SAKAGUCHI) was pasted beneath the lower copper block to adjust the hot side temperature. Since the thermal conductivity of copper is approximately two orders of magnitude higher than TEM, the presence of copper block can be assumed to be negligible. In addition, through copper block, the hot side temperature distribution across face of TEM can be thought as uniform. A heat sink was designed for cold side of TEM to obtain good cooling effect. Then, the copper blocks, TEM and heat sink were fixed using a thermal grease to reduce the thermal contact resistance. The test section was insulated lastly to minimize the conduction of heat loss.

In an effort to get consistent experiment data, the temperature of hot sides was adjusted by temperature controller. When started the program, the temperature

controller functioned until reaching a steady state in the temperature and voltage output. Then the voltage drop across the rheostat was measured for selecting temperature. Measurements were taken using a voltage recorder (KEYENCE NR-2000, resolution 14 bit) and a Pt100 thermo-sensor input reader (CONTEC PTI-4, resolution 0.01°C).

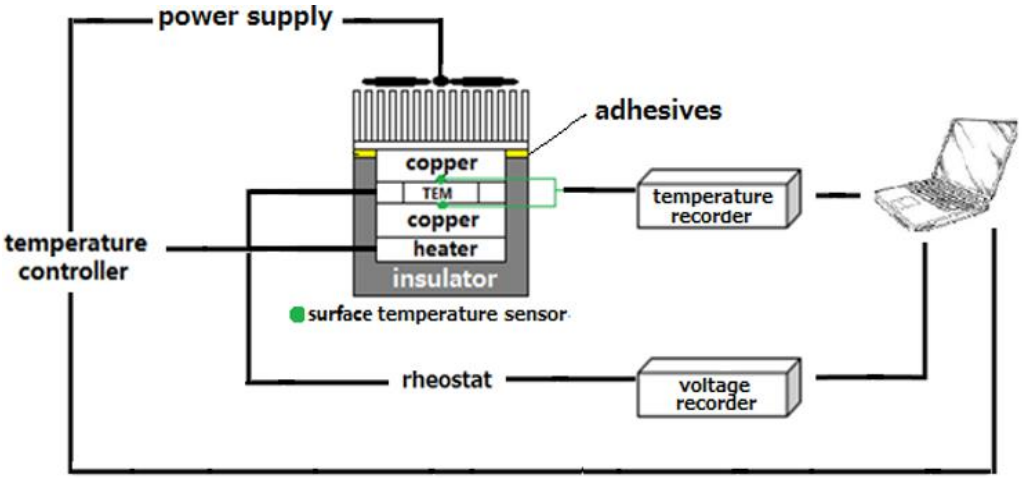

Fig. 2.13 Schematic diagram of the experiment setup

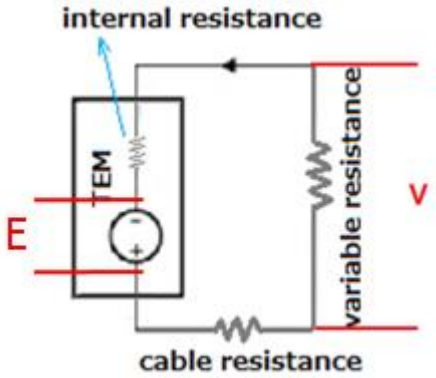

Fig. 2.14 Electrical diagram of the test system.

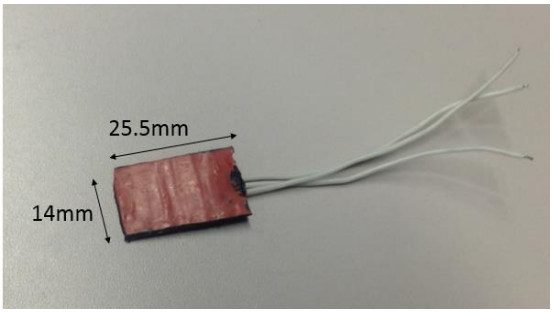

Fig. 2.15 Surface temperature sensor

The temperature can be measured in a range of -50 °C to 250°C

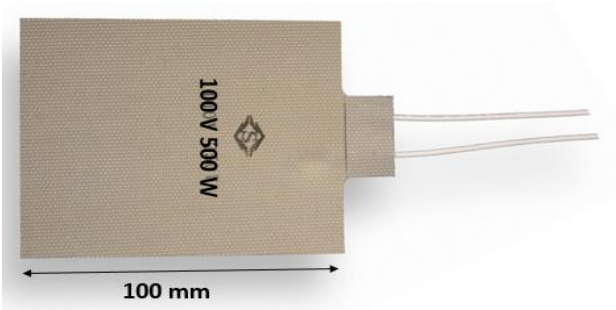

Fig. 2.16 Surface rapid heater

The maximum operating temperature is 600°C

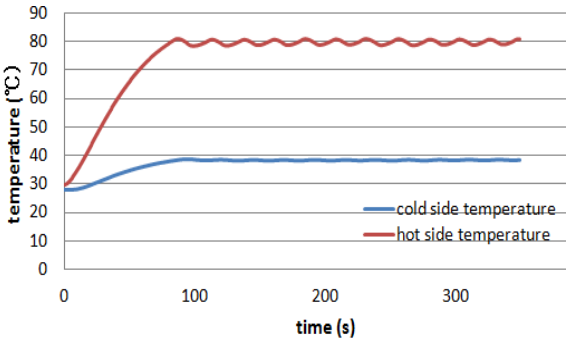

Fig. 2.17 Temperature adjustment

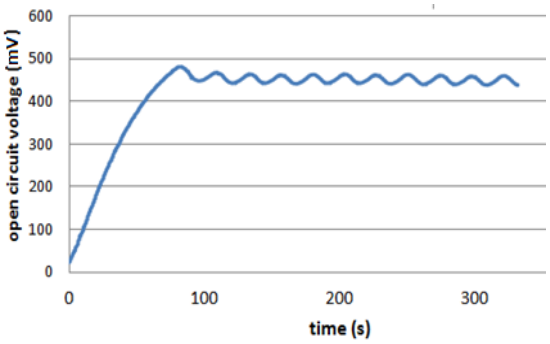

Fig. 2.18 Open circuit voltage output

The high temperature was controlled as 80°C and the temperature difference on both sides of TEM was maintained as 40°C. The oscillation range of the temperature was around 2°C.

When the temperature difference on both sides of TEM was maintained as 40°C, the output voltage was about 0.45V and the oscillation range of the voltage was around 0.02V.

Fig. 2.17 and Fig. 2.18 are the temperature and open circuit voltage output of TEM when the hot side temperature was 80°C, and the temperaure differnece on both side was 40°C. The curves behaved as periodic oscillation around a certain value that is a reflection of on-off control of heater. The oscillation range of temperature was 2°C, and for open circuit voltage that was 20 mV. The voltage across external resistor at selecting tempeautre was recored for at least a period and then the average value was taken.

The voltages, current and power output across the external resistor in various thermal conditions are plotted in Fig. 2.19 (a), (b) and (c), respectively. From these curves, it is obvious that the output voltage, current and power were increased significantly according to the temperature differences on TEM. The output power can be expressed as

$$P = (\frac{E}{r+R})^2 \cdot R \qquad (2.7)$$

Where r , R , E and P are internal resistance, external resistance, induced voltage and output power, respectively. Through differential deduction $\frac{dP}{dR} = \frac{R-r}{(R+r)^3} E^2$, it can be known that the maximum output power can be obtained which is $P_{\max} = E^2 / 4r$ when $R = r$.

Referred to the data sheet, the internal resistance of TEM Hi-Z14 is 0.28Ω. This matches with the value of external resistance where the maximim power output was obatined as shown in Fig. 2.19 (c). Comparing Fig. 2.12 with Fig. 2.19 (c), under the same thermal conditions (e.g. Th = 100°C, Tc = 35°C), the output power measured was 25% of the manufacture's datasheet by using this test system.

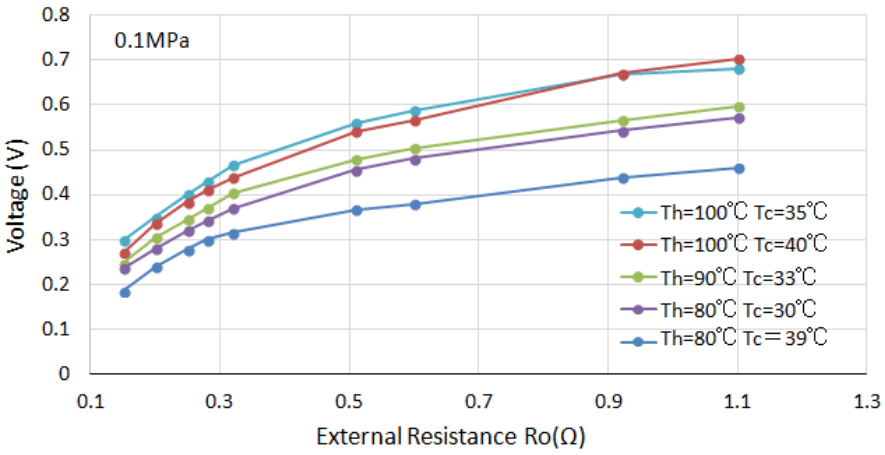

(a) External resistance vs. output voltage

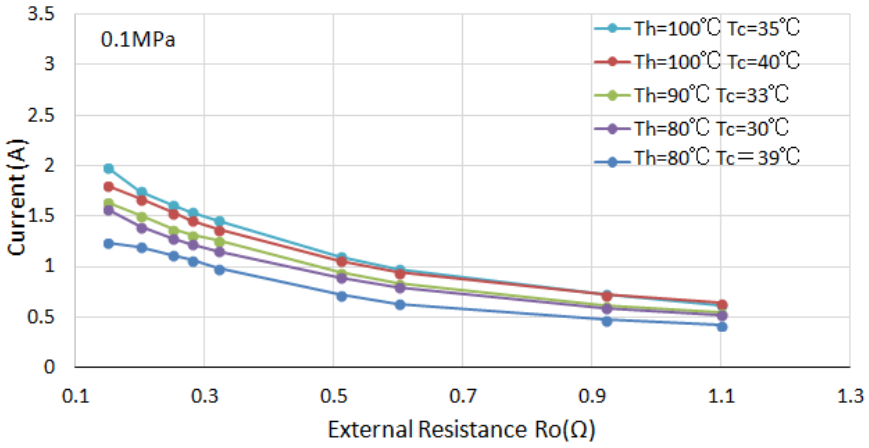

(b) External resistance vs. output current

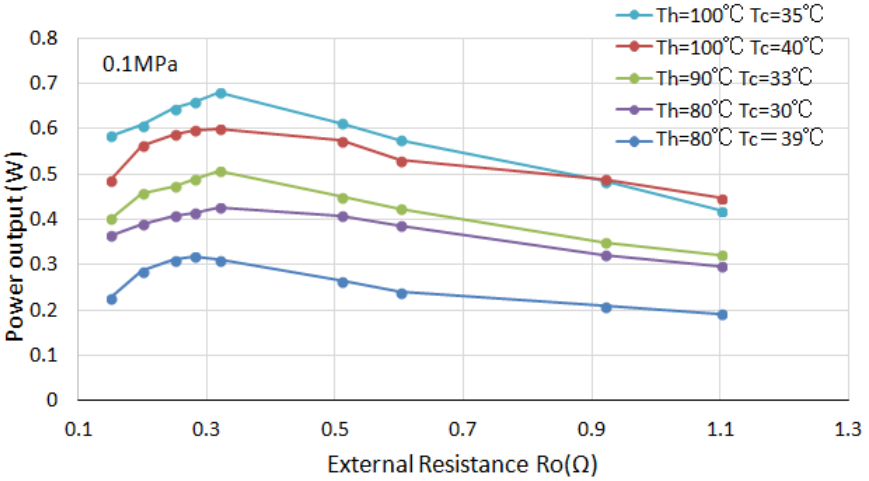

(c) External resistance vs. output power

Fig. 2.19 External resistance vs. ouput

The parameters used to describe the thermoelectric materials properties, such as Seebeck coefficient S , thermal conductivity k_s and electrical resistivity ρ_s are temperature-dependent. In other researches, it has already proved S and k_s can be treated as constant value, because the variation according to the operating temperature is very small, while ρ_s strongly relies on the thermal conditions [46] [47]. However, from this test it is found the resistivity of TEM Hi-Z14 is nearly irrespective of temperature, which can be considered as constant.

2.6 Performance of TEM under various pressures

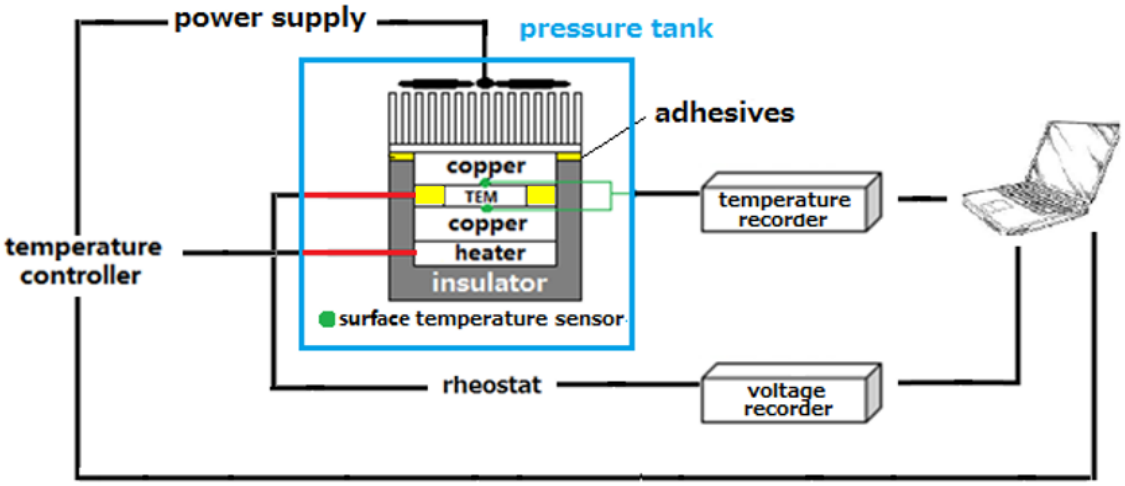

Fig. 2.20 Schematic diagram of the pressure experiment setup

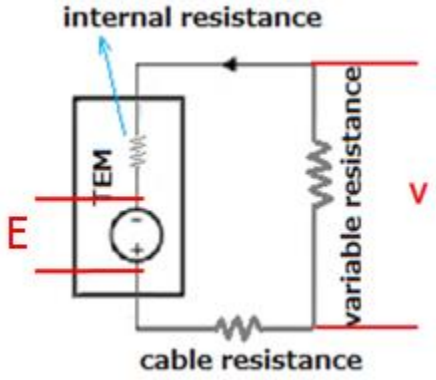

Fig. 2.21 Electrical diagram of the test system.

The power generation performance of TEM under high pressure has been tested in pressure tank. As shown in Fig. 2.20, adhesives were used to fill up the prearranged space between heat sink and insulation frame which make sure the downward pressure can impose on the TEM rather than other parts of test section. Then the system was placed in the pressure tank, and surrounding the entire setup was cold

water. The underwater cables were used to transmit power to heater, transmit temperature signals, and output of TEM from the pressure tank to outside as indicated in red and greed lines in Fig. 2.20. The resistance of the underwater cable is 0.5Ω, which is nearly twice of the internal resistance of TEM, so the power loss caused by it cannot be ignored.

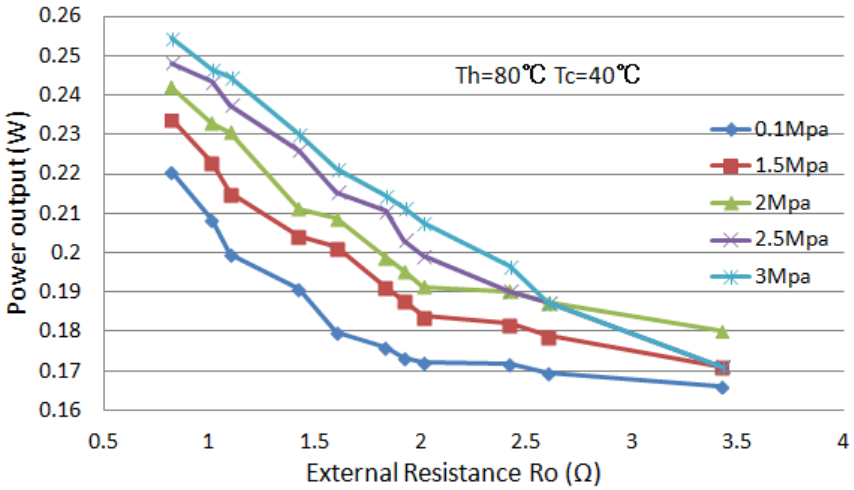

Fig. 2.22 Power output in various pressure conditions

Fig. 2.22 shows steady state results under pressure conditions that ranges from 0.1 MPa to 3 MPa. The hot side temperature was set as 80°C, and the temperature difference was maintained as 40°C. Expected trends can be seen from these curves that the higher output power was obtained as more pressure was loaded. This can be explained as the high pressure compressed both sides of TEM contact with copper plate tighter, and the gaps between them became smaller, which enhanced heat conductive transfer and bring the better performance of system. As the TEM's internal resistance is only 0.28Ω, the underwater cable used in pressure tank was about 0.5Ω, as shown in Fig. 2.19(c), only part of the power output curve was obtained. The results show TEM performs well under pressure up to 3 MPa which is the depth of hydrothermal vent we would plan to do the feasibility experiment.

2.7 Summary

TEM is a solid state device which can convert thermal energy to electric power based on the principle of the Seebeck effect. As the TEM are supposed to be used in deep sea to generate power by utilizing the temperature difference of hot fluids and cold seawater, a system was developed to test its performance in various thermal and

high pressure conditions. It is found the overall performances of TEM were in proportion to the temperature differences on both sides of TEM. Under the same thermal conditions, the output power increased as higher pressure was loaded, which can be explained as the high pressure compressed the TEM with copper plate tighter, thus brought better heat transfer.

Chapter 3 Feasibility experiment

3.1 Background

Since 2007, the first hydrothermal vent was found in Kagoshima Bay, three major active vent areas have been found until now. The vents named Tagiri and Daifukuyama are located at depth of 194 m ~ 198 m. They are at the openly venting areas which are composed by many small holes emanating from seabed. The maximum temperatures of both vents are 80°C. Yamanaka chimney is a distinct hydrothermal vent, of which the height is nearly 3 m high, flowing out with the velocity of 0.4 m/s at depth of 196 m. The outlet orifice temperature of this vent has been measured as high as 100°C and the inside temperature can be up to 190°C by analyzing the precipitated substances, and the pH ranges from 6.5 to 7.2 [48].

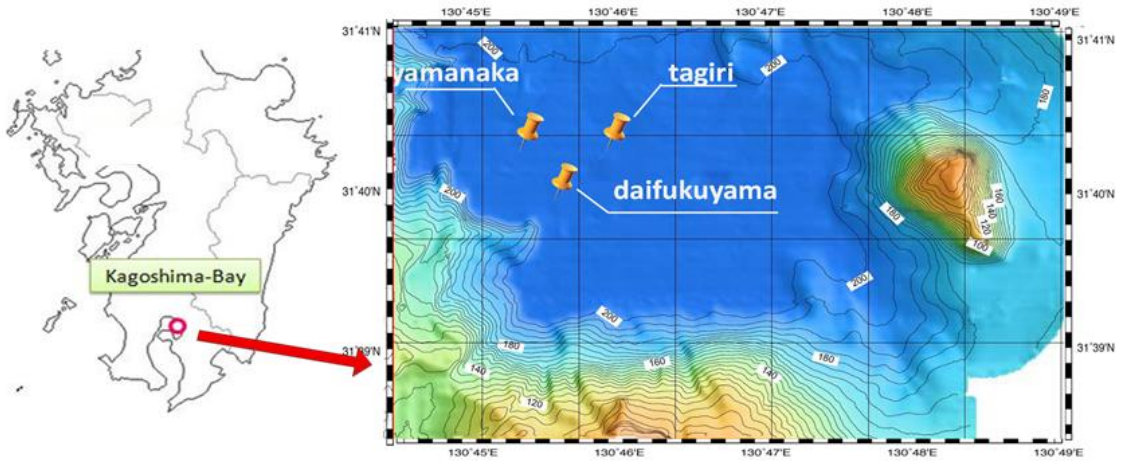

Fig. 3.1 The distribution of hydrothermal vent located in Kagoshima Bay

Hydrothermal vents located in Kagoshima Bay was chosen to do the feasibility experiment firstly because they are at a shallow depth in a very calm zone, where is easy to work and dive. In these vent places, Yamanaka vent was selected for its highest discharging temperature and obvious visible orifice.

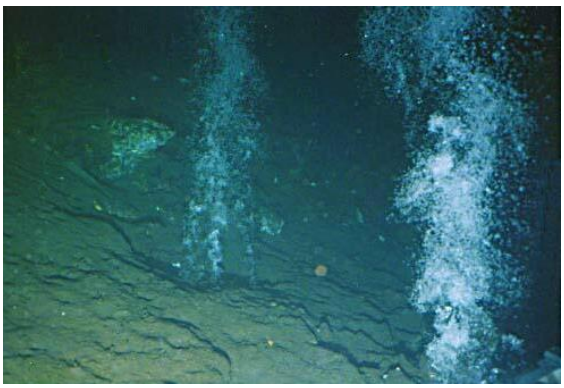

Fig. 3.2 Hydrothermal vent Tagiri [49]

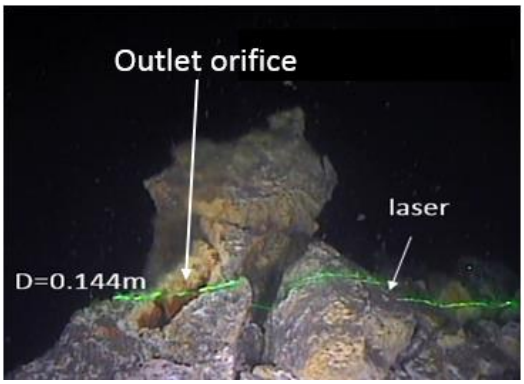

Fig. 3.3 Hydrothermal vent Yamanaka [50]

3.2 Experiment concept

As the heat discharged from hydrothermal vent is dissipated into surrounding cold seawater very quickly, the objective of this experiment is to confirm whether the water is still hot enough to drive TEM to produce power after ejection from the orifice. According to the configuration of Yamanaka chimney as shown in Fig. 3.3, the irregular orifice makes it difficult to cap the outlet orifice properly by using a pipe shape generator. If the diameter of generator is bigger than that of the vent orifice, cold water will enter from the bottom of generator and mix with the hot fluids as soon as they flow out, and this will greatly reduce the temperature of hot fluids. Reversely, if the diameter of generator is smaller, the escaped hot water will warm the outside of generator, and thus reduce the temperature differences on both sides of it.

A plate shape generator model was proposed here, in which TEMs can be housed in, as shown in Fig. 3.4. It can efficiently transfer thermal energy to the housing when the directed hot fluids flow collides against the bottom part of it. Meanwhile, the top side of housing is covered by cold seawater; the stable temperature difference formed on both sides of housing can drive TEM to produce power continuously.

The hydrothermal vent has already been penetrated by hot fluids for a long time, and the hollow mounds make it impossible to set the generator directly on top of it. Thus, the generator was decided to be held by the manipulator of ROV *Hyper-Dolphin* in a short time in the feasibility experiment.

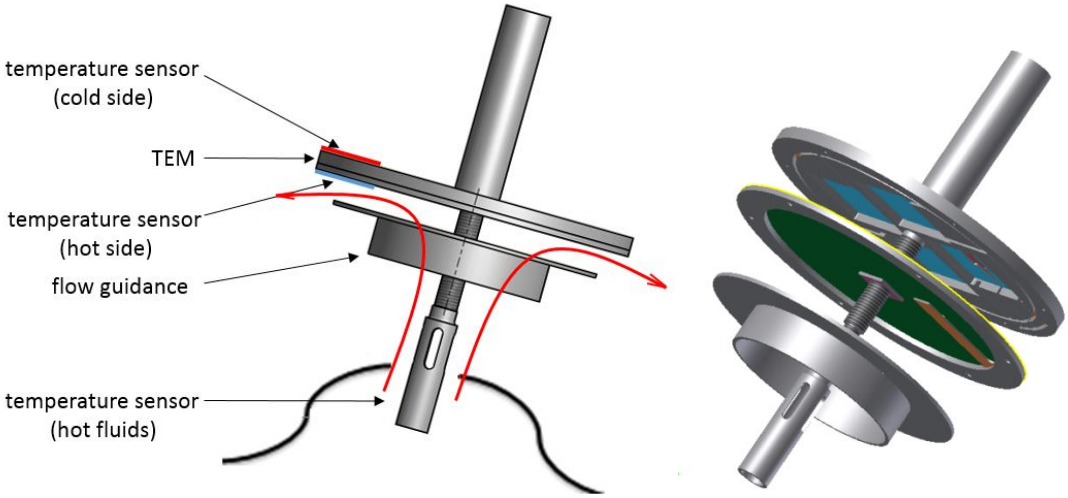

Fig. 3.4 The concept of power generator model

The directed hot fluids flow collides against the bottom part of the housing can transfer thermal energy between the surface and liquid.

3.3 Feasibility experiment

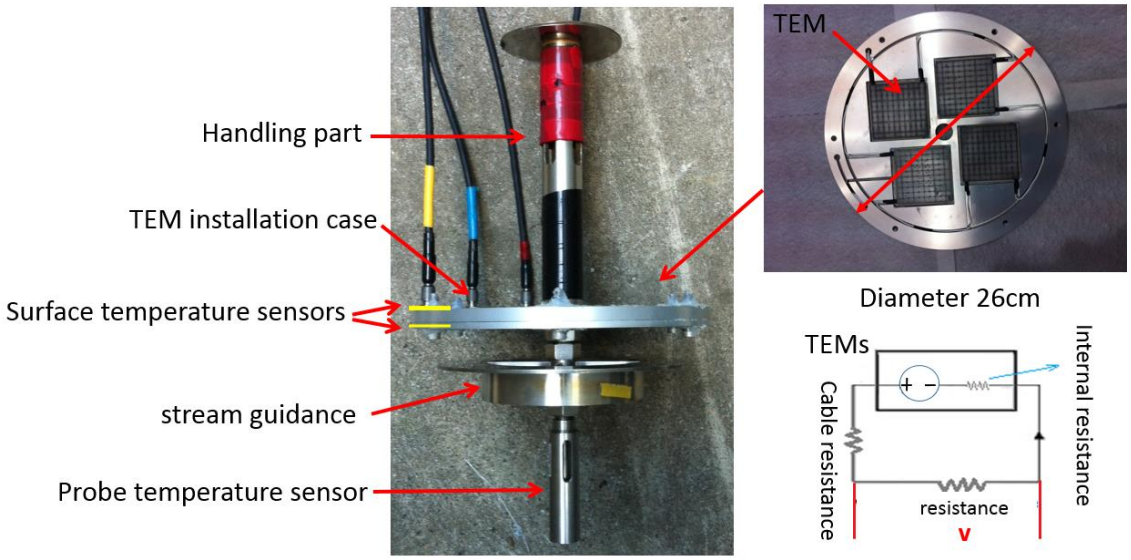

Fig. 3.5 Compact power generator model

As shown in Fig. 3.5, four pieces of TEMs were connected in series and housed in plate housing. Two surface temperature sensors (CHINO R060) were pasted on both sides of TEM to record temperature difference, and a temperature probe in bottom was used to observe the temperature of venting orifice.

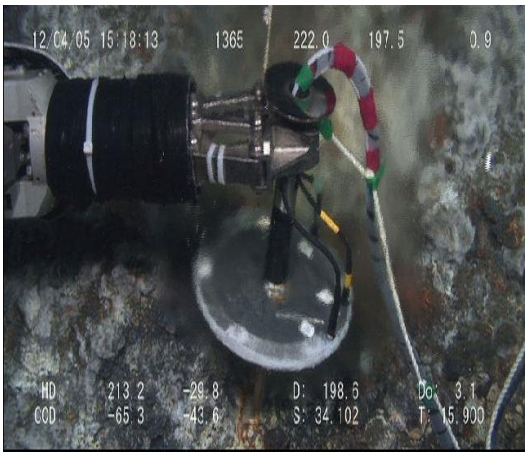

Fig. 3.6 The compact power generator

Power generator was suspended on top of vent orifice by a manipulator of ROV

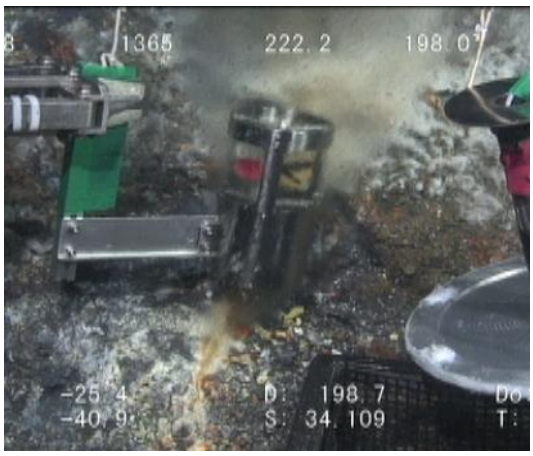

Fig. 3.7 The current meter

Current meter was placed close to the orifice by a manipulator of ROV

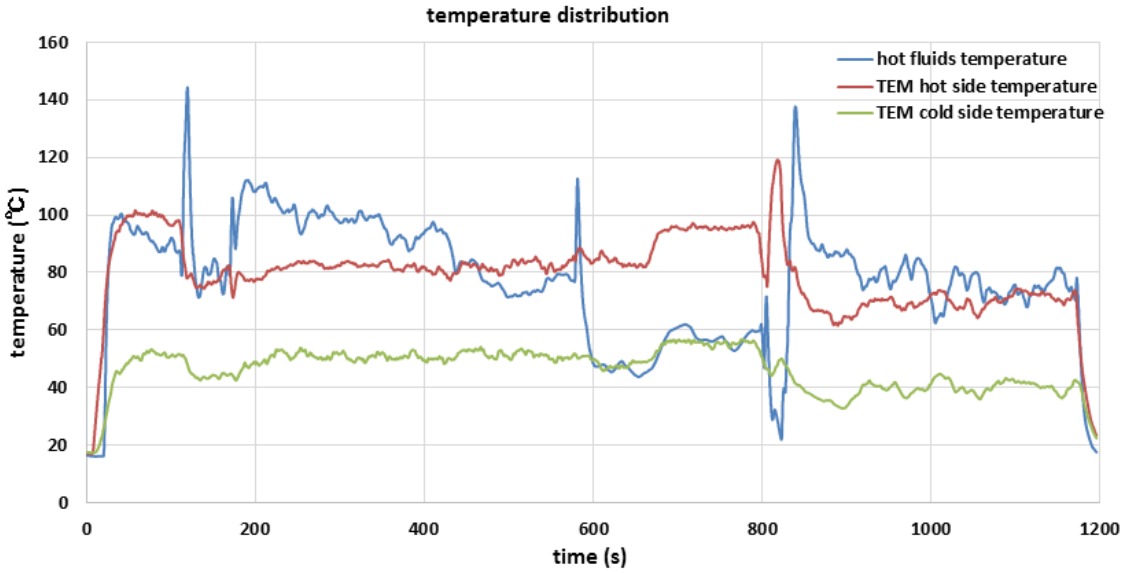

Fig. 3.8 Temperature of hot fluids and the temperature distribution on TEMs

Fig. 3.8 shows the temperature of the discharging hot fluids and the temperature distribution on TEMs. The blue line represents the temperature of venting orifice measured by the probe temperature sensor. As capped by the plate generator model, the orifice can't be seen by ROV's camera. Especially from 600s to 800s, the temperature dropped rapidly, this was due to the attitude adjustment of manipulator of ROV *Hyper-Dolphin*. Referred to other published literatures, the temperature of hot fluids inside vent can be thought as over 140°C, and temperature of outlet fluids was around 100°C. The temperature differences on both sides of the TEM ranged from 30°C to 40°C.

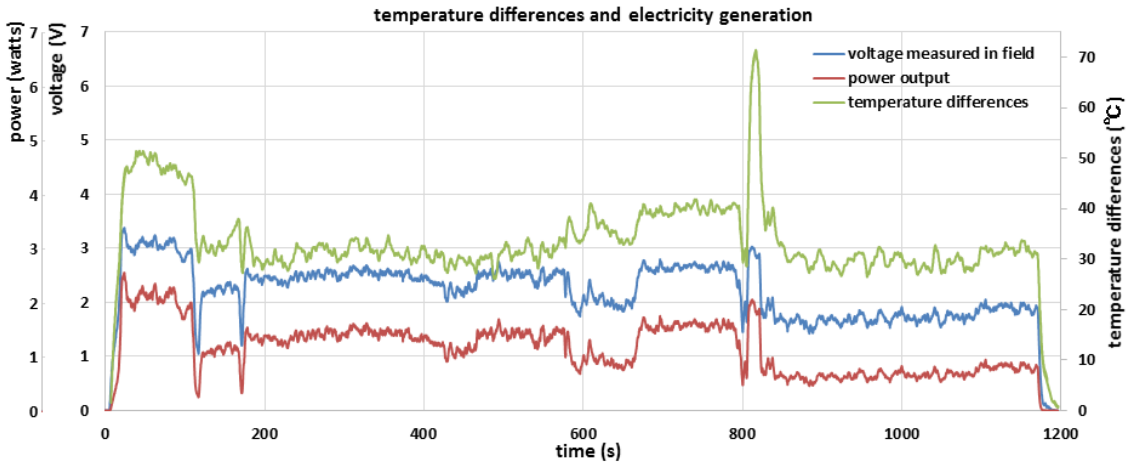

Fig. 3.9 Output voltage and the output power

Fig. 3.9 shows the output voltage and the output power of generator model. The output voltage was measured ranging from 1.8 V to 3.3 V which was in trend with the temperature difference as shown in green line. The maximum power generated by four pieces of TEMs was about 1.7 W.

This is the first power generator model by using TEMs to generate power from hydrothermal vent. Restricted by the heat flux and the area of TEMs, the power generation was very small, but it proved the feasibility of the research proposal and it is possible to generate much more power if the temperature of the discharging hot fluids is higher and surface area of generator is larger.

Chapter 4 The development of novel power generator based on numerical simulation

4.1 Concept of power generator prototype

Though verified by the feasibility experiment that the thermal energy can be utilized to generate power, the necessary power should be at least two orders of magnitude higher than the power generated at the feasibility experiment in order to charge an AUV or supply power to underwater station. To achieve this, high temperature differences on both sides of TEMs and large mounting surface area should be ensured. From these considerations, a power generator model is proposed as shown in Fig. 4.1. A conical structure with long pipe shape generator is capped on the orifice of hydrothermal vent, and then the hot fluids will be fed into the straight generator directly. Through TEMs mounted along the generator, the electrical power can be produced by utilizing the temperature differences between the hot fluids inside and cold seawater outside.

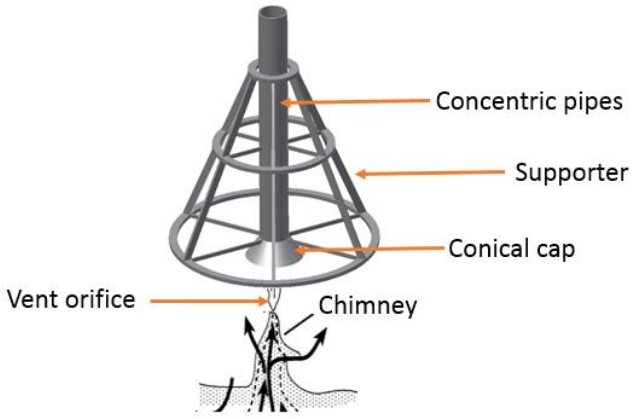

Fig. 4.1 A conceptual model of power generator

For having good pressure resistance in deep sea, an obvious shape of generator can be thought out is a concentric double-pipe structure. TEMs and the related circuits shall be installed in the annular space between two pipes as shown in Fig. 4.2. Meanwhile, the TEMs should contact with double pipes tightly to ensure good heat transfer and electric circuits need to be secured from the high pressure. Since TEM

is commonly fabricated as cuboid shape, the interfaces of the double-pipe must be flat and parallel, and the width of the annular space should be same as the thickness of TEM in order to contact with TEM well.

However, it is difficult to assemble this type of structure. The fabrication of each cylindrical pipe is not particularly difficult, but to keep the width of the annulus the same as the thickness of TEM all around is impossible. If the gap between the two cylindrical pipes is wider than the thickness of TEM, the heat transfer is compromised, and if the gap is narrower, TEMs cannot be mounted in properly.

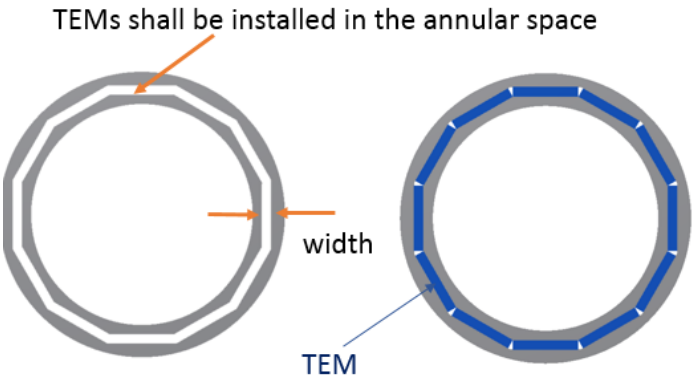

Fig. 4.2 Cross sectional view of concentric double-pipe generator

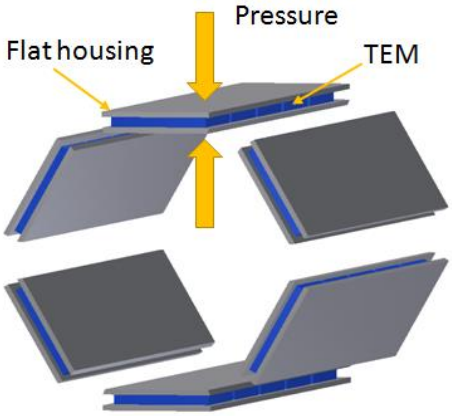

Fig. 4.3 Exploded view of polygonal generator

In order to overcome this, a novel polygonal generator is proposed as shown in Fig. 4.3. The polygonal generator performs good flexibility in mechanical design, which can facilitate to mount TEMs and related circuits. Thin flat housing is weak against pressure, but when it is supported appropriately, it can withstand against the pressure. TEM has a very strong capability to resist the 1-directional compression, and the thin flat housing supported by TEM can withstand against the pressure. At the same time, the pressure pushes the housing to contact with TEMs tightly, which brings good heat transfer between the TEM and housing. The polygonal shape generator can be easily assembled by several sets of these plate housings, and can capture the thermal energy ejected from hydrothermal vent as well.

4.2 Selection of an alternative TEM

In chapter 2, the performance of TEM Hi-Z14 in various thermal and pressure conditions were tested. The results show the generated power is in proportion to the temperature differences on both sides of TEM. It is also found the higher pressure

brings better performance, which can be explained as the higher pressure compresses the TEMs with copper plate tighter, the fewer gaps existed between them produces good thermal heat transfer.

As the internal resistance of Hi-Z14 is 0.28 Ω, when it was connected into a circuit, high output current with low voltage passing through the underwater cable caused power loss due to electrical resistance. So it becomes necessary to find a TEM that not only has high performance, but also high output voltage. An alternative TEM Tellurex G2560375 [51] is chosen, its specification is listed in Table 4.1 and shown in Fig. 4.4.

Table 4.1 The specification of Tellurex G2560375 vs. Hi-Z 14

Properties	Tellurex G2560375	Hi-Z 14
Dimensions (cm)	5.6(L)×5.6(W)×0.5(H)	6.3(L)×6.3(W)×0.5(H)
Thermal conductivity (W/m-k)	2.4	2.4
Internal resistance (Ω)	1.07	0.28
Matched load output voltage (V)	1.1 (*Th*=100°C *Tc*=35°C)	0.71 (*Th*=100°C *Tc*=35°C)
Matched load output power (W)	2.3	2.6

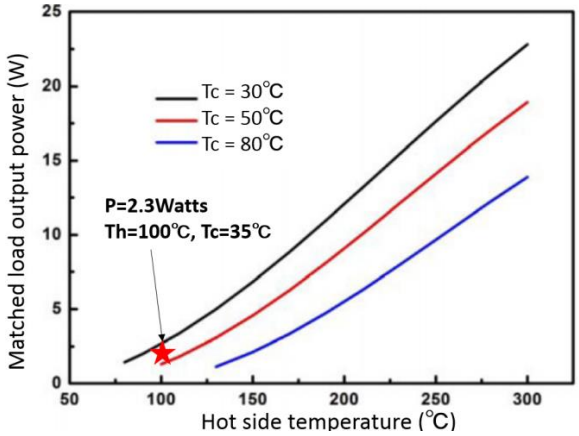

Fig. 4.4 The power generation performance of Tellurex G2560375 given by catalogue

In order to compare the performance of two TEMs, the test conditions for Tellurex G2560375 were set the same as Hi-Z 14 by using the system developed in chapter 2. Fig. 4.5 and Fig. 4.6 show the output voltage and power of Tellurex G2560375 in various thermal conditions under 0.1 MPa. When the temperature difference increased from 40°C to 65°C, the output power increased from 0.4 W to 1.04 W, which is about 1.3 times than Hi-Z 14 in the same conditions. And these values are

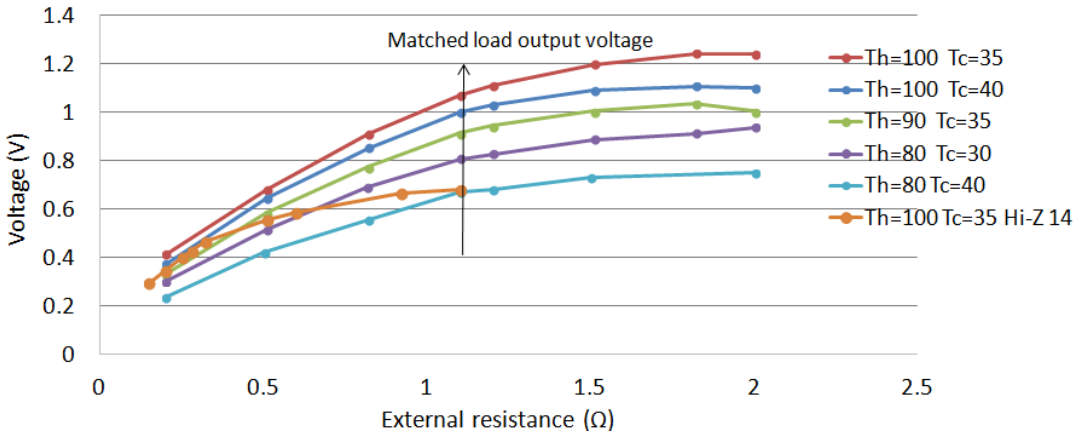

Fig. 4.5 External resistance vs. output voltage under 0.1 MPa

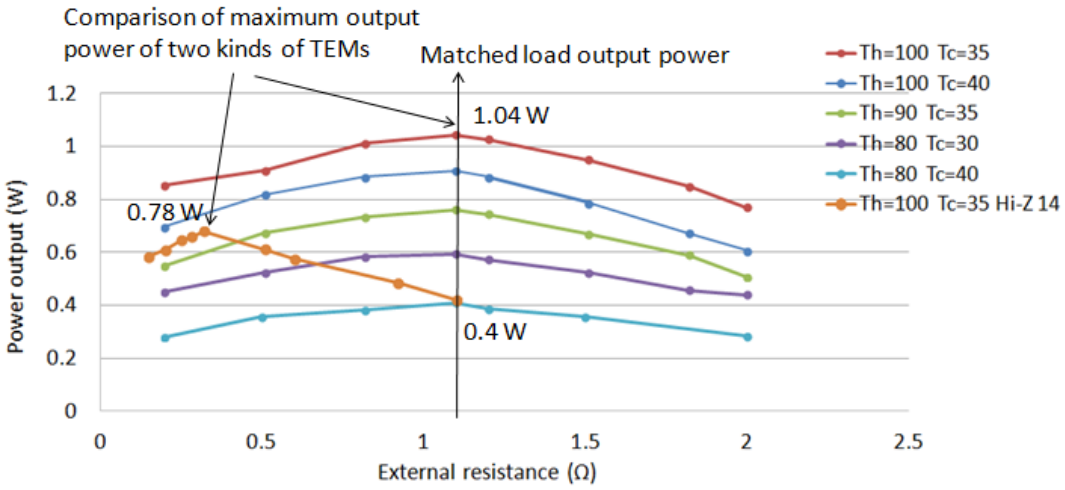

Fig. 4.6 External resistance vs. output power under 0.1 MPa

about half of the values showed in manufacture's datasheet (e.g. when Th = 100°C, Tc = 35°C, the maximum output power was measured as 1.03 W, but shown as 2.3 W in datasheet). It can also be noticed the output voltage at the matched load is higher than 0.5 V. As the minimum input limit of general DC-DC converter is 0.5 V, so this makes it possible to use a commercial DC-DC converter to boost the output voltage of TEM G2560375 into an applicable level.

In chapter 2, the power generation performance of TEM Hi-Z14 has been tested under the pressure up to 3 MPa. However, as 80% of the hydrothermal vents are distributed at the depth of 2000 m to 2500 m, power generation performance of Tellurex G2560375 has been tested up to 20 MPa in order to verify its applicability to most hydrothermal vent sites.

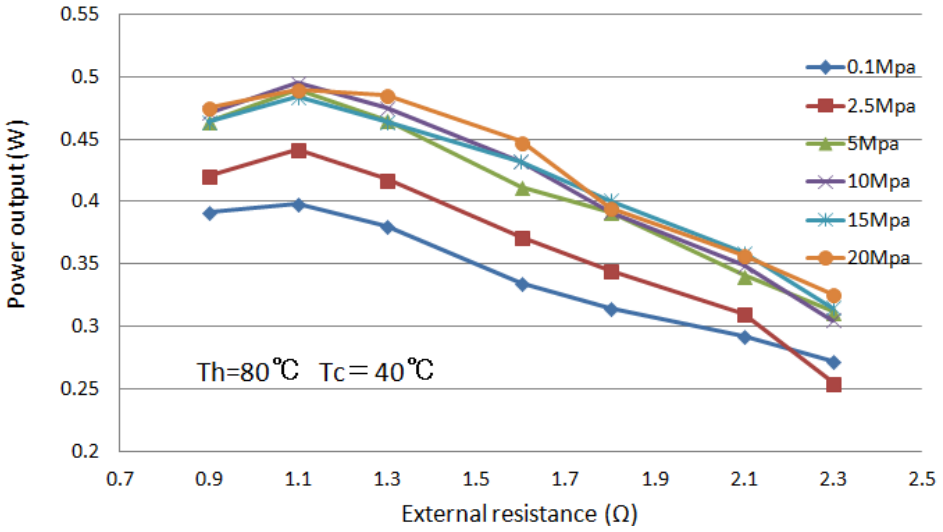

Fig. 4.7 External resistance vs. output power in various pressure conditions

From Fig. 4.7, it can be observed that the output power increased as more pressure was loaded until to 5 MPa. This can be explained as the same reason that the load pressure minimized gaps between TEM and copper plates, thus the thermal resistance between TEM and the device was reduced. From 5 MPa to 20 MPa, the power output was nearly irrespective of pressure. This can be conceived that no gap existed between TEM and contact interfaces, and it has already achieved the best heat transfer conditions at 5MPa. In the published literature, it has been validated that the physical property of TEM won't change even to 70 MPa [31], so it can be suggested that TEM can be used to produce power at most hydrothermal vents, of which the depth ranges from 2000 m to 2500 m.

All of the following discussion will be based on the specifications of Tellurex G2560375.

4.3 Numerical method and turbulence modeling

The heat transfer process in generator is analyzed by means of numerical simulation method. The flow and heat transfer process of fluid with time dependency is given as follows:

The conservation of mass equation is

$$\frac{\partial \rho}{\partial t} + \nabla(\rho \vec{V}) = 0 \tag{4.1}$$

And the conservation of momentum equation is

$$\rho(\frac{\partial \vec{V}}{\partial t} + \vec{V} \cdot \nabla \vec{V}) = -\nabla p + \mu \nabla^2 \vec{V} + \vec{f} \tag{4.2}$$

The five terms represent unsteady acceleration, convective acceleration, pressure gradient, viscosity and other body forces, such as gravity or centrifugal force, respectively. And ρ, $\vec{V}$, μ and ∇ are the density, is the velocity, dynamic viscosity and del operator, respectively [52].

Conservation of energy for fluid

$$\nabla(\rho C_p T_f) \cdot \vec{V} = \nabla(k_f \nabla T_f) \tag{4.3}$$

Conservation of energy for solid

$$\nabla(k_s \nabla T_s) = 0 \tag{4.4}$$

where C_p is the thermal capacity, T_f, T_s are the temperature of fluid and solid, k_f and k_s are the effective thermal conductivity of fluid and solid, respectively.

The governing equations on mass, momentum and energy were solved by commercial program Fluent, which is a CFD computer code developed and marked by Ansys Inc. The codes provide mesh flexibility by unstructured meshes. All the codes solve the discretized equations in a segregated manner, with the SIMPLE (Semi-Implicit Method for Pressure-Linked Equations) algorithm, or its "consistent" variant, SIMPLEC [53], and they are used to achieve the pressure-velocity coupling for stability [54]. Turbulence closures range from one-equation turbulence model up to RSTM (Reynolds Stress Transport Modeling) [55].

For turbulence modeling, several models are available in Fluent, such as Spalart Allmaras, $k-\varepsilon$, $k-\omega$ and etc. Most of them are derived from the standard $k-\varepsilon$ model introduced by Launder and Spalding [56] with different treatments of wall region.

In $k-\varepsilon$ model, the high Reynolds number version is obtained by neglecting all the terms containing the kinematic viscosity. However, in the proximity of solid walls, viscous effects become important and this assumption no long holds. Several modifications have been proposed: in the two layer formulation [57], a simpler model is used close to the wall and then the eddy viscosity is patched at a certain distance from the wall. In the damping functions approach [58] algebraic functions are introduced to correct the behavior of turbulent quantities close to the wall. Several different choices are available in the open literature [54]. In this work, the model introduced by Launder and Sharma [59] was used, which is available in all the codes

and can be expressed by two questions as follows:

For turbulent kinematic energy k

$$\frac{\partial(\rho k)}{\partial t}+\frac{\partial(\rho \overline{V}_i k)}{\partial x_i}=\frac{\partial}{\partial x_j}[(\mu+\frac{\mu_t}{\sigma_k})\frac{\partial \varepsilon}{\partial x_j}]+P_k-\rho\varepsilon \tag{4.5}$$

For dissipation ε

$$\frac{\partial(\rho \varepsilon)}{\partial t}+\frac{\partial(\rho \overline{V}_i \varepsilon)}{\partial x_i}=\frac{\partial}{\partial x_j}[(\mu+\frac{\mu_t}{\sigma_\varepsilon})\frac{\partial \varepsilon}{\partial x_j}]+C_{1\varepsilon}P_k\frac{\varepsilon}{k}-C_{2\varepsilon}\rho\frac{\varepsilon^2}{k} \tag{4.6}$$

where μ_t is the turbulent viscosity, P_k is the production of k which can be expressed as, $P_k=-\rho\overline{u_i u_j}\frac{\partial u_j}{\partial x_i}$, σ_k, $C_{1\varepsilon}$, $C_{2\varepsilon}$, σ_ε are model constants.

To simplify the calculation, the flow is assumed as steady and incompressible. The initial conditions set in FLUENT are based on data measured at Yamanaka vent located in Kagoshima Bay, where the hot fluids flow into the generator around 100°C with the velocity of 0.4 m/s, and the temperature of the surrounding seawater is 10°C. The housing of the prototype is assumed to be made of A6063 and the thermoelectric materials is fully filled up in the space.

4.4 Simulation in various conditions

Ideally, if the thermoelectric materials can be constructed flexibly and in an appropriate thickness, it is possible to fill them in the annular space of concentric-double pipe properly. In order to compare the heat transfer between the concentric double-pipe configuration which has good pressure resistance and polygonal shape which is easy to mount TEMs, the heat transfer of two prototypes was simulated and discussed in different geometrical conditions. For convenience, hexagonal shape generator was used as the representative of polygonal shape generator in the simulation, as shown in Fig. 4.8.

(1) Under the condition of same sectional area

The inner diameter of concentric pipe is supposed to be 12 cm and inscribed circle diameter of hexagonal prototype is 11.4 cm, so the inlet mass flux and inlet heat flux are same for both prototypes. The length of the generator is temporally determined as 50 cm.

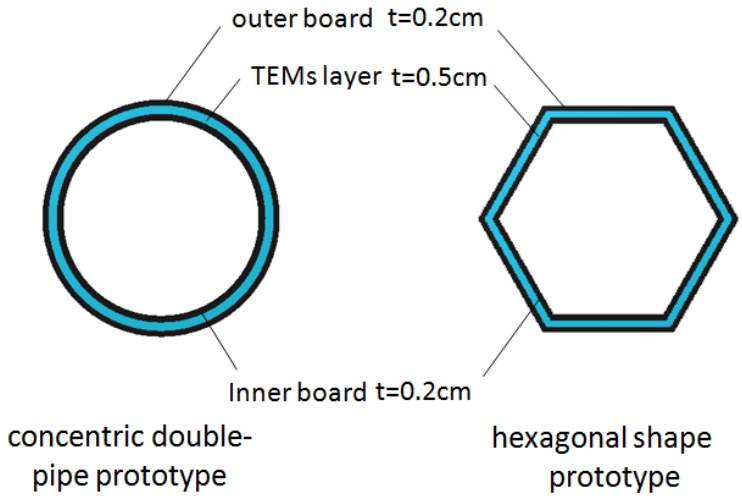

Fig. 4.8 The cross sectional view of two types prototypes

Fig. 4.9 shows the cross sectional view of temperature distribution and velocity profile of the concentric double-pipe prototype. From the temperature gradient contour showed in the left, it can be observed that near the inside wall region, the temperature is nearly the same as the hot fluids, but near the outside wall region, the temperature is obviously higher than the cold seawater because the heat cannot be dissipated into surrounding cold seawater very quickly. The temperature difference on both sides of TEM is about 40°C. It also can be found the temperature of the hot fluids keeps high in the pipe but drops significantly once they flow out of the pipe. The same trend can be found in the velocity profile. Therefore, it is very critical to capture the hot water into generator once discharging from hydrothermal vent.

Fig. 4.10 shows the cross sectional view of the temperature distribution of hexagonal prototype. It can be found the temperature keeps high inside generator and the thermal distribution is similar to that in concentric double-pipe prototype. Fig. 4.11 shows the temperature distribution on the surface of hot side of TEM layer. The temperature in the corner part is lower than that in the middle area, because the relatively lower velocity in the corner part results in the thicker thermal boundary layer there. But this area is not so large, so it can be considered the temperature distribution on the whole TEMs is nearly uniform.

From Fig. 4.12, it can be found that the temperatures on TEMs drop slowly along the flow direction for both generator prototypes. This drop comes from the heat dissipation through TEMs layer and housings continuously. At the same time, because the thermal conductivity of TEM is only 2.4 W/m-K, it prevents the heat

from dissipating rapidly. This also implies that though the temperature drops very quickly as soon as the hot fluids flow out of the generator, inside the generator, sufficient temperature differences on both sides of TEMs can be maintained in long length.

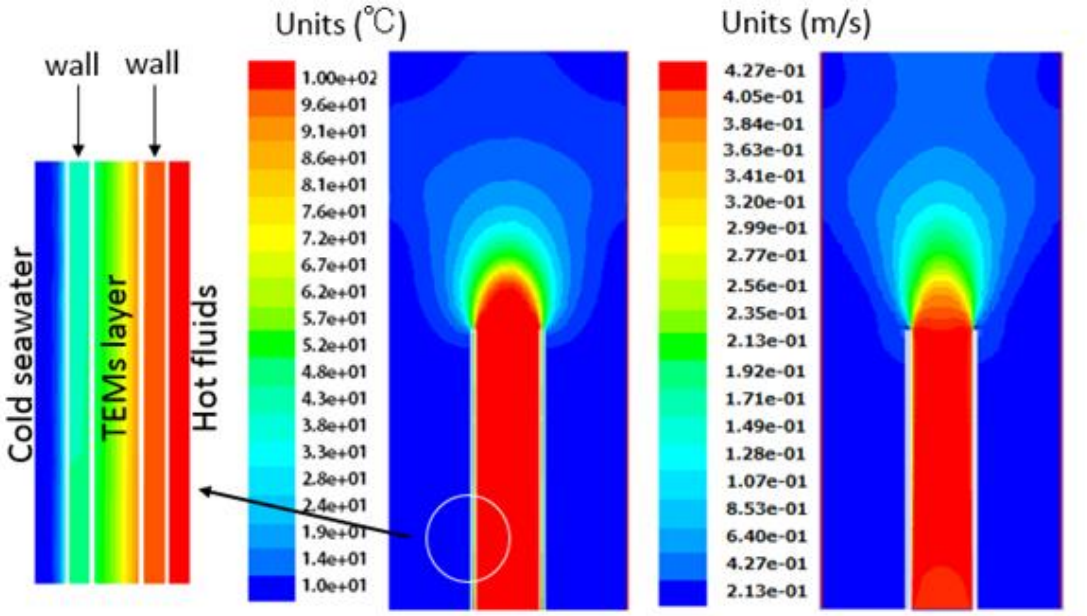

Fig. 4.9 Cross sectional view of temperature distribution and velocity profile of concentric double pipes prototype

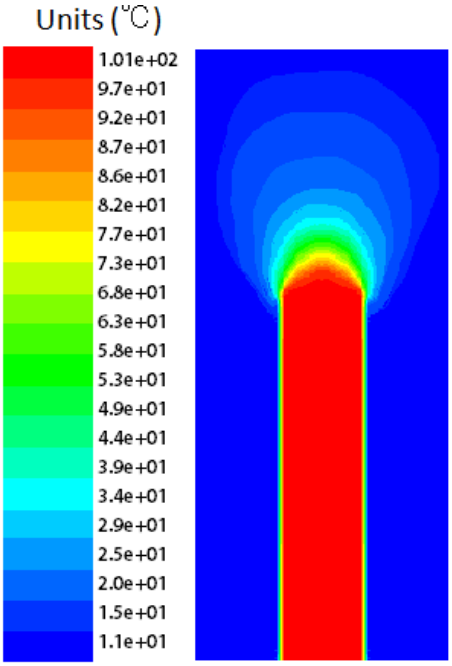

Fig. 4.10 Cross sectional view of temperature distribution of hexagonal prototype

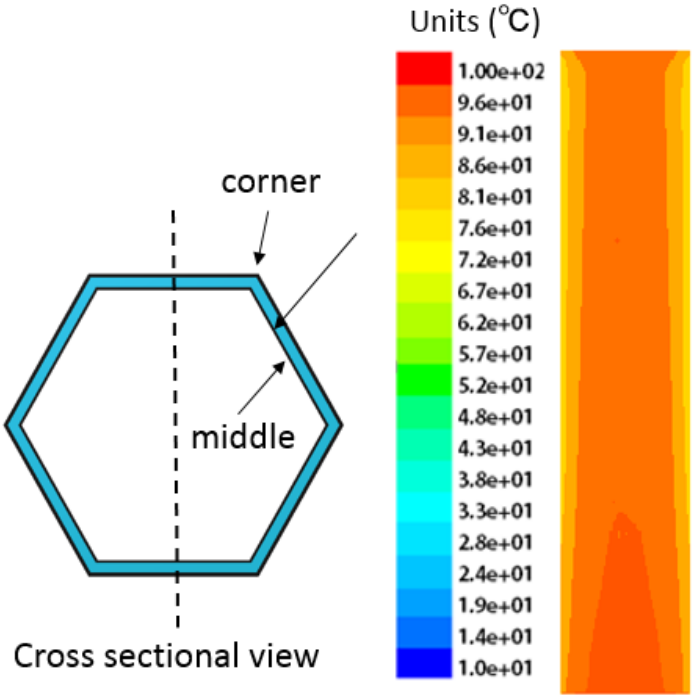

Fig. 4.11 Temperature distribution on inner TEM layer of hexagonal prototype

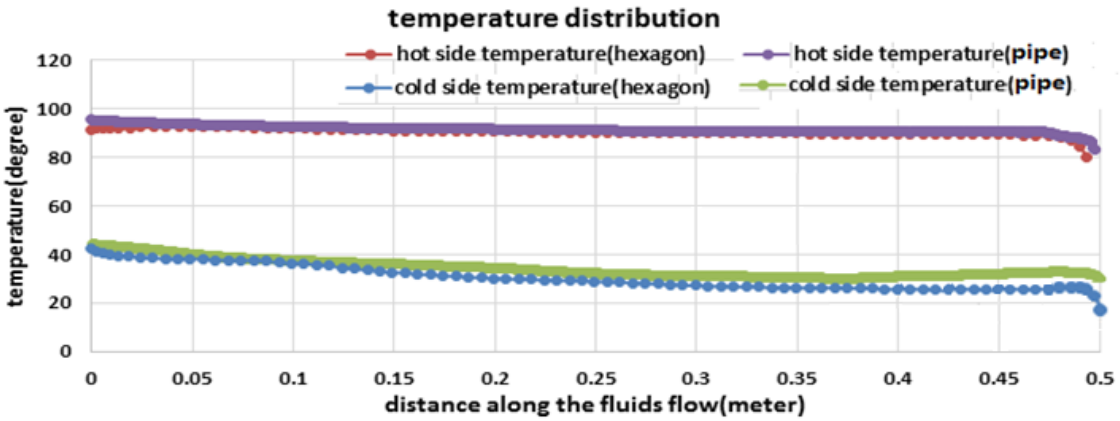

Fig. 4.12 Temperature distribution on TEMs along the flow direction

When both prototypes have same sectional area, the hexagonal prototype has larger heat transfer area. Fig. 4.12 shows larger temperature difference on TEM layer is also produced by hexagonal prototype, allowing it to generate much more power than concentric double-pipe prototype.

(2) Under the condition of same heat transfer area

In this case, the heat transfer areas of both prototypes are supposed to be the same, and the dimension of the cross sectional area of hexagonal prototype is kept the same as the former case. Under this condition, the dimension of the cross sectional area of concentric double-pipe prototype is larger than that of hexagonal prototype, as shown in Fig. 4.13.

For concentric double-pipe prototype, the enlarged cross sectional area results in a decrease in velocity along the flow direction. Because of this, the dissipation of the

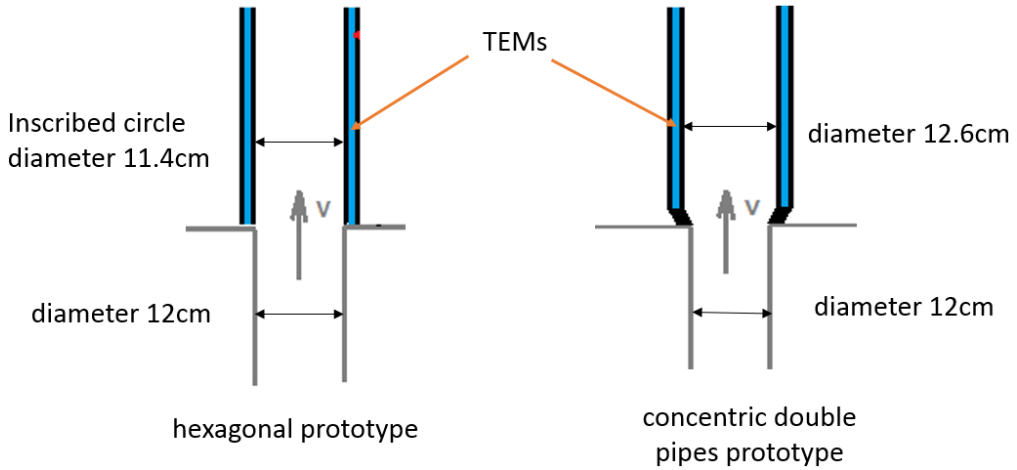

Fig. 4.13 Simulation models of both prototypes

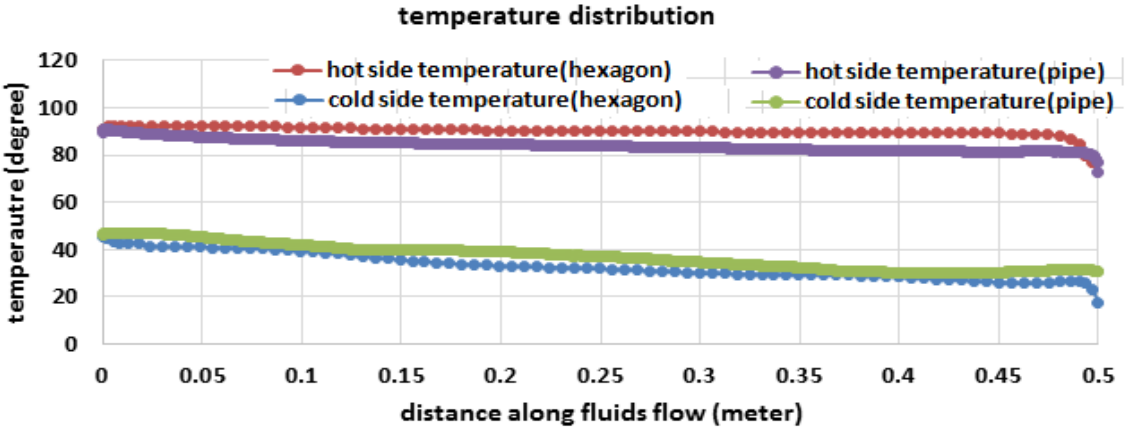

Fig. 4.14 Temperature distribution on TEMs along the flow direction

thermal energy into surrounding water becomes much easier, and the temperature difference on both sides of TEMs becomes smaller than that of hexagonal prototype as shown in Fig. 4.14. Therefore, under the condition of same heat transfer area, much more power can be produced by hexagonal prototype.

(3) System efficiency

The efficiency η_2 of the power converted from inlet thermal energy can be defined as the product of the generator efficiency η_1 and TEM conversion efficiency η. The efficiency of the generator η_1 is defined as the ratio of the heat passing through the TEM layer and inlet heat flux. And the efficiency of TEM conversion η is defined in chapter 2 that is the ratio of power generation and thermal energy pass through the generator. The total efficiency η_2 can be expressed as follows:

$$\eta_2 = \frac{heat\ pass\ through\ the\ generator}{inlet\ heat\ flux} * \frac{power\ generation}{heat\ pass\ through\ the\ generator} \quad (4.7)$$

The efficiency of generator under both cased are shown in Table 4.2.

Here, Q_i is the inlet heat flux rate from hydrothermal vent, Q_u is the heat conducts

Table 4.2 Heat transfer and the efficiency of generator

	Inlet heat flux Q_i	Heat flux pass through the generator Q_u (W)	η_1 (%)
Hexagon case(1)	1.71E6	5660	0.33
Concentric case(2)	1.71E6	5010	0.29
Concentric case(2)	1.71E6	4730	0.28

through the TEM layer, which can be calculated by the Fourier's law of conduction.

For hexagonal prototype, if the temperature distribution on the hot side of TEM layer is considered as uniform, Q_u can be defined as:

$$Q_u = \frac{CL\Delta T}{\delta_{in\_Al}/\lambda_{Al} + \delta_{TEM}/\lambda_{TEM} + \delta_{ou\_Al}/\lambda_{Al}} \tag{4.1}$$

where C and L are the perimeter and length of generator respectively; ΔT is the temperature difference on both sides of TEMs; δ_{in_Al}, δ_{TEM} and δ_{ou_Al} are the thickness of the inner aluminum wall, TEMs layer and outer aluminum wall respectively. For concentric double pipes prototype, it defines as:

$$Q_u = \frac{2\pi L\Delta T}{\ln(d_2/d_1)/\lambda_{Al} + \ln(d_3/d_2)/\lambda_{TEM} + \ln(d_4/d_3)/\lambda_{Al}} \tag{4.2}$$

where d_1 , d_2 , d_3 and d_4 are the diameters of inner aluminum pipe, inner TEMs layer, outer TEMs layer and outer aluminum pipe, respectively, as shown in Fig. 4.15.

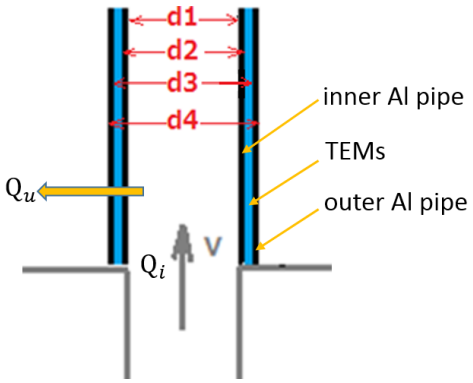

Fig. 4.15 The marking of parameters in the calculation

Because of the low thermal conductivity of TEMs layer, the efficiency of the generator is calculated less than 0.5%. But efficiency increases when the generator is elongated.

(4) Under the condition that hydrothermal vent is partially clogged by solidified particles

In most hydrothermal vent sites, hot fluids always contain many tiny metallic sulfide particles when they flow out of the vent. These minerals solidify when the hot fluids are cooled down, forming chimney-like structures. "Black smokers" are chimneys formed from deposits of iron sulfide, while the "white smokers" are chimneys form from deposits of barium, calcium, and silicon [60]. All of these minerals are very easy

to pile up, so the chimneys are growing up all the time. When the power generator is set on top of the hydrothermal vent, the limited space inside the generator will prevent the particles from dissipating into surrounding environment free and quickly, which will instead aggravate the growing of chimney. In this process, the hydrothermal vent possibly gets clogged, and the particles also maybe adhere to the inner surface of generator that will weaken the heat transfer through the wall. The simulations of these conditions were done using the concentric double-pipe prototype for simplifying the numerical calculation.

In the simulation, the original diameter of venting outlet orifice is set as 12 cm. Assuming the outlet velocity of hot fluids is 0.4m/s and keeps constant when the vent is partially clogged by solidified particles, as shown in Fig. 4.16.

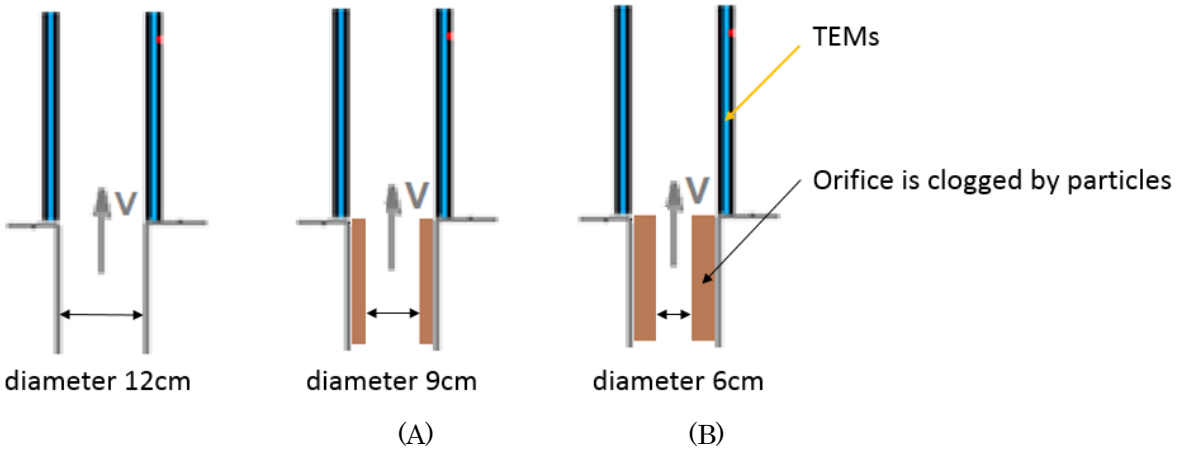

Fig. 4.16 Under the condition that the orifice of hydrothermal vent is partially clogged by solidified particles

Compared with Fig. 4.9 and Fig. 4.17, it can be found, the velocity drops rapidly along the flow direction when hot fluids flow out from the clogged orifice into an enlarged cross sectional area pipe. From Fig. 4.18, the temperature shows big fluctuations on the hot side of TEM layer at entrance part, and the average temperature difference on both sides of TEM along the flow direction is obviously lower than that of the non-clogged vent condition. The non-uniform temperature distributions in the bulk flow area and near wall region result in the difference in fluids' viscosity. Near the wall region, the relatively high viscosity caused by lower temperature and thick turbulent boundary layer caused by lower velocity, produce a thick thermal boundary layer, therefore results in poor heat transfer. It can also be observed the heat transfer will become poorer if the clogged layer is thicker.

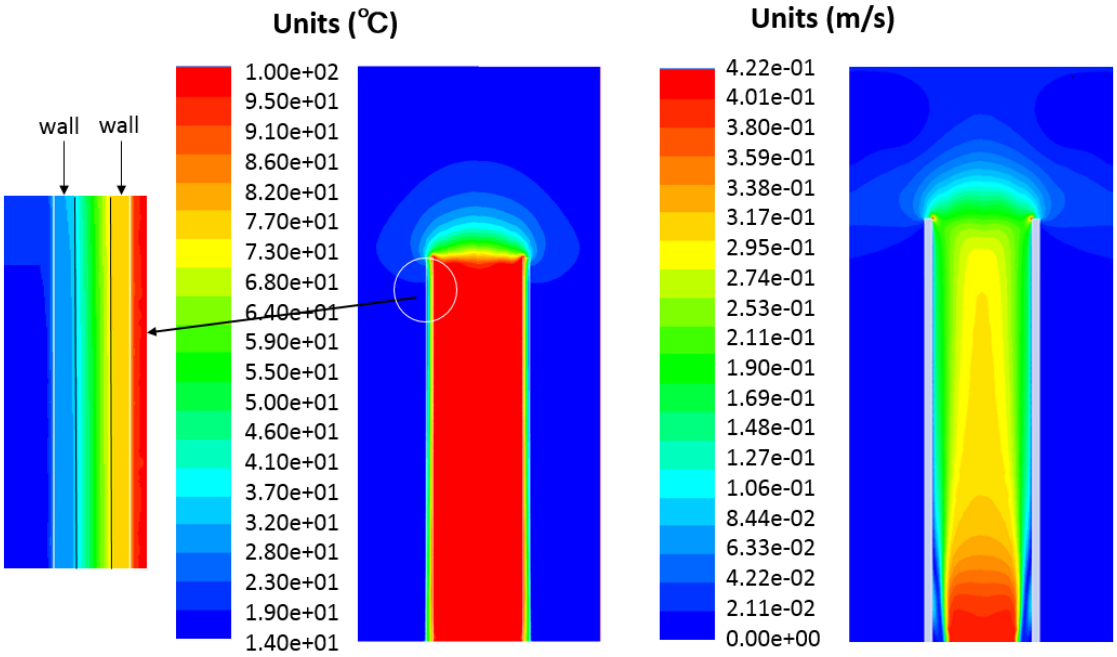

Fig. 4.17 The cross sectional view of temperature distribution and velocity profile if the orifice of hydrothermal vent is partially clogged by solidified particles

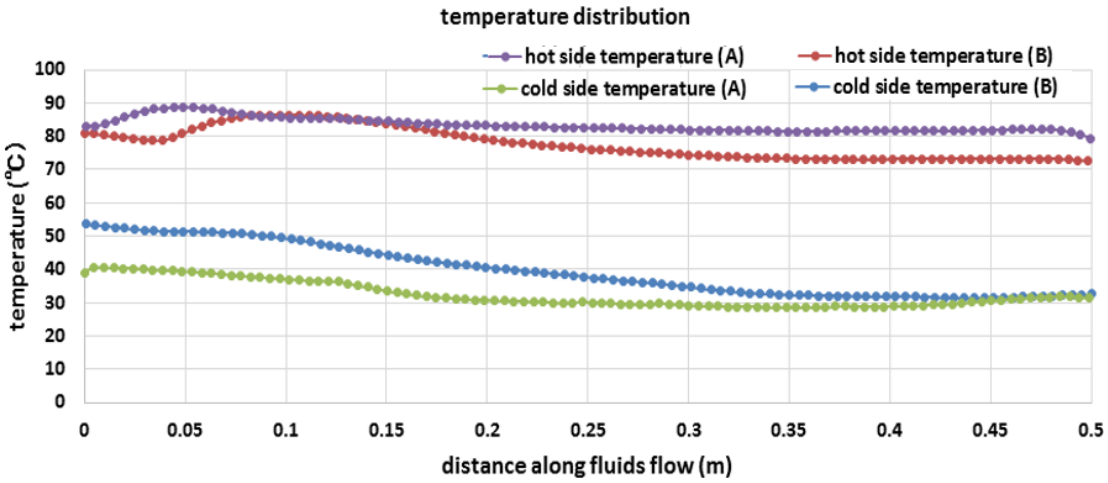

Fig. 4.18 The temperature distribution on both sides of TEMs when the vent orifice is partially clogged by solidified particles.

(5) Under the condition that inside surface of the generator is covered by solidified particles

In the simulation, the original diameter of venting outlet orifice is set as 12 cm. Assuming the outlet velocity of hot fluids is 0.4 m/s and keeps constant when the vent is partially clogged by solidified particles and inner surface of generator is covered by sulfide particles, as shown in Fig. 4.19.

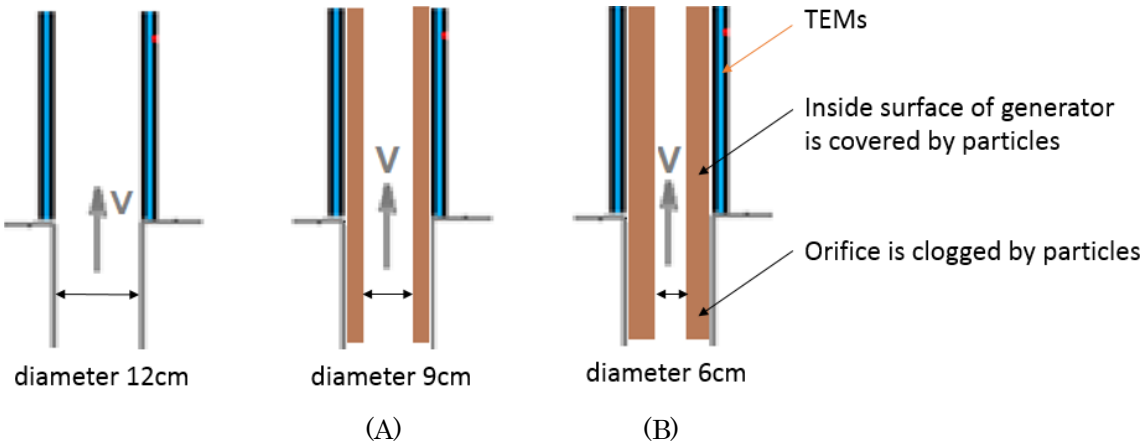

Fig. 4.19 Under the condition that inner surface of generator is covered by solidified particles

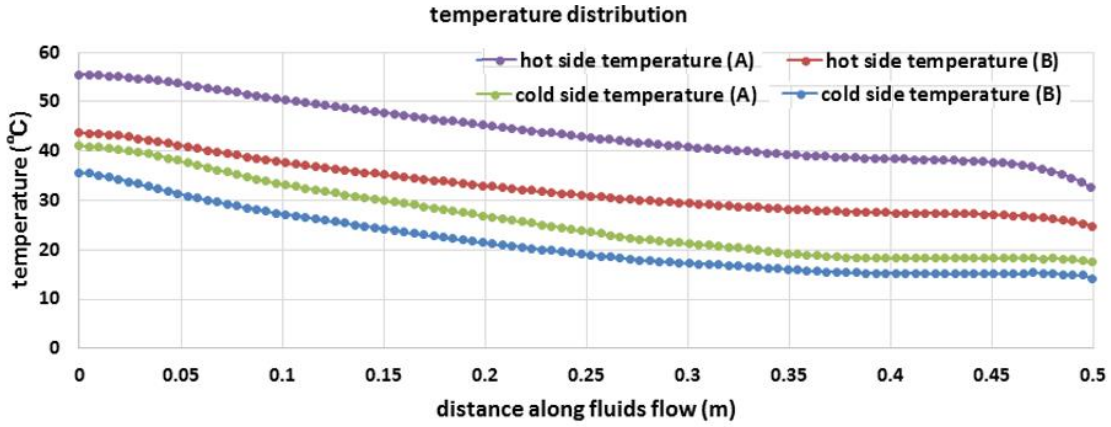

Fig. 4.20 The temperature distribution on both sides of TEMs when the inner surface of generator is covered solidified particles

It is possible that the inner surface of generator is covered by solidified particles over time. Because the thermal conductivity of sulfide is low, this will greatly influence the thermal transfer and power generation performance. As there is no accurate data about the thermal conductivity of solidified particles, the thermal conductivity is assumed to be the same as the TEM for convenience. Assuming the solidified particles that covered on the inner surface of generator are homogenous along the flow direction, the temperature distribution on both sides of TEMs are shown in Fig. 4.20.

Compared with Fig. 4.12, the average temperature difference on both sides of TEM is reduced apparently. When the inner surface is not covered by solidified particles, the temperature difference on both sides of TEM layer is 50°C. And it drops to 15°C and 10°C when the thickness of the covered particles is 3 cm and 6 cm respectively. It is obvious that the power generation performance is seriously influenced by the

covered solidified particles because of less inlet heat flux and low thermal conductivity of them. This should be considered in the practical design.

4.5 Summary

In this chapter, the structure of generators and the heat transfer process of them were calculated and discussed. Referring to the general pressure vessel, a concentric double-pipe prototype was proposed, while considering the flexibility of manufacture and convenience for mounting TEMs and related circuits, a hexagonal prototype was proposed later.

From feasibility experiment using Hi-Z14, it was found that power loss was caused when the low voltage with high current output pass through underwater cables, because of the relative small internal resistance. So it is necessary to find a new TEM which not only has high output power, but also high output voltage.

An alternative of TEM Tellurex G2560375 was chosen and tested. It is found its performance is better than Hi-Z 14 under the same test conditions, and the higher output voltage makes it possible to find a commercial converter to boost it into an applicable level. The pressure test was done up to 20 MPa which is the depth of most hydrothermal vents are exist, the good performance verified the applicability of applying TEM to the most hydrothermal vents.

The heat transfer process of both prototypes in various conditions were done and compared based on the CFD numerical calculation software Fluent. The conclusions from calculations can be summarized as follows:

(1) Under the ideal condition that the hydrothermal vent is not clogged and inner surface of generator is not covered by solidified particles, for both prototypes, the temperature distribution on both sides of TEMs drops slowly because of low thermal conductivity of TEM, of which is only 2.4 W/m-K.

(2) Under the condition of same sectional area, comparing with concentric double-pipe prototype, the hexagonal prototype exhibits better performance for its larger heat transfer area and larger temperature difference on both sides of TEMs.

Under the condition of same surface transfer area, if both prototypes still have the same inlet mass flow rate and same inlet heat flow rate, hexagonal prototype can produce much more power for its uniform thermal distribution along the fluids flow and higher temperature differences on both sides of TEMs.

(3) According to the calibration data of Tellurex TEM, the conversion efficiency is about 1.1%. Under the initial condition, about 124 W can be produced by hexagonal prototype per meter long. Though the efficiency of generator is very low, it increases as the length of the generator increases.

(4) Big temperature fluctuation at the entrance part of generator will be caused if the vent is partially clogged by metallic sulfide solidified particles. And it is also found that the thickness of the layer of clogged solidified particles influences the temperature distribution on inner surface of generator greatly.

(5) It is possible that the inner surface of generator will be covered by the solidified particles over time. The less inlet heat flux and low thermal conductivity of covered particles cause the poor heat transfer and low power generation. This should be considered in the practical design.

Chapter 5 The development of power generation system

Following the simulation on power generator described in chapter 4, a deep sea power generation system was designed, constructed and tested. This is the first experiment platform that can generate power by utilizing the thermal energy ejected from hydrothermal vent. In this chapter, the main part of the research is carried out to verify the research concept, theoretical developments, simulation models and access to the practical applications.

The power generation system is composed of the power generator and power management system. Comparing with the land use generator and according to the field conditions, a comprehensive study of power generator on stress intensity, corrosion resistance, heat transfer and flexibility in mechanical design was done. In power management solutions, MPPT control method was applied which can extract maximum power under any thermal conditions and without being influenced by the different loads. The TEMs connection topologies in large TEMs power generation systems were analyzed and discussed.

5.1 Field selection and system design concept

The hydrothermal vent sites that can be potentially used for electricity generation should have high discharging temperatures, and be convenient for installation. Regarding to natural hydrothermal vent sites, as stated in chapter 3, the porous and hollow structure make it difficult to set a power generator on top of it directly. Since 2004, several artificial vents have been drilled in Iheya-North field in Okinawa Trough for better understanding the core and diverse biosphere in subsea floor of hydrothermal fluids flow, as shown in Fig. 5.1 ~ Fig. 5.3. The hard structure of the artificial hydrothermal vents provides an available platform to set the power generator on top of it in long term. It also has been observed the superhot fluids were ejecting at a rate of ~1 m/s, and the average temperature was above 250°C [15]. The sufficient discharging thermal energy makes it possible to produce enough

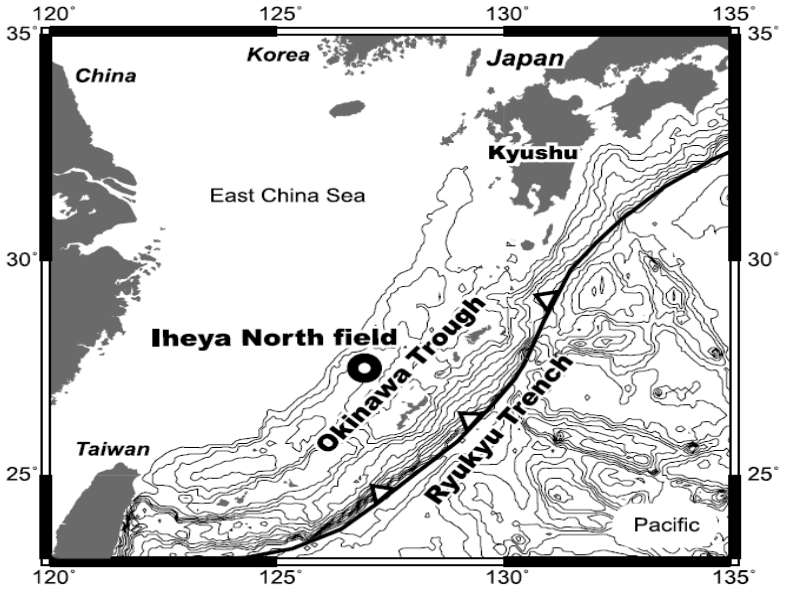

Fig. 5.1 Iheya-North Field in Okinawa Trough [15].

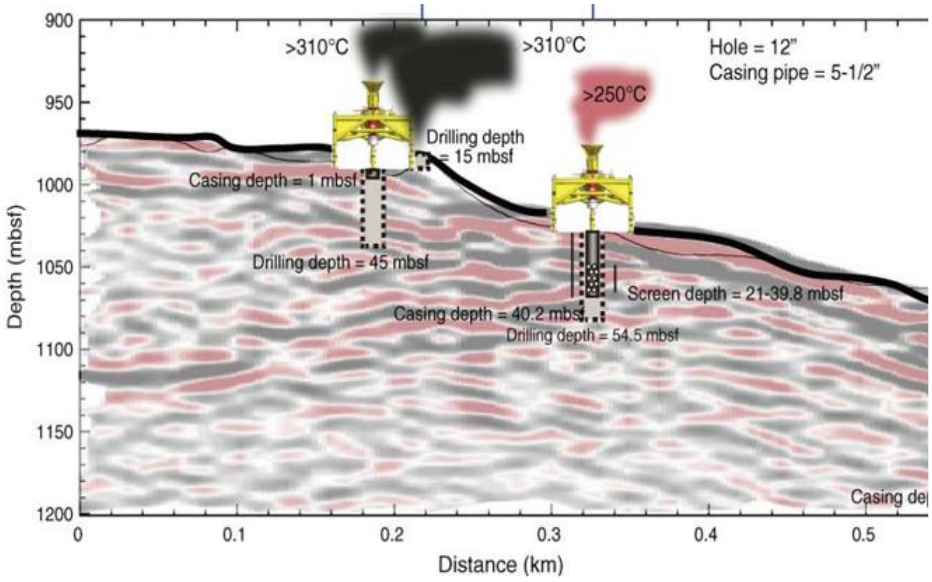

Fig. 5.2 Schematic illustration of artificial hydrothermal vent [61].

power to supply for AUV and seabed station. The design of the generator will be based on the parameters of the artificial hydrothermal vent. Despite various land use thermoelectric power generators have been developed, as the field environment is totally different from the land use conditions, some special approaches have to be taken to overcome these new challenges.

(1) Since the thermal energy dissipate into the surrounding sea water very quickly, a pressure resistive structure that can collect and utilize heat efficiently must be designed.

(2) Because of the low pH value of hydrothermal vent, the materials fabricated for generator is required to have good corrosion resistance and good thermal conduction simultaneously. The heat transfer influenced by materials must be studied, and the strength of the generator decided by material and structure should also be calculated.

(3) To ensure high performance of the power generator, high thermal convective coefficient between TEMs and the cooling side is expected. Because it is difficult to apply the same water circulation system as land use generator, the approaches to improve the heat transfer must be thought of.

(4) The output power of single TEM depends on the thermal conditions, thus the method that can extract maximum power under any thermal conditions should be considered. The non-uniform temperature distribution always causes power loss problem if the TEMs are connected simply in series or parallel, the efficient and reliable electric topology of TEMs must be established.

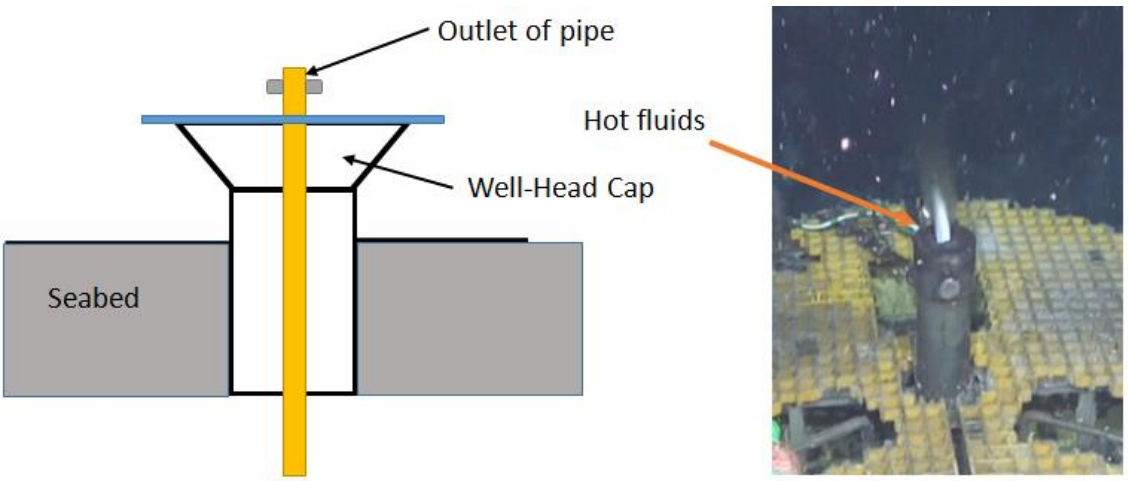

Fig. 5.3 The configuration of artificial hydrothermal vent.

5.2 Development of the power generator

5.2.1 Mechanical design

For the general pressure vessels used in deep sea, the cylindrical shape is commonly adopted for their good pressure resistance. However, as stated in chapter 4, it is difficult to keep the TEMs in good thermal contact with the surfaces of concentric double-pipe generator over large surface area. Testing results also show that some of the TEMs are in good contact while the others are not [44]. In deep sea, the large pressure will be imposed over the entire surface area of the generator that can

improve the contact effect to some extent, but the uneven TEMs arrangement may result in the bad O-ring seal effect and hidden water leaks.

Generally, the related electric circuits for improving the performance of the system are laid in pressure vessel rather than in generator for their irregular shape and temperature sensitivity. In order to solve the power loss problem caused by the resistance of underwater cables, it is better to boost the output voltage of TEMs into a high level before the output current conducts through underwater cables. But for cylindrical shape generator, it is difficult to place the circuit boards well in the annular space between the double pipes without crushing them.

Based on these, the new design goes from a cylindrical shape to a hexagonal shape which is composed of six sets of flat housings as shown in Fig. 5.4. Each set of housing is composed of inner board and outer case which are directly in contact with hot fluids and cold seawater, respectively. The flat housing design is much easier to mount TEMs and electrical circuits properly. The hexagonal shape could also supply sufficient area to mount TEMs without increasing the flow cross sectional area. For

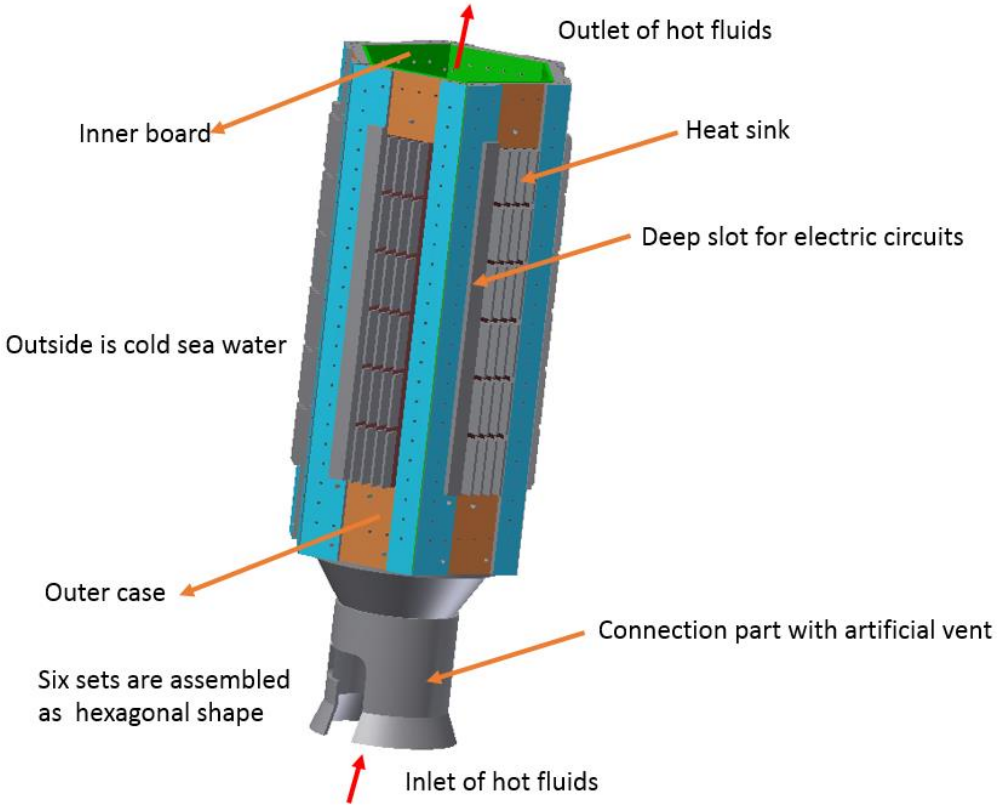

Fig. 5.4 The concept design of the hexagonal shape generator

one single plate, the expansion or contraction problem will occur when submerged in

hot water or cold water over time, this problem will be alleviated if six sets of housings are fixed as hexagonal shape, because each of housings restrains the deformation of its neighbor.

As shown in Fig. 5.5, the TEMs were mounted in the outer case and extended longitudinally. Two pairs of temperature sensors were pasted on both hot side and cold side of TEMs along the flow direction at inlet and outlet. The boards that are in

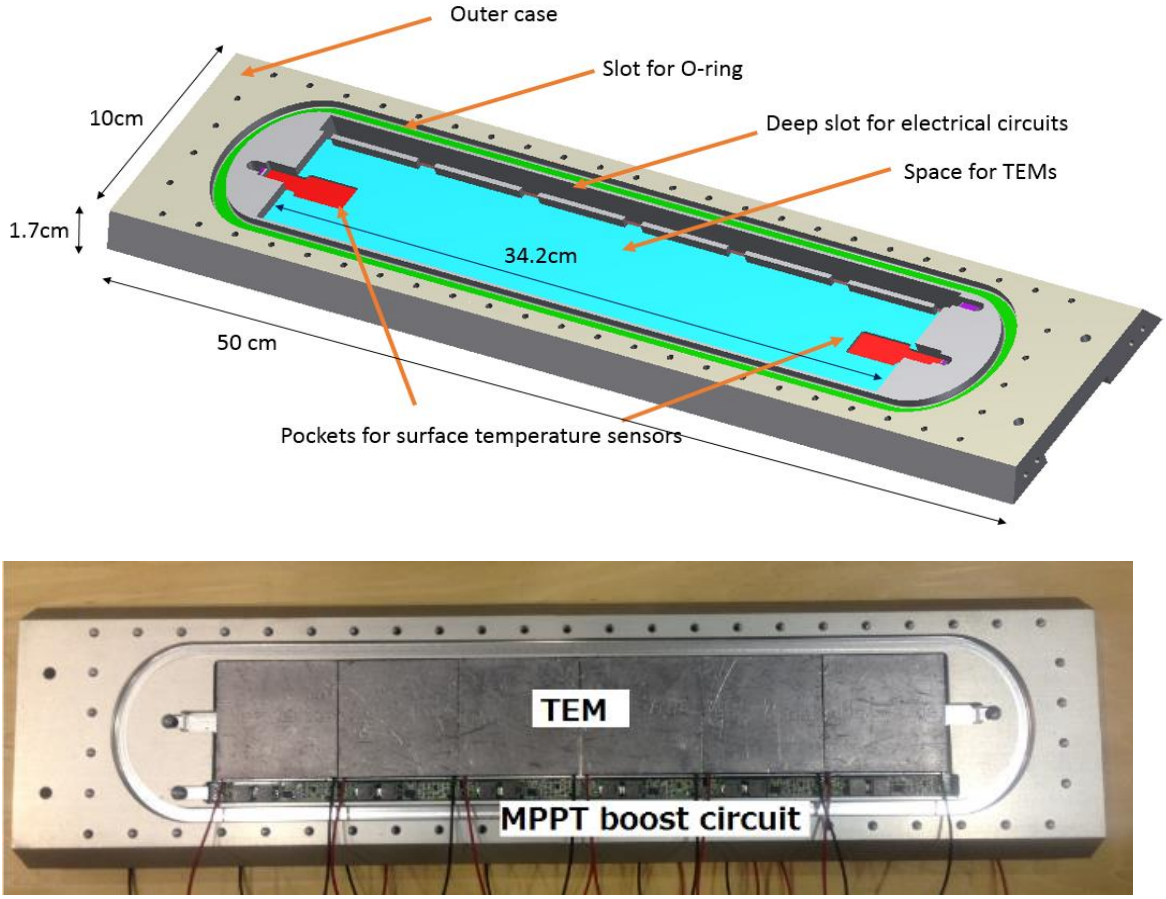

Fig. 5.5 The outer housing and the layout of components

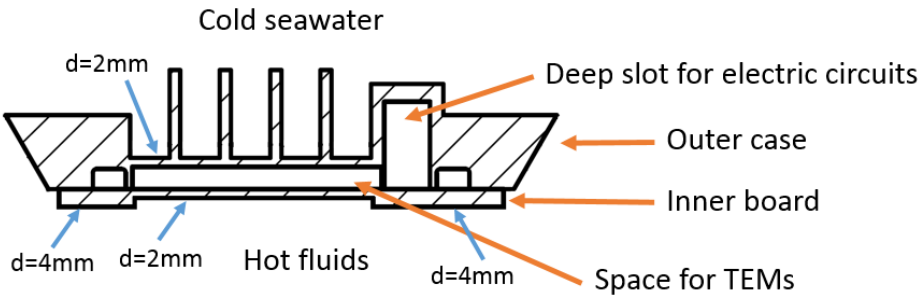

Fig. 5.6 Cross sectional view of one set of housing

contact with TEMs should be as thin as possible to obtain good heat transfer, but the electric circuits should be far away from hot fluids because most of the electric components are sensitive to temperature. A deep slot was designed to place the circuits in bottom of it, as shown in Fig. 5.6. The strength of the whole structure was designed to enable it can be used under the depth of artificial hydrothermal vent located in Iheya-North field where the field experiment would be carried out. On the other hand, the center parts of inner board and outer case that are in contact with TEMs should be thin enough to reduce thermal resistance. However, the plate will become flexible if it is too thin; the thickness of the center section was designed as 2 mm combining with the machining technology lastly. The pressure resistance of this irregular shape generator was verified in pressure tank up to 11 MPa. These dimensions will be used in the following discussions.

5.2.2 Materials selection

Besides the corrosion by seawater, the hot fluids discharged from hydrothermal vent always show extremely low pH, and at some places it is really acidic enough to corrode metals. The main compositions of hot fluids are sulfur, hydrogen sulfide and other kinds of minerals. As reported in some researches, in Okinawa Trough, the pH value of hot fluids ranges from 4.7~5.8 among the 20 hydrothermal vents [15]; in Manus basin, one vent named Desmos is characterized by very low pH which is lower than 2. Based on this, the materials fabricated for power generator should have three basic properties: good thermal conductivity, high corrosion resistance, and high strength in high temperature environment. From these considerations, three kinds of materials, ceramics, aluminum alloy and stainless steel have been compared.

Table 5.1 Physical properties of three kinds of materials

Physical property	C AIN[62]	A 6063	SUS 316
Thermal conductivity (W/m-K)	220	218	17
Thermal expansion coefficient (e-6/K)	4.6	23.4	15.9
Density (g/cm^3)	3.26	2.7	7.98
Tensile strength (MPa)	500	145	205
Young's modulus (GPa)	343	69	197
Corrosion resistance	Strong	Medium	Strong
Manufacture difficulty	Difficult	Easy	Medium

Ceramics, like AIN ceramic have been used in airspace engine for their high temperature strength. They are also possible to be used directly for deep sea power generator at hydrothermal vent sites for their high thermal conductivity and corrosion resistance.

Aluminum alloy A6063 is an alloy composed of aluminum, magnesium and silicon. It has strong corrosion resistance characteristics and performs well in the slight acid environment where pH ranges from 4~8, but will be corroded rapidly when pH is lower than 4, as shown in Fig. 5.7.

Tufram coating is a very convenient and effective way to improve corrosion resistance, which is one kind of anodic oxide coating methods. The surface of Tufram film has a large number of microspores and exhibits much greater corrosion resistance than conventional hard anodizing. Tufram treated surface areas show no effect when they are immersed in acid with a pH range of 3.5~4.0 and in an alkaline solution with a pH range of 8.5~9.0 for three months [63].

Stainless steel SUS 316 is widely used in applications requiring corrosion resistance and elevated temperature strength. It has corrosion resistance to marine environment and is useful for sulfuric acid environment. The corrosion speed is less than millimeters per year when they are immersed in high aggressive acid and alkaline environments. The experiments show the corrosion speed is around 0.002 mm and 0.05 mm per year in the sulfuric acid pH=1 and hydrochloric acid pH=1 environment, respectively [64].

Besides the consideration of corrsosion resistance of genrator, the simulation was made to understand the difference in heat transfer of three kinds of materials. The thickness of the housing is set to 2 mm as explained above. The dimension of the

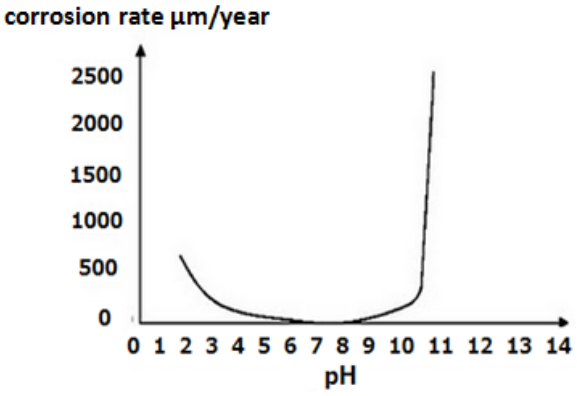

Fig. 5.7 Corrosion rate of A6063 with pH [65]

inlet orifice and inlet hot water temperatrue were initialied with the same values of the field conditons, where the diameter of artificial vent is 9 cm and the temperature of inlet hot fluids is 300°C.

From the simulation shown in Fig. 5.8 ~ Fig. 5.10, the temperature distributions on both sides of TEMs for three kinds of materials are nearly the same because of the low thermal conductivity of TEMs. As the TEMs are mounted in the middle part of outer housing, the temperature at the start and end parts of TEMs are mainly influenced by the thermal conductivity of housing fabricated materials.

When the housing are fabricated by ceramic AIN, aluminum alloy A6063 and stainless steel SUS 316, the corresponding average temperature differences on both sides of TEMs are 166°C, 164°C and 158°C, respectively. As the thickness of the inner and outer plates that are in contact with TEMs is only 0.2 cm, the difference in heat transfer of three kinds of materials is slight. It also can be observed, the higher the thermal conductivity of fabricated materials, the higher the temperature on hot side of TEM. This is because the high thermal conductivity contributes in increasing the thermal efficiency of the generator by decreasing the temperature drop between the hot fluids and TEMs surface.

From the simulation, it can be seen that the heat transfer through TEMs is not only decided by the thermal conductivity, but also the thickness of housing. In high pressure environment, to maintain enough strength intensity is much more important which is decided by the structure and its thickness. Though the ceramic AIN is the most efficient on heat transfer, the manufacturing difficulty makes it not very appropriate to be used for complex design. Regarding to the strength intensity and easiness of fabrication, aluminum alloy A6063 is the most suitable for power generator application here. To strengthen the corrosion resistance, the generator has been coated with Tufram to cope with acid environment of artificial hydrothermal vent area.

5.2.3 Optimization of the structure

The largest thermal resistance in the path between the fluids and generator is the thermal boundary layer. The convective heat transfer between the surfaces of generator and fluids is related to the heat transfer coefficient, and the wetted surface area. As shown in

$$R_f = \frac{1}{h \cdot A} \tag{5.1}$$

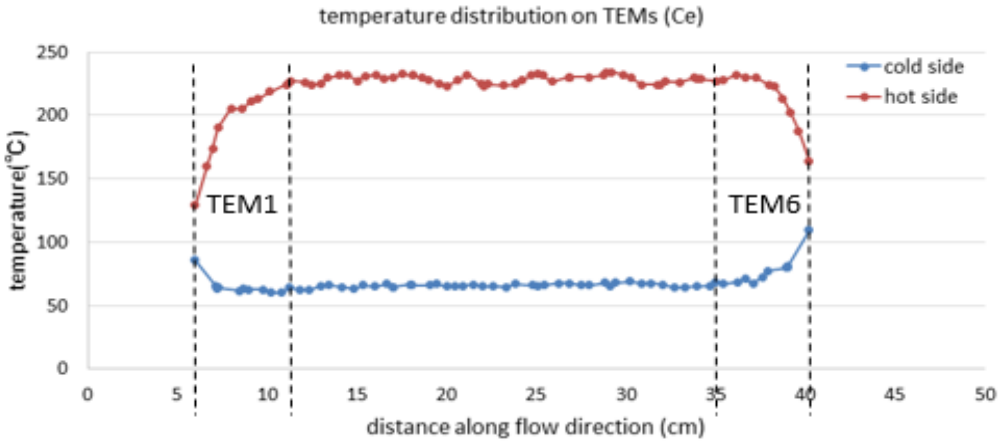

Fig. 5.8 The temperautre distribution on TEMs when the housing is made of ceramic AIN

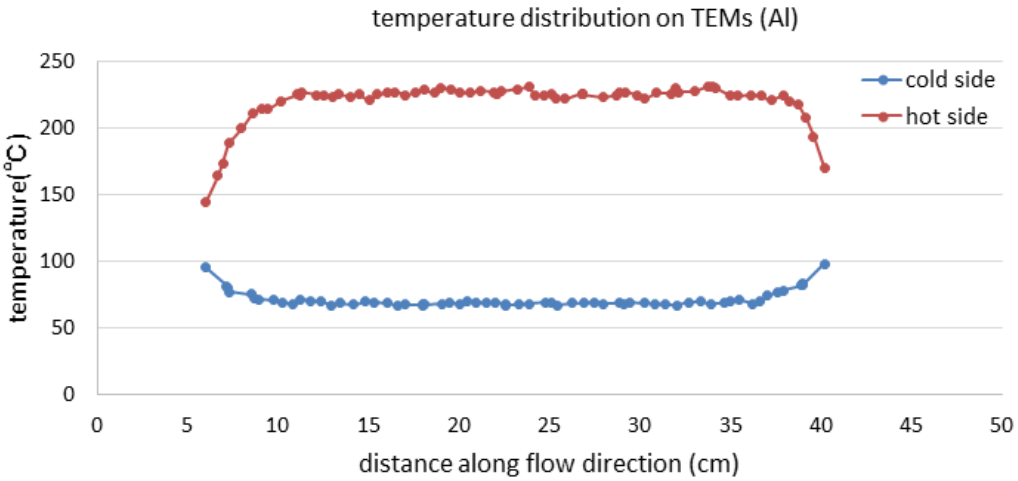

Fig. 5.9 The temperautre distribution on TEMs when the housing is made of A 6063

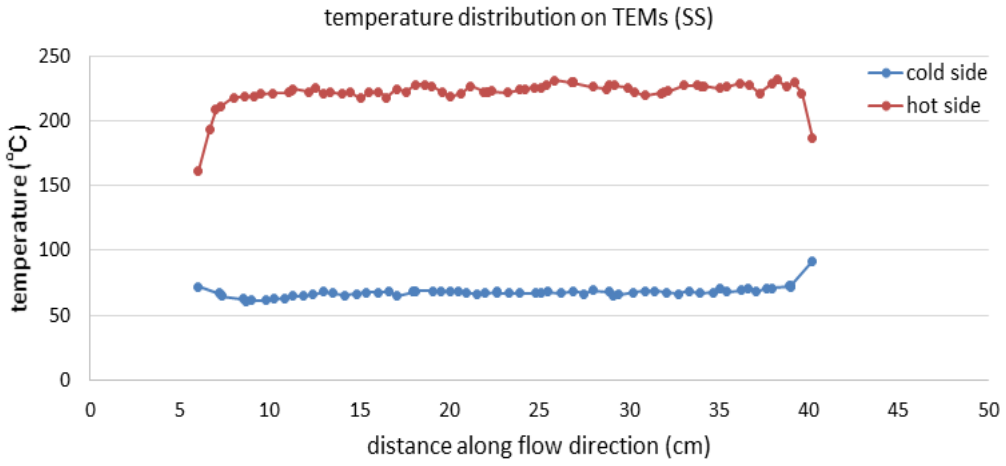

Fig. 5.10 The temperautre distribution on TEMs when the housing is made of SUS 316

where R_f is the thermal resistance, h is the heat transfer coefficient and A is the surface area. An increase in either the heat transfer coefficient or the surface area or both of these quantities can reduce thermal resistance and enhance the heat transfer effect.

Inside generator, sulfide and mineral particles will adhere to the inside surface over time with the outflow of hot fluids. Though the attached fins can extend surface area and get much more heat, they will also exacerbate the adhesive effect and the adhesions covered on the inner surface would result in poor heat transfer.

Outside generator, the conductive heat transfer coefficient could potentially enhanced with an increase in approach velocity, but in the deep sea, especially near the seabed area, the water currents are mainly caused by density differences and thus relatively small [66]. The natural heat convection between the slow flowing or the stagnant sea water and generator causes the poor heat transfer. Comparing with the land use generator of which the water circulation system is always employed to enhance heat transfer through forced heat convection, it is not practical to use a propeller to drive seawater to move to enhance the heat dissipation on the outside surface, because the high flow resistance results in the power consumed by motor far exceeding the output increment of TEMs.

Another alternative for reducing the thermal resistance can be achieved by increasing the outside surface area, which is typically achieved by attaching fins to the surface. Different from forced heat convection, heat will be accumulated in the space between the neighboring fins, and cannot dissipate effectively if the fin density is high. Combining with the machining technology, the fin array was designed with relatively wide interval.

The whole configuration of power generator is shown in Fig. 5.11. Six sets of housings were assembled to a hexagonal shape. In a small pressure vessel, which was fixed beneath the generator, six power output cables drawn from six housings respectively were united into one electric cable, then the power was transmitted to loads. To prevent damage of generator or electric cables during the installation process, the supporters were mounted on its outside surface.

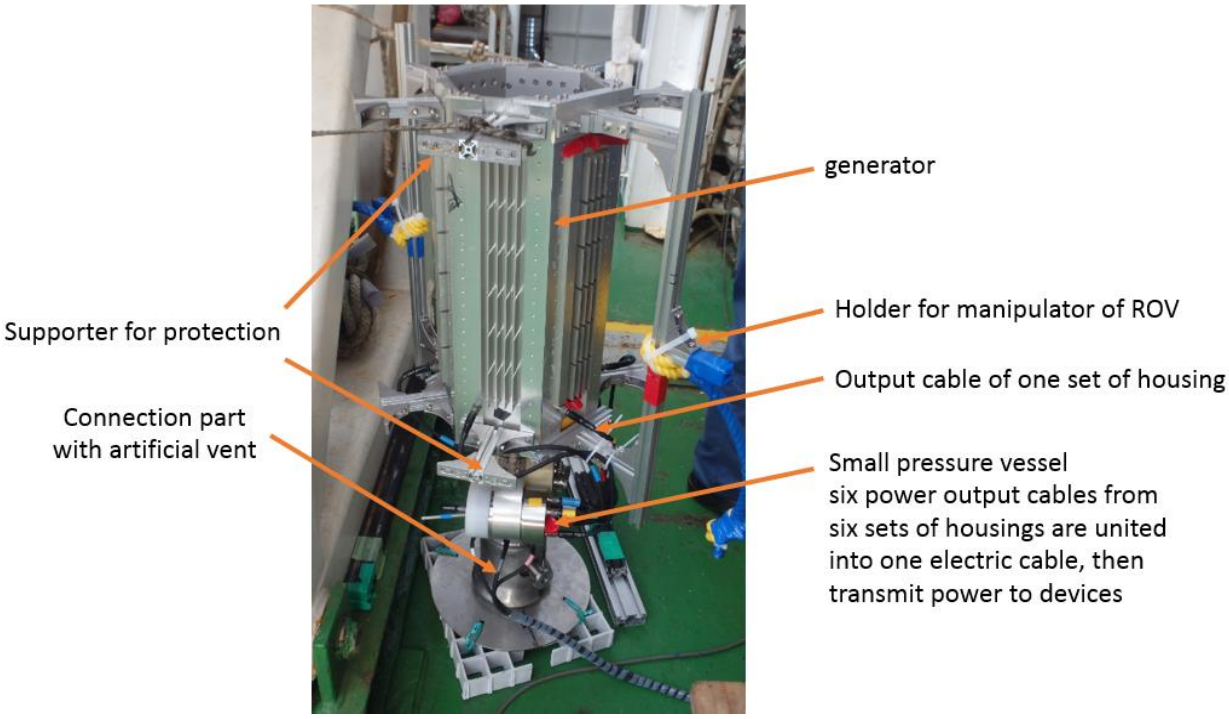

Fig. 5.11 The configuration of power generator

5.3 Electrical system design and analysis

5.3.1 Introduction of MPPT method

In general applications, restricted by the thermal conditions and the power generation ability of TEM itself, the temperature difference on both sides of it is always within 300°C, and the power generated by each TEM is within 5 W [39]. In practical applications, it is necessary to extract the maximum power from TEMs and boost the output voltage of TEMs into a required level simultaneously. The goal of this research is to supply power to robots, power storage systems, or to enable TEMs power generation system as a viable part of electrical grids system. In order to realize this, two problems have to be solved:

(1) To extract the maximum output power from TEM

The output power of single TEM is decided by temperature difference on both sides of it. And the maximum output power can only be obtained when the external resistance is equal to the internal resistance of TEM. Actually, this is not feasible that the generated power should be applicable to various appliances.

In order to make sure the maximum output power can be extracted under any thermal conditions and can supply to various loads, maximum power point tracking

(MPPT) algorithm is employed here to reduce the potential mismatch power loss.

(2) To avoid power loss when many TEMs are connected in a grid system.

Because the output of single TEM is relatively small, many TEMs are generally connected in series to achieve required voltage. Ideally, when TEMs are wired in series, the output voltage of the string is the sum of that of each module, and the current will remain that of a single module. But in large power generator systems, it is possible that the temperature distributions on both sides of all TEMs are not identical, and thus the output powers of all TEMs are not same. When the dissimilar modules are wired in series, voltage will be additive. However, the current will be just above the lowest current in the string, and thus results in the power loss. Therefore, it is necessary to analyze the connection topology of TEMs combined with MPPT method in large power generation system.

MPPT is an electronic form of tracking that utilizes algorithms and control circuits to search for the maximum energy point, and thus allow a converter to harvest the maximum power available from a TEM. There are two characters that are different from conventional PWM voltage boost converter.

Firstly, through the converter embedded with MPPT, the voltage and current generated by TEM will be monitored, and the maximum power point will be calculated and tracked all the time. Secondly, MPPT controller can convert the maximum power point (MPP) from a point into a wide range, of which the maximum and minimum limits are decided by the topologies of converter itself. If the output voltage of MPPT converter is higher than the working voltage of load, when it is connected with load, the output voltage of MPPT converter will drop to the load's voltage, and the excessive voltage can be converted into output current. This can guarantee the maximum power to be supplied to various loads as long as their operating voltage is in the range of MPPT converter. The working principle of MPPT is explained in Fig. 5.12.

MPPT is first developed to work with the photovoltaic applications, and it can be realized by simple microcontrollers. Since TEM and photovoltaic bear similarities in voltage-current relationship, MPPT is introduced into the TEM field in recent years [67~70]. As the various algorithms and simulation models have already been studied in many researches, in this thesis work, the topology of TEMs will be mainly analyzed according to the thermal distribution in generator.

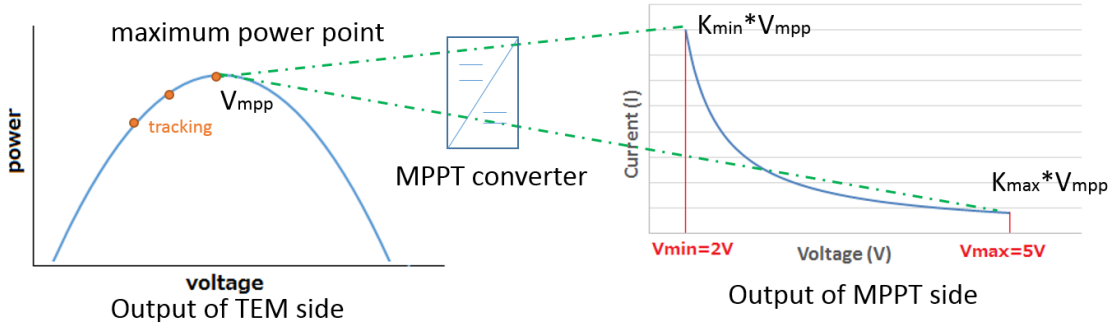

Fig. 5.12 Working principle of MPPT

Through MPPT algorithm, the maximum power point is tracked all the time, and this point can be converted from a point into a wide range

5.3.2 Electric topology of TEMs

(1) Centralized MPPT architecture

From Fig. 4.12, it is observed that the temperature distribution on both sides of TEMs almost maintains the same along the direction of hot fluids flow in generator, which implies the output power of TEM is similar to each other. Under this condition, centralized MPPT converter topology can be applied.

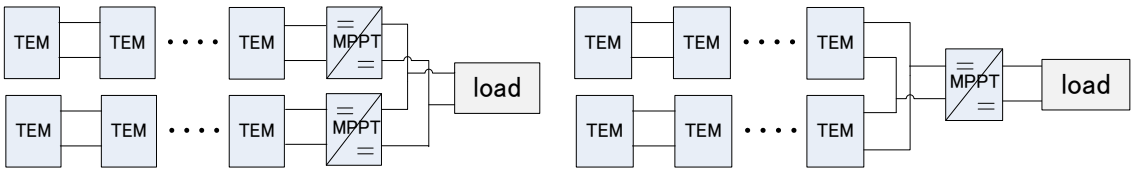

Fig. 5.13 Centralized MPPT architecture

As shown in Fig. 5.13 (a), several TEMs are connected in series to meet the minimum working limits of MPPT converter, and then boost the input voltage into required level through MPPT converter. Several strings are connected in parallel to supply the maximum output power to load; or multiple strings of TEMs are connected in parallel and they feed the input of a grid-tied MPPT converter. The conventional batteries grid-tied systems generally use a single MPPT converter as shown in Fig. 5.13 (b). The process tracks one maximum power point from array input, varying the ratio between the voltage and current delivered to get the maximum power it can.

Regarding to the field conditions, it has been observed that the orifice of hydrothermal vent was partially clogged by the metallic solidified particles since Dec. 2012. For the power generator developed in Fig. 5.11, the simulation of temperature

distribution on TEMs was done under this condition, and the result is shown in Fig. 5.14.

It can be found that the temperature difference on both sides of each TEM is not identical, so each TEM has their own MPP which is different from the others. If the centralized MPPT architecture is applied here, the array's MPP will become a compromise between all TEMs' variances and two problems may be caused.

One is that it is possible to make the centralized MPPT controller becomes confused, stopping on a local maximum point and setting in a sub-optimal point of the voltage to power configuration; another one is that the voltage point of the MPP can be very diverse due to irregular conditions, going beyond the scope and voltage range of the centralized MPPT converter [71]. So the disadvantage of centralized MPPT architecture cannot be ignored when the output power of TEM is not identical to each other.

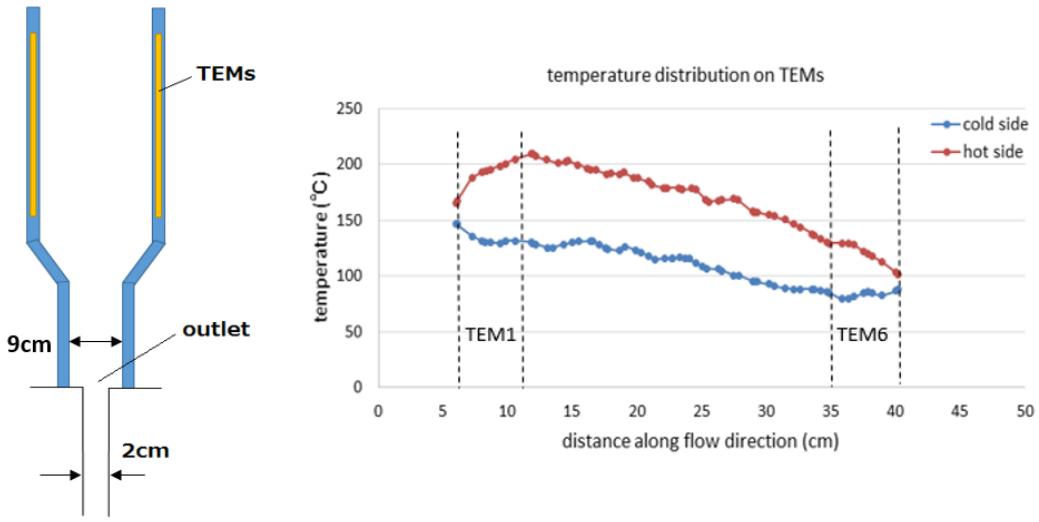

Fig. 5.14 Temperature distribution on TEMs of practical power generator

(2) Distributed MPPT architecture

According to the above mentioned problems, distributed MPPT architecture is proposed. Each TEM shall be attached with each MPPT converter firstly and then several MPPT converters connect in series to achieve load's required voltage, as shown in Fig. 5.15. On the one hand, each MPPT track the local MPP of each TEM, and boost the output voltage of each TEM into a higher level; on the other hand, the series connected MPPT converters communicate with each other in an indirect way. Some MPPT converters lower the output voltage of weak TEMs, raising their current

to match that of stronger ones, others raise the output voltage of strong TEMs, lowering their current to match that of weaker ones. They adjust themselves until achieving a total string optimum to create a fixed string voltage and current. The working principle of this process is shown in Fig. 5.15 (right).

(3) Performance of distributed MPPT architecture

Ideally, the distributed MPPT architecture can solve any mismatch problem, but actually this is not feasible [72]. As stated in section 5.3.1, the mismatch power problem is caused by two conditions. One is the dissimilar output power between

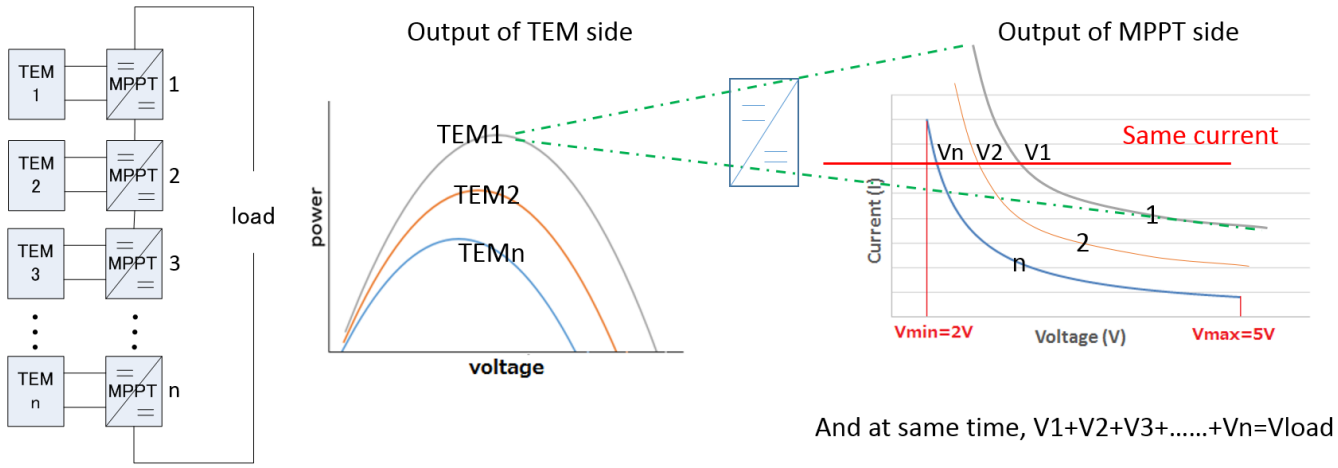

Fig. 5.15 Distributed MPPT architecture

In Fig. 5.15, MPPTn lower the output voltage of TEMn, raising its current; meanwhile, MPPT1 raises the output voltage of TEM1, lowering its current to match with others until reaching a total string optimum.

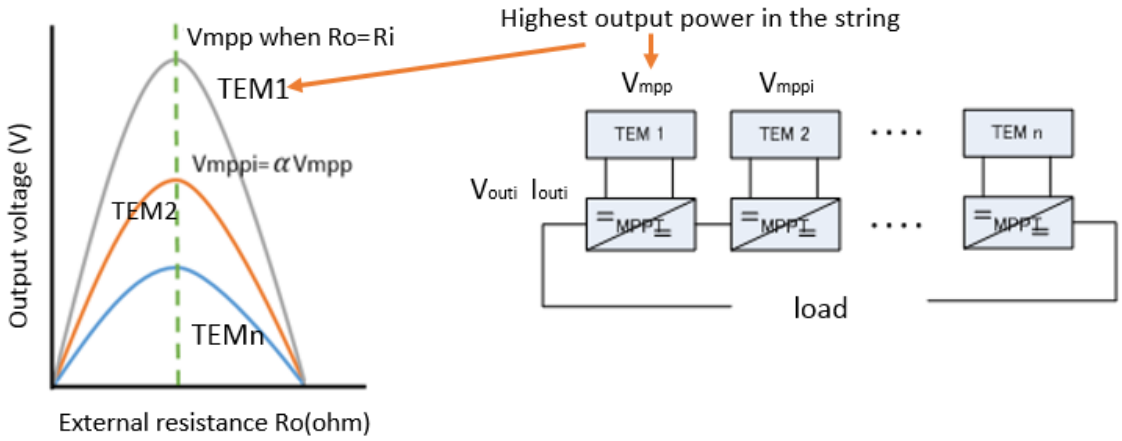

Fig. 5.16 Output characteristic of TEM in distributed MPPT architecture

each TEM, and this problem can be solved by distributed MPPT architecture as

illustrated in Fig. 5.15. Another one is the mismatch resistances problem when the TEMs are connected with load. In other words, the output voltage of distributed MPPT architecture should be in the operating range of the load's voltage. However, this limitation has not been devoted enough attention in other researches. In this research work, the characteristic of distributed topology applied to TEM is studied.

As stated above, when the temperature distribution on both sides of TEM is nonuniform, every TEM has their own maximum output point. Assume V_{mpp} and I_{mpp} are the maximum output voltage and current of the TEM which has the highest output power in one string. If the internal resistance of TEM is constant, the maximum output voltage of other TEMs V_{mppi} in the same string can be expressed as:

$$V_{mppi} = \alpha_i V_{mpp} \qquad (0 \le \alpha_i \le 1\ ) \tag{5.2}$$

as shown in Fig. 5.16. Correspondingly, the electrical current from TEM to MPPT converter is:

$$I_{mppi} = \frac{V_{mppi}}{r} = \frac{\alpha_i V_{mpp}}{r} = \alpha_i I_{mpp} \tag{5.3}$$

Through MPPT converter, the output voltage of TEM will be boosted into a higher level. Supposing the voltage after boost is V_{outi}, which can be described as:

$$V_{outi} = k_i V_{mppi} \tag{5.4}$$

where k_i is the conversion ratio of MPPT converter, for boost conversion $k_{\min} = 1$, and for buck conversion $k_{\max} = 1$. The electric current flowing out from each MPPT converter can be written as:

$$I_{outi} = \frac{P_{mppi}}{V_{outi}} = \frac{\alpha_i V_{mpp} \cdot \alpha_i I_{mpp}}{k_i \cdot \alpha_i V_{mpp}} = \frac{\alpha_i}{k_i} I_{mpp} \tag{5.5}$$

In a series connected string, the current flowing through each converter is same:

$$I_{outi} = I_{outj} \tag{5.6}$$

Substituting I_{out} from(5.5), it can be obtained:

$$\frac{\alpha_i}{k_i} I_{mpp} = \frac{\alpha_j}{k_j} I_{mpp} \tag{5.7}$$

$$\frac{\alpha_i}{k_i} = \frac{\alpha_j}{k_j} \tag{5.8}$$

The total output voltage of distributed MPPT architecture is:

$$V_{sum} = \sum_{i=1}^{N} V_{outi} = \sum_{i=1}^{N} k_i V_{mppi} = \sum_{i=1}^{N} k_i \cdot \alpha_i V_{mpp} \tag{5.9}$$

From(5.9), it can be seen the total output voltage is decided by k_i which is the conversion ratio of MPPT converter and α_i which is affected by the temperature distribution.

In order to confirm the range of output voltage of the distributed MPPT architecture is in the operating range of load, the maximum and minimum output voltage of distributed architecture is analyzed in the worst condition. To simplify the study, several assumptions are made. Supposing N TEMs with MPPT converters are connected in series, m of them has the same maximum output and n of them have less output power. Equation (5.9) can be written as:

$$V_{sum} = \sum_{i=1}^{m} k_a \cdot \alpha_a V_{mpp} + \sum_{i=1}^{n} k_b \cdot \alpha_b V_{mpp} \tag{5.10}$$

Define a is m/N and b is n/N, if m TEMs have the same highest output power, α_a is equal to 1. Equation (5.10) can be simplified as:

$$V_{sum} = NV_{mpp}(a \cdot k_a + b \cdot k_b \alpha_b) \tag{5.11}$$

Combined with(5.8), (5.11) can be described as:

$$V_{sum} = NV_{mpp} \cdot k_a (a + b \cdot \alpha_b^2) \tag{5.12}$$

From(5.12), two conclusions can be obtained. One is that it is possible to know the output voltage of distributed MPPT architecture when all TEMs are working at their maximum output point. Another one is the total output voltage is greatly decided by V_{mpp} , k_a , a which are the parameters of highest output TEMs, and restricted by α_b , which is the ratio of maximum output voltage of the highest and weakest output TEM. It also shows in order to get a high output voltage, it would be better to keep the temperature distributed identically rather than seeking a local high output power.

Deduced from(5.12), when $k_a = k_{\max}$, the maximum output voltage can be obtained:

$$V_{sum\_\max} = NV_{mpp} \cdot k_{\max}(a + b \cdot \alpha_b^2) \tag{5.13}$$

And the minimum output voltage can be got if $k_b = k_{\min}$:

$$V_{sum\_\min} = NV_{mpp} \cdot k_{\min}(\frac{a}{\alpha_b} + b \cdot \alpha_b) \tag{5.14}$$

Equation (5.13) and (5.14) are two essential equations to calculate the range of output voltage of distributed MPPT architecture. And this range should be in the operating range of the load's voltage to prevent mismatch power problem.

In this work, it is expected the produced power can charge a 24 V 17 Ah battery, so the output voltage of the circuits should be in the range of 25 V~ 30 V. A MPPT converter SPV1040 is employed, which can boost the output voltage of single TEM up to maximum 5.2 V. And it has been found the efficiency of this converter is about 75% when the temperature difference on both sides of TEM is 80°C. The configuration of TEMs with MPPT converters is shown in Fig. 5.17. Six pieces of TEM are connected with converter respectively, and then connected in series to obtain an output voltage as high as 30 V.

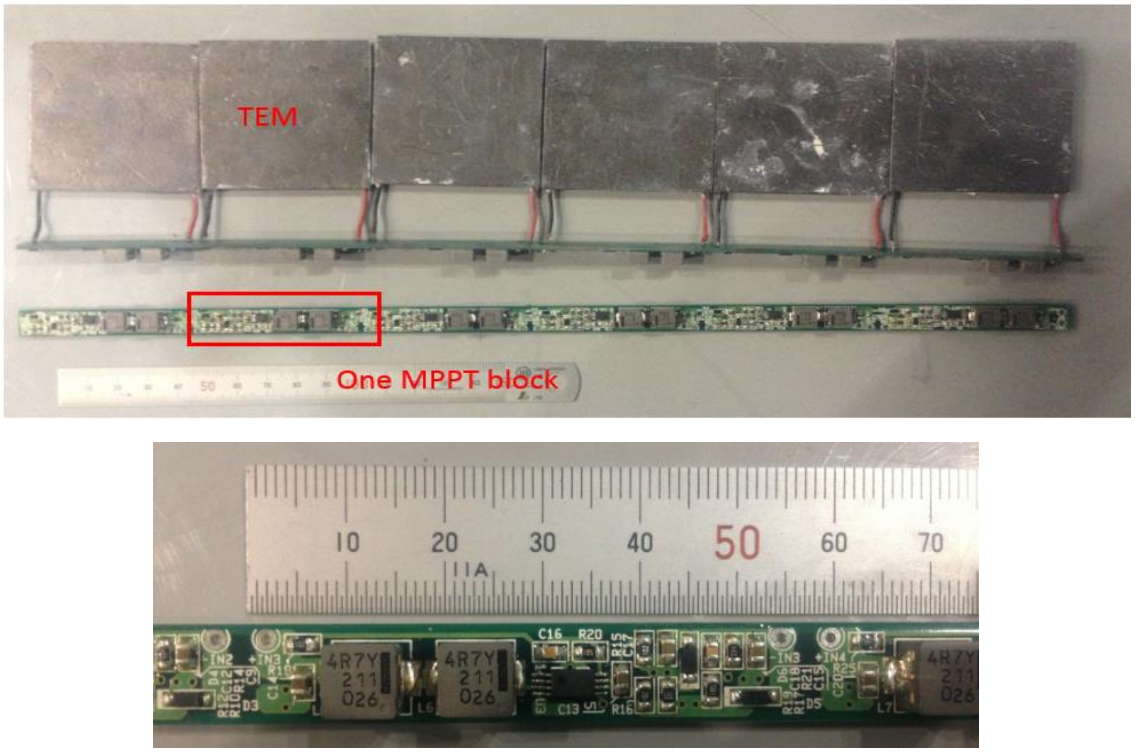

Fig. 5.17 Six pieces of TEMs with MPPT converters are connected in distributed MPPT architecture

According to the temperature distribution on TEMs as shown in Fig. 5.14, the maximum output power of each TEM can be estimated. The output power of the first and last TEM are about 0.4 W and 0.35 W respectively; and the maximum output power of other four TEMs are 0.8 W. Based on (5.4), (5.8) and (5.13), the maximum output voltage of distributed architecture can be approximated as 24.8 V which is a little lower than required charging voltage and cannot recharge the battery in a safe mode.

(4) Solution of the limitation of distributed MPPT architecture

In order to satisfy the charging voltage of battery, one solution to improve the performance of one stage distributed architecture is to add a second stage MPPT converter to boost the output voltage again. As shown in Fig. 5.18, the output current of the first stage MPPT converters adjust TEMs working at their own maximum output point and boost the output voltage to a certain level. Then the second stage MPPT will track the MPP of the first stage and at same time, convert input voltage into a required level.

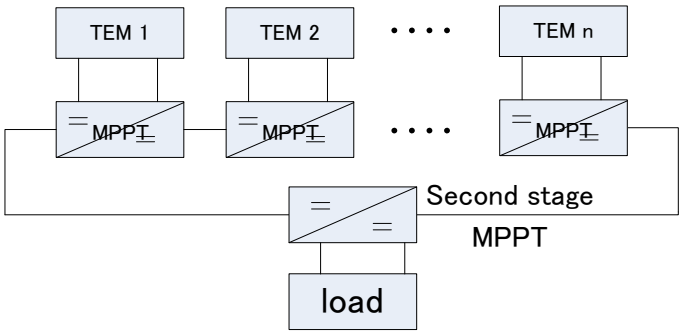

Fig. 5.18 Two stages MPPT architecture

Since the power loss will be caused by the second stage MPPT converter, a mechanical modification has been made to improve the heat distribution along the flow direction. As concluded from (5.11), it would be better to keep the temperature distribute identically rather than seeking a local high output power, a plate was fixed on top of the generator in order to prevent hot fluids dissipate quickly and enable the temperature difference on both sides of TEM are similar to each other. As shown in Fig. 5.19, the nearly identical temperature differences obtained from structure modification will facilitate to achieve the required charging voltage of battery.

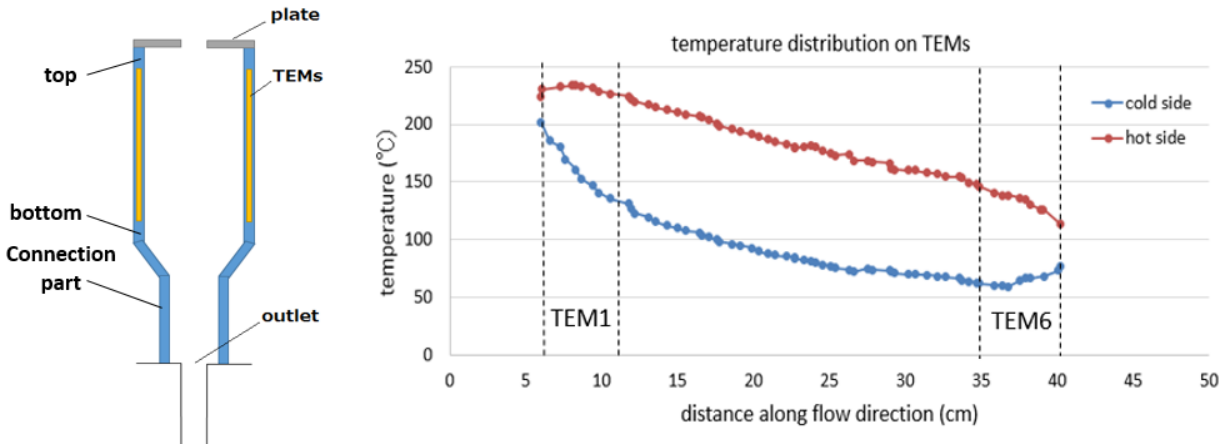

Fig. 5.19 Temperature distribution on TEMs if a plate is fixed on top of generator

5.4 Field experiment

As shown in Fig. 5.20, the power generation system is composed by a hexagonal shape power generator, and power management system. A plate was fixed on the top of generator to improve the heat distribution on the inner surface of generator as stated in section 5.3.2.

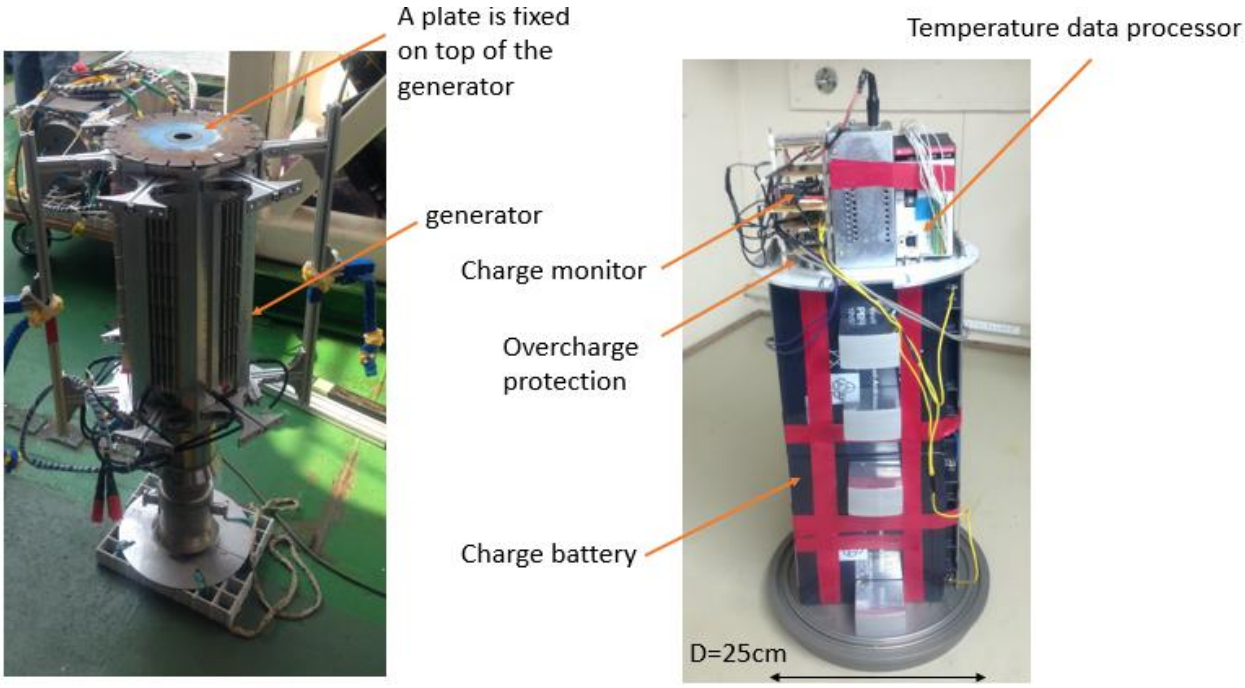

Fig. 5.20 Power generator and power management system

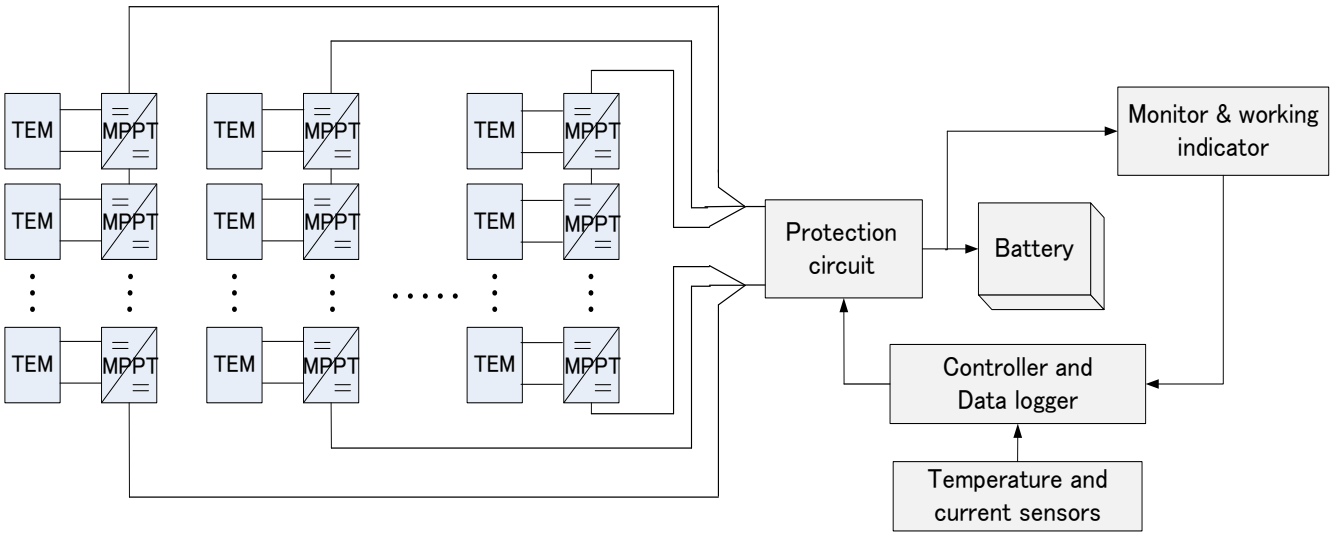

Fig. 5.21 The electrical system chart of the power generation system

The electrical system chart of the power generation system is shown in Fig. 5.21. Six TEMs are attached with MPPT converter respectively and then connected in series as a string. Then, six strings are connected in parallel to obtain high electrical current. The charging voltage, current and current accumulation are recorded continuously. An overcharge protection circuit is combined to prevent overcharging.

Table 5.2 The specification of charge battery

Battery classification	Nominal voltage (V)	Nominal capacity (Ah)
Lead cell	24	17

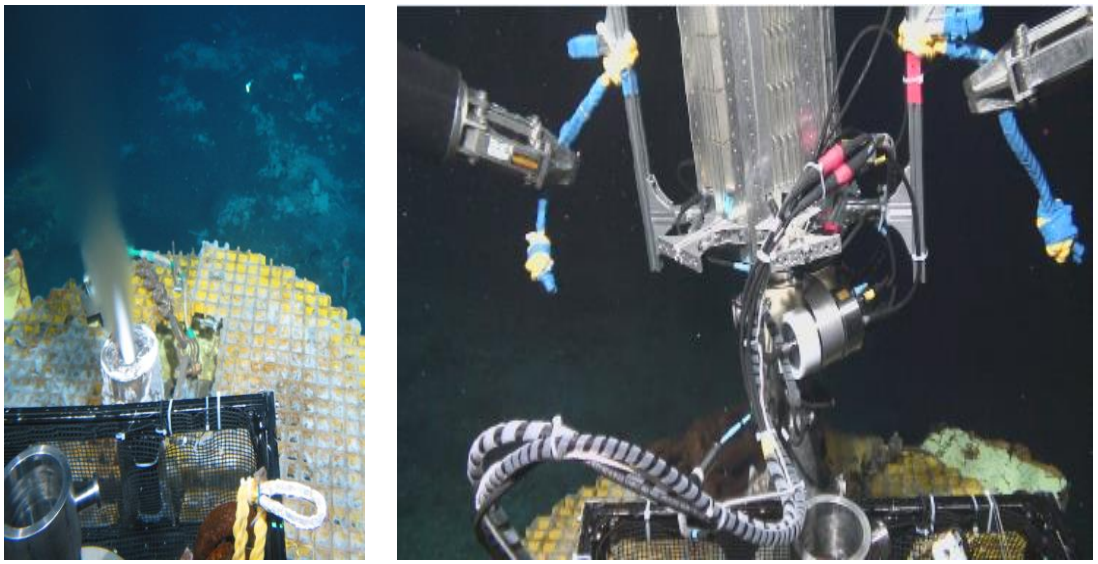

(A) (B)

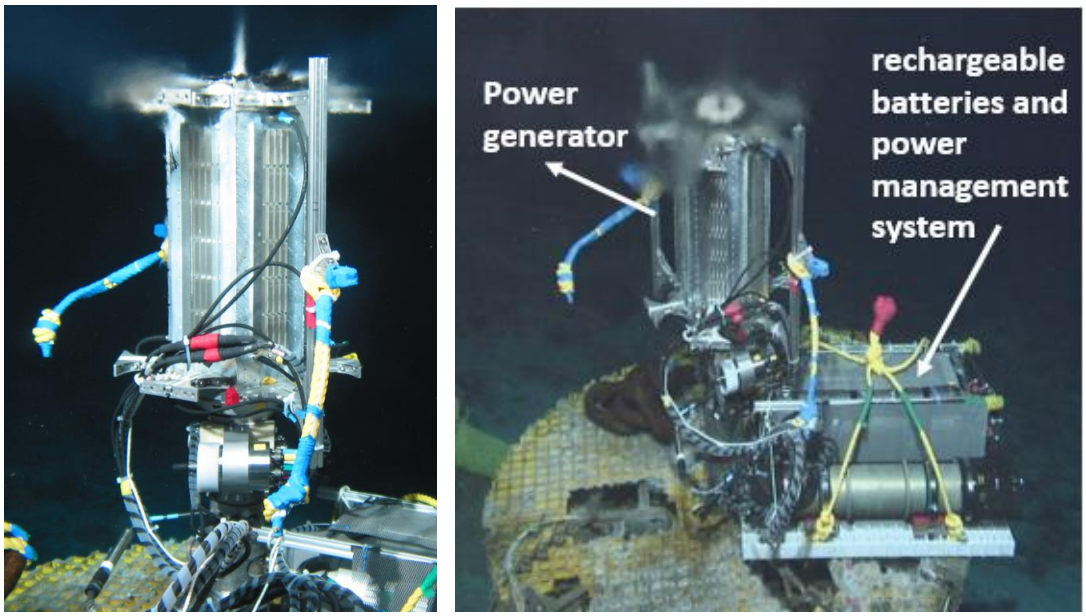

(C) (D)

Fig. 5.22 The condition of the field experiment

(A) The configuration of artificial hydrothermal vent
(B) The configuration of installing process helped by ROV Hyper-Dolphin
(C) The power generator is installed on the artificial hydrothermal vent, superhot water were ejecting from the small hole in the center of plate drastically
(D) Power management system is laid on the platform of hydrothermal vent.

The field experiment was done at an artificial hydrothermal vent located in Okinawa Trough of which the depth is 1069 m on Nov 23th, 2013. The installation work was helped by ROV *Hyper-Dolphin* and the whole experiment was lasted for one and a half hour.

5.5 Results and discussion

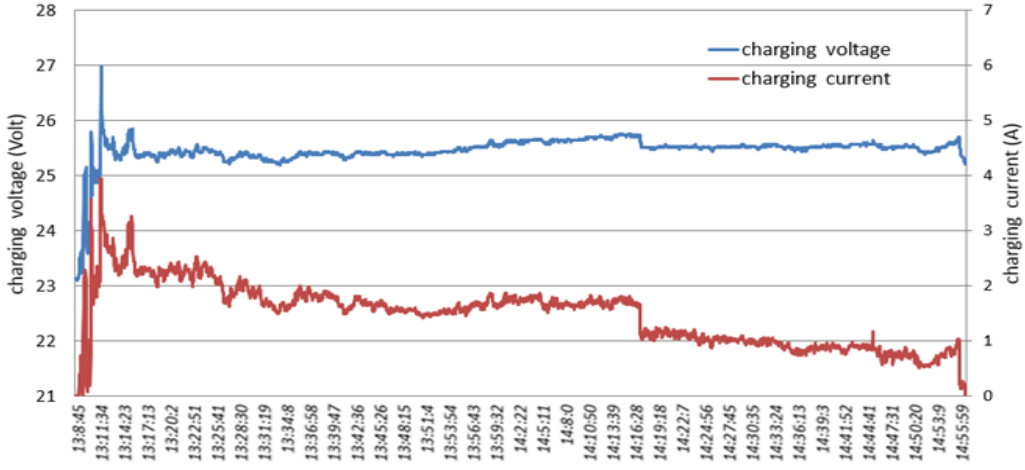

Fig. 5.23 Charging voltage and current

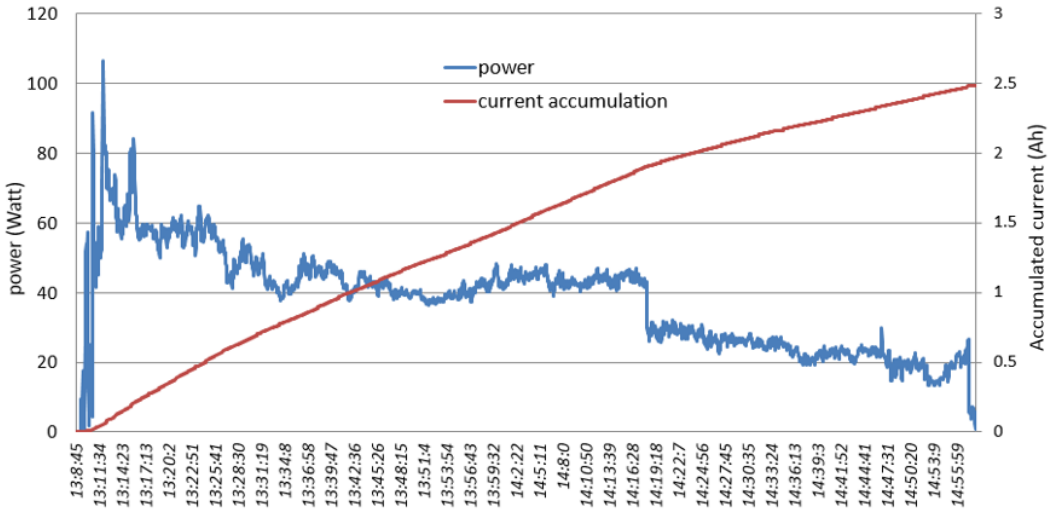

Fig. 5.24 Power and current accumulation

Fig. 5.23 shows the results of charging voltage and current. The charging voltage was maintained relatively stable as 25.5 V, while the charging current was decreasing with the time. Fig. 5.24 shows the results of generated power from TEMs and current accumulation. The maximum and average power produced was around 60 W and 45 W, respectively. About 2.5 Ah got charged during the whole experiment. Based on this data, it needs nearly 10 hours to fully charge the battery of AUV TRI-TON. It is also possible to supply this magnitude of power to a small seabed sensor. It can be noticed the test values obtained from field experiment were very close to the results of theoretical development. This verified the correctness and rationality of the theoretical developments, thermal transfer simulation and electric power system.

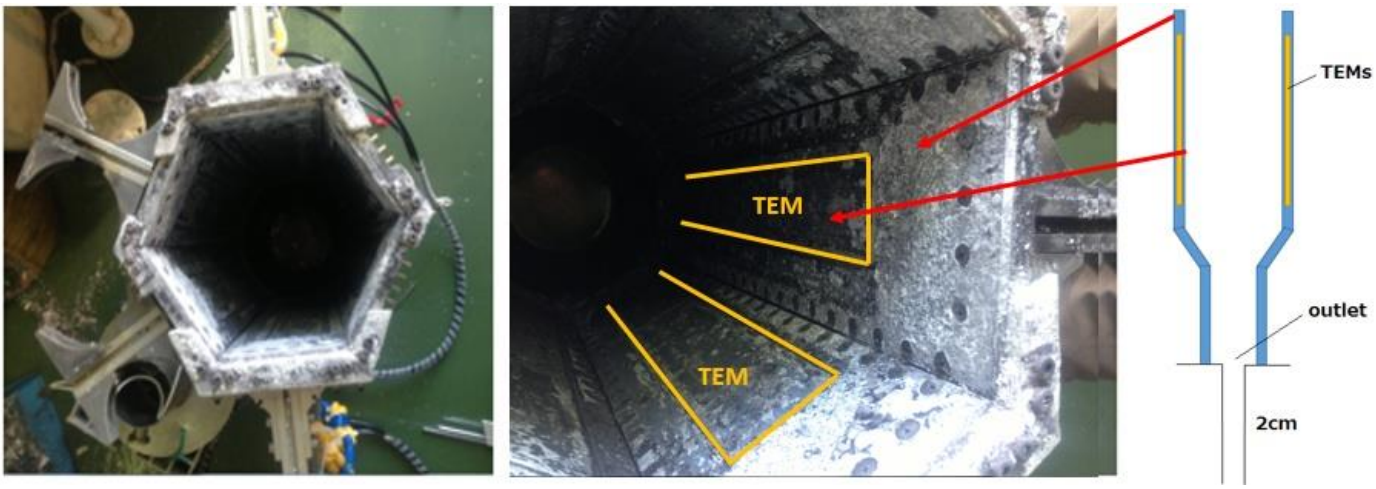

Fig. 5.25 Solidified particles covered on the inner surface of generator

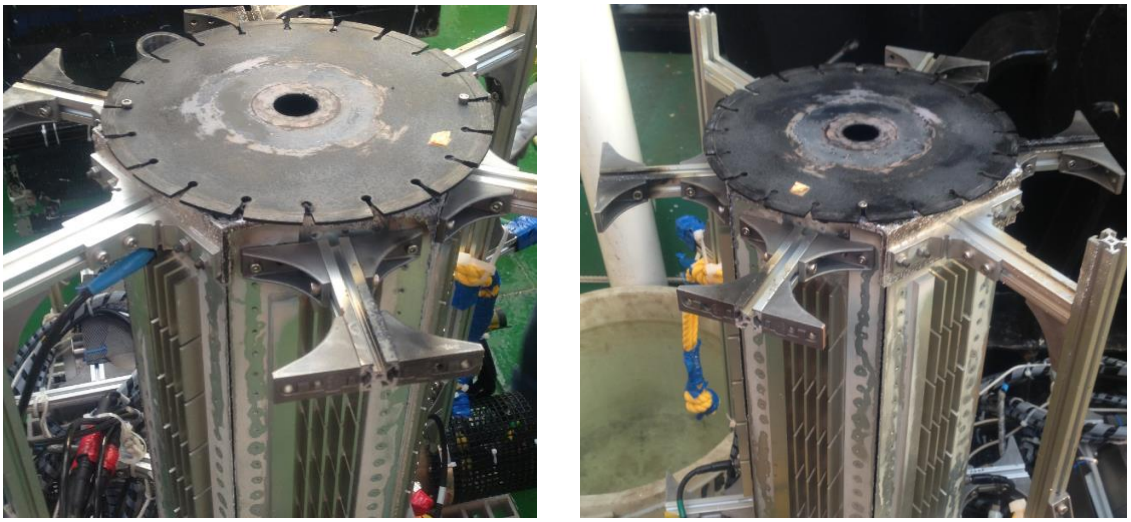

Fig. 5.26 Solidified particles covered on top of the plate

When the generator was recovered from seawater, it was found the inner surface of generator and the plate were covered by the metallic sulfide solidified particles as shown in Fig. 5.25 and Fig. 5.26. The reason is that the generator and the plate on top of the vent prevented particles scattering to surrounding water quickly, and instead aggravated the adhesion speed. With the enlargement of cumulate particles area, the TEMs areas are possibly to be covered gradually and thus the heat transfer will be weakened.

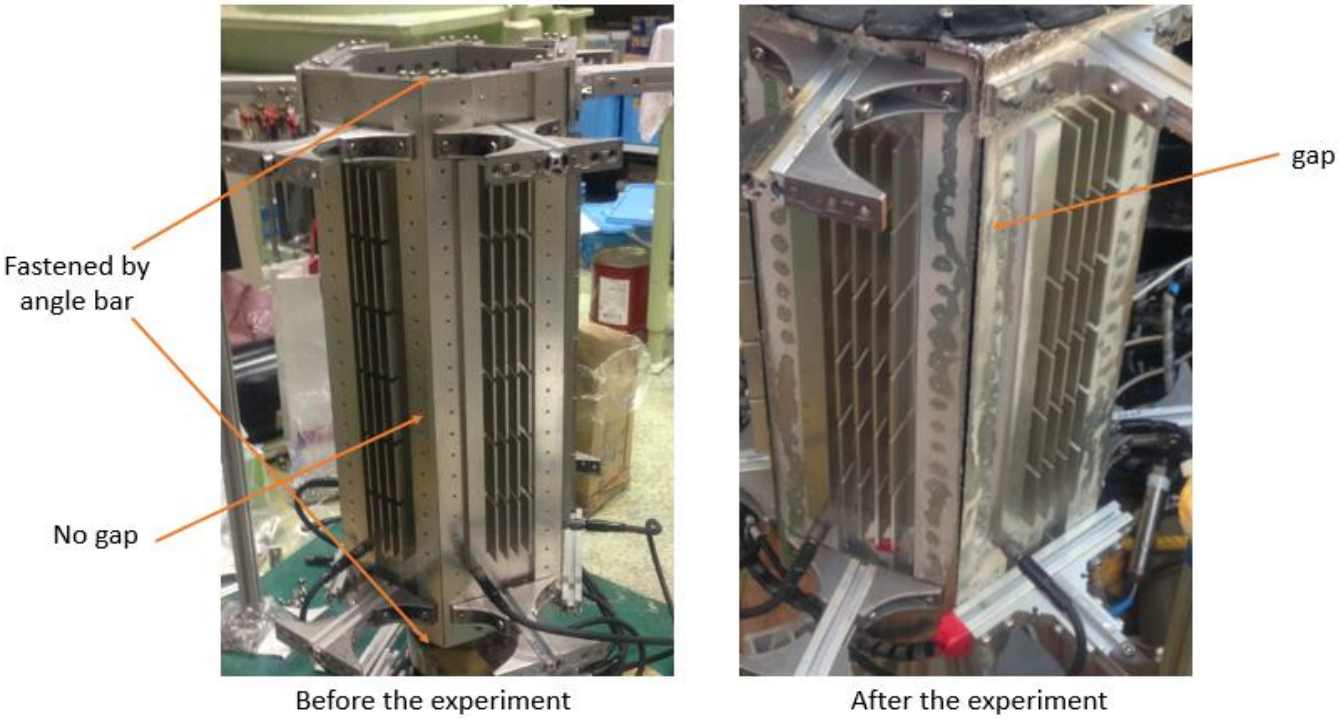

Fig. 5.27 The deformation of the structure

The thermal expansion coefficient of aluminum alloy A6063 is only 23.4×10^{-6} /°C at 25°C ~ 400°C, the expansion is nearly negligible when it is emerged in hot water. But after experiment, a gap was formed in the middle part of generator, as shown in Fig. 5.27. On the hot fluids side, the aluminum was expanded; meanwhile, it was contracted on the cold side. The gap was possibly formed by the large temperature gradient across the housing.

Because of the complex sea condition, the whole experiment was only lasted for one and a half hour. For the long term and large scale power generation, several aspects should be paid attention and modified.

(1) Decease of the charging current

From Fig. 5.23, the charging current deceased slowly in the first hour and dropped suddenly at 14:16. The slow decrease of the current is considered to be caused by the poor heat transfer between the stagnant seawater and generator. As there was nearly no sea current in the field, the heat on the cold side of the generator cannot dissipate into the surrounding cold seawater and accumulated gradually, which resulted in the reduction of current. On the other hand, the hot fluids leaked from the gaps between adjacent housing also warmed up the outside and thus reduced the temperature difference on both sides of TEM layer as shown in Fig. 5.27.

The suddenly drop of current at 14:16 is considered to be caused by the dysfunctional electrical circuits. In the electrical system, TEM and MPPT converter pairs are connected in series bypass configuration as shown in Fig. 5.28. As one MPPT converter can boost the output voltage of TEM into 5.2 V, the battery can still get charged even if one MPPT converter does not work well.

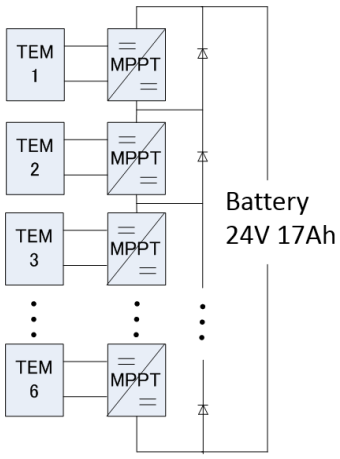

Fig. 5.28 Bypass structure

Through the test after experiment, it was found three MPPT converters became dysfunctional in one series-connected string and thus the output of this string could not flow into the battery. This resulted in the sudden deduction of the charging current. It is possible that the temperature distributed over the interface of electrical components was relatively high and some of them were working over their operating temperature.

In order to overcome this, a modification has been suggested as shown in Fig. 5.29. The plate covered on the housing is made of thermal insulation materials (yellow) to prevent heat conduction to the housing and electrical circuits. The housing is made of high thermal conductivity material (white) to dissipate heat efficiently. The insulation material (brown) is also filled in the slot to isolate heat to electric circuits. Though the insulation materials covered on the hot side of TEM will lower the efficiency of thermal energy transmits to TEM, the influence can be ignored because it is very thin as analyzed in Fig. 5.8 ~ Fig. 5.10.

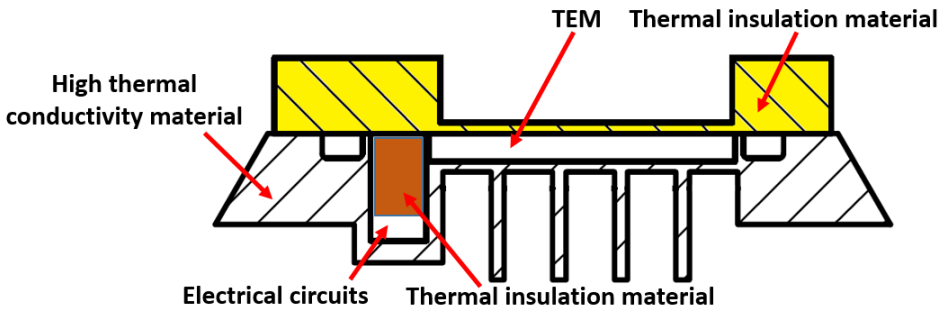

Fig. 5.29 Modification of current design

(2) Adhesion of solidified particles

It has been found the particles were covered on top of the inner surface of the generator especially at the outlet area. This may be because the particles are less adhesive in the high temperature region, but attach to generator easily when cooled down. According to this, one way to attenuate the effect of adhesion is to maintain a high temperature in the outlet region.

From Fig. 5.30, it can be seen though the thermal energy were prevented from dissipating quickly and the temperature kept relatively high inside when the plate was covered on top of the generator, the particles would still adhere to the top part as found in the field experiment. This is because the whole housing was constructed by Al 6063, it was cooled fast at outlet for its high thermal conductivity.

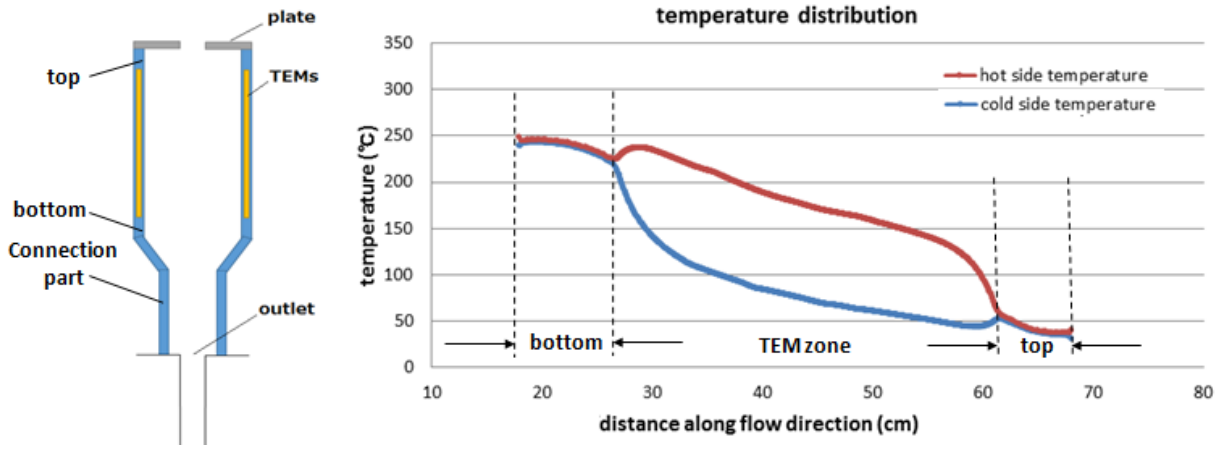

Fig. 5.30 Temperature distribution along the wall surface (Al 6063 with plate)

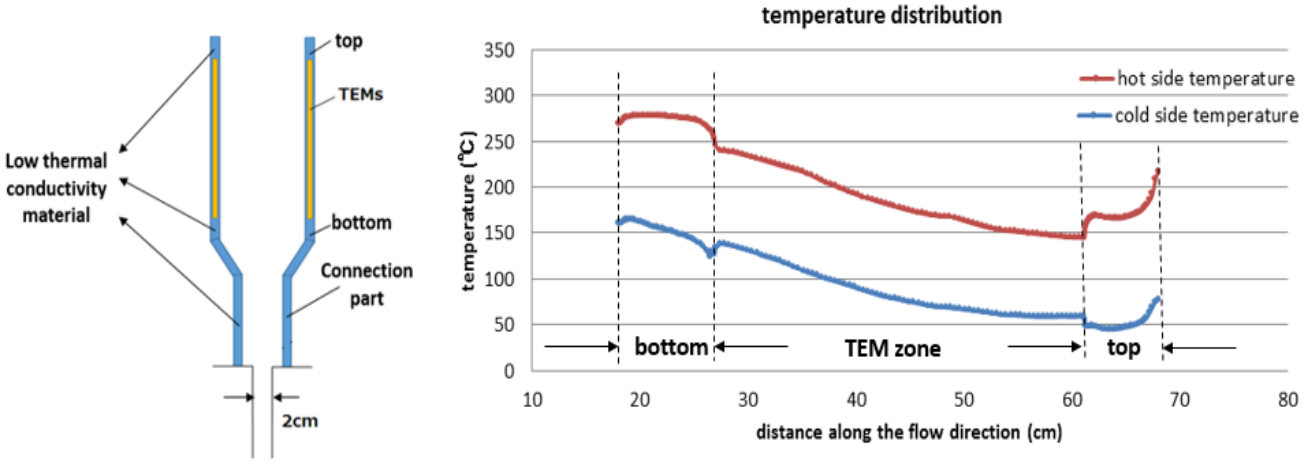

Fig. 5.31 Temperature distribution along the wall surface
(low thermal conductivity material 2.4 W/m-K)

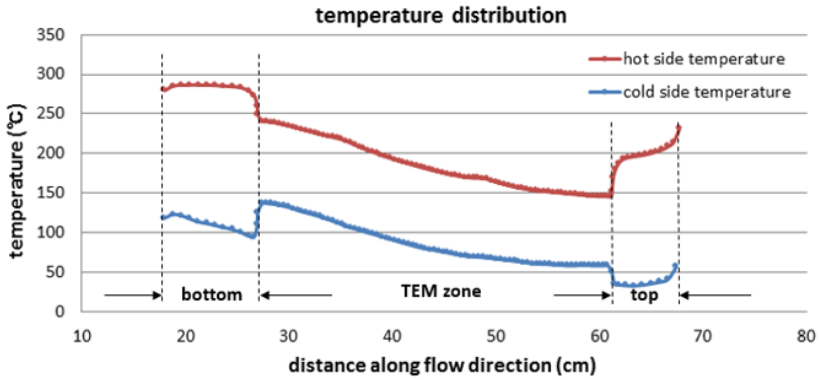

Fig. 5.32 Temperature distribution along the wall surface
(low thermal conductivity material 1 W/m-K)

Comparing with Fig. 5.30, the temperature differences along the wall surface are maintained higher along the flow direction as shown in Fig. 5.31, if the connection, bottom and top part are changed into thermal insulation material of which the thermal conductivity is as low as TEM. Under this condition, the particles are difficult to adhere to the inner surface of generator in the outlet region.

Comparing with Fig. 5.31, the temperature of the inner surface at outlet will become higher if the thermal conductivity of the material constructed for housing and connection parts is lower, as shown in Fig. 5.32. From these figures, it can be seen besides the field condition, the temperature distribution inside the generator is mainly relied on the thermal characteristic of the constructed material. In the future design, the thermal insulation material should be applied which can not only keep high and stable temperature distribution in TEM area, but also attenuate the effect of adhesion.

(3) Slight deformation of mechanical structure

The gaps formed by the temperature gradient across the generator will reduce the durability of it, and the hot fluids leaked from these gaps also warm up the outside. In the future design, the middle part of the generator should also be fixed next to each other to increase the stability and durability of the system.

(4) For long term and large scale power generation

Firstly, in order to ensure the high temperature difference along the generator, it is necessary to trap the hot fluids completely once discharging from vent orifice. The leak of the hot fluids from the bottom part of generator will warm up the cold side of TEMs, and thus weaken the heat transfer. On the other hand, the solidified particles covered on the inner surface of generator insulate heat conduction from hot fluids to TEMs that also greatly reduce the temperature difference across them. For long time power generation, the adhered particles should be removed by some cleaning robots, or the generator itself should be changed in a certain time.

For large scale power generation, the produced power is in proportion to the length and cross sectional area of generator. When the hot fluids are trapped properly, sufficient temperature differences on both sides of TEMs can be maintained in long length to obtain enough power as shown in Fig. 5.33. If the length is extended to the twice of the current generator, maximum 120 Watts can be extracted and one battery of the AUV Tri-ton can get fully charged in 5 hours. Actually, the length of

the

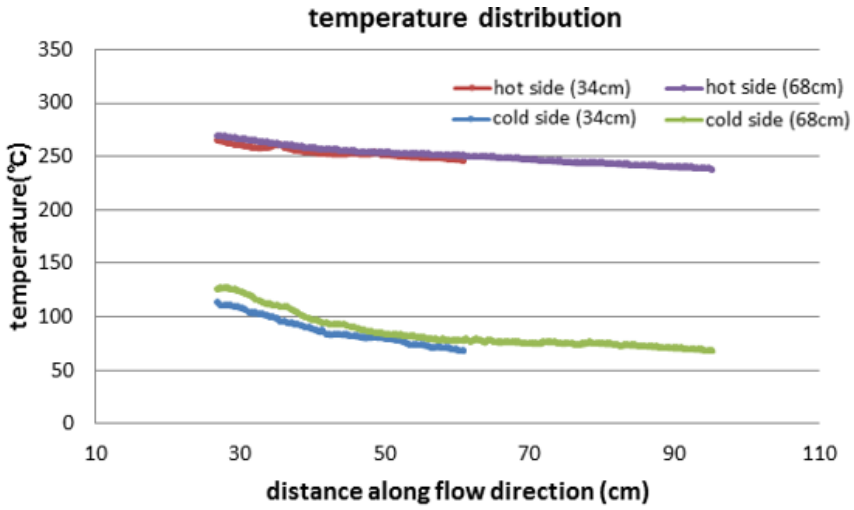

Fig. 5.33 The power generation vs. the length of generator

generator is decided by the discharging temperature, velocity, pressure, adhesion of particles and other factors, so it becomes necessary to do the observation on hydrothermal vent in long term to understand its basic characteristic in the next research phase.

The large power generation can also be realized by the arrangement of several power stations in the same area simultaneously. The integration of these stations will provide a stable and sufficient power for underwater vehicles and observation stations.

5.6 Summary

This chapter follows the design and construction of the deep sea power generator system by utilizing the thermal energy discharged from hydrothermal vent. This is a platform developed as main part of this research to verify the associated theoretical developments, simulation models and access the practical applications of the structure design and electrical system topology.

The simulation shows the heat transfer is not only decided by the thermal conductivity of materials, but also the thickness of it. The difference in temperature distribution is slight if the housing is relative thin. The experiment demonstrates that, in contrast to the traditional cylindrical pressure vessel, the new hexagon generator performs good flexibility in mechanical design. The hexagon shape could

also provide sufficient area to mount TEMs without increasing the flow cross sectional area and take advantage of the inherent thermal expansion in generator as the cylindrical shape generator.

In the power management, MPPT method is applied here to extract the maximum power without affected by various loads. For large TEMs power generation system, distributed MPPT architecture is an effective topology to facilitate the power loss reduction which is caused by the differences in output of TEMs from each other. But it is also found the poorest output TEM greatly influences the performance of the whole architecture. It would be better to keep the temperature distributed identically rather than seeking a local high output power.

The field experiment was done at artificial hydrothermal vent located in Okinawa Trough in Nov. 2013. Maximum 60 W and average 45 W were generated from TEMs and a 24 V 17Ah battery was partly got recharged in one and a half hour. This is the first deep power generation system that really realized to produce power from hydrothermal vent. From the experiment, it should also be noticed the solidified particles will adhere to the inner surface of generator soon which will affect the heat transfer and reduce the generated power. The strength of the material should be carefully studied when there is a large thermal gradient across the housing.

Chapter 6 Conclusions and future work

The goal of this research has been the developments of a deep sea power generation system that is capable of generating, storing and supplying power to underwater vehicles, seabed stations and other seabed sensors. To achieve this, it requires a method that can convert power contained in seawater into electricity; a generator which can support the system to work under this high pressure and low pH environment; and a power management system that can extract the maximum power generation all the time, and store, supply power in a safe mode.

In this research work, thermal energy discharged from hydrothermal vent is utilized as a power source; a novel power generator is developed which has good pressure and corrosion resistance, high thermal conduction and good flexibility in mechanical design; also the topology of the electrical power generation diagram is studied and discussed.

6.1 Contributions and conclusions

This is the first deep sea power generation system by utilizing the thermal energy discharged from hydrothermal vent in the world.

It is widely known that vast energy contained in the superhot fluids discharged from hydrothermal vent, and some ideas of thermal energy utilization have been proposed, but no one has had realized power production from it. In order to solve the power supply problem near hydrothermal vent areas where are one of the most attractive places for researches now, a new method was applied to convert the thermal energy into electricity.

This is the first time to apply thermoelectric module in deep sea as a medium to produce power. So it becomes necessary to understand its performance under high pressure. A system was developed to test the power generation ability of TEM under various thermal and high pressure conditions. As 80% of the hydrothermal vents are located at depth of 2000 meters to 2500 meters, the pressure has been added up to 20 MPa. The result shows it performed well and the efficiency of the system even

became higher. This can be explained as the high pressure compressed the TEM with the contact interfaces tighter, and less gap existed between them brought good heat transfer, and thus much more power were produced by TEM.

A compact power generator model was developed in order to confirm whether the water is still hot enough to drive TEM to produce power after ejection. This feasibility experiment was carried out at Yamanaka vent located in Kagoshima Bay in Apr. 2012. The model was made as a plate shape in which four pieces of TEMs were housed in. When the model was set on top of the vent, the hot fluids collided against the bottom of it to transfer heat energy, but cold seawater maintained a low temperature on the top side of it. By utilizing this temperature difference, the power output has been recorded as 1.7 W from four series connected TEMs. This is the first model to generate power from hydrothermal vent, and the results verified it is possible to produce power from hydrothermal vent if the thermal energy is captured properly as soon as the hot fluids flow out.

However, the necessary power should be at least two orders of magnitude higher than the power generated from feasibility experiment in order to charge an AUV or supply power to underwater station. For practical application, the power generator should not only have good pressure resistance and thermal conduction, but also can mount TEMs and related circuits properly. To achieve this, a novel hexagonal generator prototype was proposed which is composed by several sets of housings. Though the thin flat plate is weak against pressure, but when it is supported appropriately, it can withstand against the pressure.

The differences in heat transfer of concentric double pipes prototype and hexagonal prototype were simulated and compared. Under the condition of same sectional area and same heat transfer area for both prototypes, it is found the temperature drops very slowly along the flow direction because of the low thermal conductivity of TEM layer. Hexagonal prototype shows better performance because of the larger temperature difference maintained on both sides of TEM layer under both conditions. The simulation results also shows the heat transfer becomes poor obviously if the orifice of vent is partially clogged or the inner surface of generator is covered by metallic sulfide particles.

According to the theoretical developments and simulation results, a power generation system was designed, constructed and tested. The mechanical design shows that the new hexagonal generator performs good flexibility in contrast to the

traditional cylindrical pressure vessel. The hexagonal shape could also provide sufficient area to mount TEMs without increasing the flow cross sectional area and take advantage of the inherent thermal expansion in generator as the cylindrical shape generator. The strength of this irregular structure is confirmed based on the structure dynamic calculation, and the pressure resistance is verified in pressure tank up to 11 MPa.

For one single TEM, the output power is decided by the temperature differences on both sides of it. MPPT method was employed, which can extract the maximum output power from TEM under any thermal conditions and without being influenced by the different loads. However, in large power generation system, the output power is not only concerned with the temperature differences on single TEM, but also the topology of TEMs connection methods. According to the thermal distribution, centralized architecture and distributed architecture were compared and the limitations of both methods were analyzed. Ideally, the distributed architecture can solve any mismatch problem, but actually this is not feasible. Combined with the simulation results, the power mismatch problem caused by the non-uniform temperature distribution on TEMs was studied, and the solutions for distributed architecture were proposed. The modification of the system has been done to enable the output voltage of TEMs is in the operating range of load.

The field experiment was carried out at artificial hydrothermal vent located in Okinawa Trough in Nov. 2013. This is the first deep sea power generation system which has really produced electrical power by utilizing the thermal energy released from hydrothermal vent in the world, and above 60 W were obtained. The experiment verified the rationality and correctness of theoretical developments, simulation results and electric power management system. This research provides a reference for the development of large power generation system in deep sea.

6.2 Future work

This work has built a test platform of power generation from hydrothermal vent sites. There are still some issues need to be solved in the future.

It is noticed when the hydrothermal vent is partial clogged by the solidified particles, the temperature differences on both sides of TEM are different from each other. This will result in the power mismatch problem if all the TEMs are connected in series. The theoretical analysis showed the output voltage of TEMs still could not be boosted

into an expected value, even if all the TEM all working at their maximum output point. It would be better to keep the temperature distributed identically rather than seeking a local high output power. The problem can possibly be solved if second-stage MPPT controller is added, which can boost the low output voltage from the TEMs again to achieve an expected voltage. The algorithm and efficiency of the second-stage MPPT controller should be studied in the future.

After the experiment, it was found the middle part of generator was expanded and a 0.2 cm gap was formed between two housings as shown in chapter 5. Though the thermal expansion coefficient of aluminum 6063 is only 23.4×10^{-6}/°C at 25~400°C, the gap was possibly formed by the large temperature gradient across the thickness of housing. In the post design, the deformation of materials in the large temperature gradient environment should be carefully considered and studied.

After the experiment, it is found the metallic sulfide particles are adhered to the inner surface of power generator. This will greatly weaken the heat transfer and thus lower the power generation performance of the system. The next major target in the development of power generator is to investigate how to remove these particles in mechanical and chemical methods. Another way is to fabricate generator with some other materials which reject these particles to attach to the surface.

The power generated from single hydrothermal vent is limited, in order to realize the large-scale grid-tied systems that can generate, store and supply power, an intelligent power management system is necessary. This will be a subject of future study.

References

[1] Bird, P., An updated digital model of plate boundaries, Geochem. Geophys, Geosyst.,4,1027, doi:10.1029/2001GC000252, 2003

[2] Baker, E.T., and German, C.R.: On the Global Distribution of Hydrothermal Vent Fields, In German, C.R., Lin, J.and Parson, L.M. (eds.) Mid-Ocean Ridges: Hydrothermal Interactions Between the Lithosphere and Oceans, Geophysical Monograph Series, 148, (2004), 245-266.

[3] Haase, K. M.; et al. (2007). "Young volcanism and related hydrothermal activity at 5°S on the slow-spreading southern Mid-Atlantic Ridge". Geochemistry Geophysics Geosystems 8 (11): Q11002.

[4] Haase, K. M; et al. (2009). "Fluid compositions and mineralogy of precipitates from Mid Atlantic Ridge hydrothermal vents at 4°48'S". PANGAEA.

[5] http://www.whoi.edu/page.do?pid=83560&tid=4142&cid=71854

[6] http://usatoday30.usatoday.com/tech/columnist/aprilholladay/2005-01-07-wonder quest_x.htm

[7] http://www.underwatertimes.com/news.php?article_id=95461073018

[8] http://www.uib.no/geobio/en/research/research-themes/geodynamics-of-the-deep- seafloor/about-deep-seafloor-dynamics

[9] http://www.divediscover.whoi.edu/tectonics/tectonics-subduct.html

[10] http://www.udel.edu/PR/experts/weirdworm.html

[11] Zhai Shikui, The distribution and mineralogical Characteristics of pumice in Okinawa Trough, Oceanologica et Limnologia Sinica, 1986, 17(6): 504.

[12] http://www1.kaiho.mlit.go.jp/GIJUTSUKOKUSAI/kaiikiDB/kaiyo28-2.htm

[13] Kimura, M. et al., Research result of the 284, 286, 287 and 366 dives in the Iheya

Depression and the 364 dive in the Izena Holl by “SHINKAI 2000”, Proceedings of JAMSTEC Symposium on Deep Sea Research, No. 7, Japan Marine Science and Technology Center,1991, 147

[14] Nedachu, M. et al., Hydrothermal ore deposits on the Minami- Ensei Knoll of the Okinawa Trough-Mineral assemblages, Proceedings of JAMSTEC Symposium on Deep Sea Research, No. 8, Japan Marine Science and Technology Center, 1992, 95 106

[15] Kawagucci. S, Chiba. H, Ishibashi. J, et al, Hydrothermal fluid geochemistry at the Iheya North field in the mid-Okinawa Trough: Implication for Origin of Methane in Subsea floor Fluid Circulation Systems, Geochemical Journal, Vol. 45, pp.109-124, 2001

[16] http://www.mpi-bremen.de/en/strange%20ecosystem.html

[17] Baker, E.T., and S.R. Hammond, Hydrothermal venting and the apparent magmatic budget of the Juan de Fuca Ridge, J. Geophys, Res. , 97, 3443-3456, 1992.

[18] http://www.newscientist.com/article/dn9843-extreme-seabedsurvival-boosts-hope-of-aliens.html#.UqMCs8RdWEk

[19] http://happy.ap.teacup.com/ibaraki-doji/520.html

[20] http://scixchange.missouri.edu/blog-post/can-you-stand-the-heat/

[21] Ursula Ginster and Michael J.Mottl, Heat flux from black smokers on the Endeavour and Cleft segments, Juan de Fuca ridge, Journal Of Geophysical Research, Vol, 99, No. B3, Pages 4937-4950, March 10, 1994.

[22] Hiriart, G., and Espindola, S. Submarine Geothermics; Hydrothermal Vents and Electricity Generation, Proceedings World Geothermal Congress 2010, Bali, Indonesia, 25-29 April 2005.

[23] www.marshallsystem.com

[24] Yamamoto, M. et al. 2013. Generation of electricity and illumination by an environmental fuel cell in deep-sea hydrothermal vents. Angewandte Chemie, online DOI: 10.1002/ange.201302704

[25] http://en.wikipedia.org/wiki/Hydrothermal_vent

[26] Peter Lonsdale and Keir Becker, Hydrothermal Plumes, hot springs and

conductive heat transfer in the Southern Trough of Guaymas Basin, Earth and Planetary Science Letters, 73(1985), 211-225

[27] www.hi-z.com

[28] http://www.adafruit.com/blog/2013/04/19/new-product-peltier-thermo-electric-cooler-module-5v-1a/

[29] R. D. Abelson, Thermoelectrics Handbook (CRC Press, Boca Raton, FL, 2006), chap. 56, pp. 1–29.

[30] Lon E. Bell, Cooling, Heating, Generating Power and Recovering Waster Heat with Thermoelectric systems, Science, Sep. 12, 2008.

[31] M. Kyo and T. Itoh, Fundamental experiment of thermoelectric module for the deep sea use, the fifteenth Japan Symposium on Thermo physical Properties, 1994

[32] Morena, John J (1988). Advanced Composite Mold Making. New York: Van Nostrand Reinhold Co. Inc. pp. 124–125. ISBN 978-0-442-26414-7.

[33] http://www.digikey.com/us/en/techzone/energy-harvesting/resources/articles/thermoelectric-energy-harvesting.html

[34] http://en.wikipedia.org/wiki/Thermoelectric_effect

[35] G. S. Nolas, J. Sharp, and H. Goldsmid, Thermoelectrics: Basic Principles and New Materials Developments, Springer, New York, 2001

[36] A. J. Minnich, M. S. Dresselhaus, Z. F. Ren and G. Chen, Bulk nanostructured thermoelectric materials: current research and future prospects, Energy Environ. Sci, 2009, **2**, 466-479

[37] J. P. Heremans et al., Science 321, 554 (2008).

[38] T. Kajikawa, S. Sano, J. Morimoto, “The new edition of thermoelectric energy conversion system”, realize Science &Engineering, 2004.

[39] H. Ohta. Thermoelectrics based on strontium titanate. Materials today, Oct 2007

[40] “Basic Principles of Thermoelectric Materials”. www. Ferrotec.com

< http://www.ferrotec.com/technology/thermoelectric/thermalref02/>

[41] Kajikawa T, Present status of research and development on thermoelectric

power generation technology in Japan, Journal of Thermoelectricity №1, 2009

[42] T. Shindo, Y. Nakatani and T. Oishi. Thermoelectric Generating System for Effective Use of Unutilized Energy, Toshiba review, Vol. 63 No2, 2008

[43] EF Thacher, Testing of an automobile exhaust thermoelectric generator in a light truckProceedings of the Institution of Mechanical Engineers, Part D: Journal of Automobile Engineering January 1, 2007 221: 95-107

[44] Doug Crane, John Lagrandeur and etc. TEG On-Vehicle Performance and Model Validation and What It Means for Further TEG development

[45] Bass, J., Elsner, N.B., and Leavitt, A. (1995), Performance of the 1 kW thermoelectric generator for diesel engines. Proc. Of the 13th International Conference on Thermoelectrics, B. Mathiprakisam, ed., p. 195. AIP Conf. Proc., New York.

[46] O. Yamashita, "Effect of temperature dependence of electrical resistivity on the cooling performance of a single thermoelectric element," App. Energy, vol. 85, pp. 1002-1014, 2008.

[47] O. Yamashita, "Effect of linear and non-linear components in the temperature dependence of thermoelectric properties on the cooling performance," App. Energy, vol. 86, pp. 1745-1756, 2009.

[48] J. Ishibashi, M. Nakaseama, M. Seguchi, Marine shallow-water hydrothermal activity and mineralization at the Wakamiko crater in Kagoshima bay, south Kyushu, Japan, Journal of Volcanology and Geothermal Research 173 (2008) 84-98

[49] http://senkakushizen.iinaa.net/page014.html, the hydrothermal vent "tagiri" located in Kagoshima Bay

[50] http://underwater.iis.u-tokyo.ac.jp/robot/TS/TunaSand.html

[51] www.tellurex.com

[52] http://en.wikipedia.org/wiki/Navier%E2%80%93Stokes_equations

[53] Vandoormaal, J.P., and Raithby, G.D.,1984, "Enhancement of the SIMPLE Method for Predicting Incompressible Fluid Flows", Number. Heat Transfer, 7, pp. 147-163.

[54] Gianluca laccarino, "Predictions of a Turbulent Separated Flow Using

Commercial CFD Codes", Journal of Fluids Engineering, Dec 2001, Vol. 123.

[55] Kim, S.E.,2001, "Unstructured Mesh Based Reynolds Stress Transport Modeling of Complex Turbulent Shear Flows, " AIAA Paper 2001-0728.

[56] Launder. B. E. and Spalding. D.B., 1972, Mathematical Models of Turbulence, Academic Press, London.

[57] Rodi, W.,1991, "Experience with two-layer models combining the $k-\varepsilon$ model with a one-equation model near the wall ", AIAA Paper 91-0216.

[58] Speziable,C. G., Abid. R, and Anderson, E. C.,1990, "A critical evaluation of two-equation models for near wall turbulence", AIAA Paper 90-1481.

[59] Launder, B. E., and Sahrna, A., 1974, "Application of the Energy-Dissipation Models of Turbulence to the Calculation of Flow Near a Spinning Disk", Lett. Heat Mass Transfer 1, pp. 131-138.

[60] http://oceanservice.noaa.gov/facts/vents.html

[61] http://publications.iodp.org/preliminary_report/331/331_f9.htm

[62] http://www.scielo.br/scielo.php?pid=S0366-69132004000300012&script=sci_arttext

[63] http://www.magnaplate.com/literature/brochures/pdf/tufram.pdf

[64] http://www.doxsteel.com/corrosionProtection.html

[65] http://www.kobelco.co.jp/alcu/technical/almi/1174614_12412.html

[66] http://geography.about.com/od/physicalgeography/a/oceancurrents.htm

[67] Mateu L, Pollack M, Spies P Step-up Converters for Human Body Energy Harvesting TEGs PowerMEMS 2007 (Freiburg, Germany, 28-29 November 2007) 213-216

[68] H. Nagayoshi, K. Tokumisu and T.kajikawa, Evaluation of Multi MPPT Thermoelectric Generator System, Thermoelectrics, 2007. ICT 2007. 26th International Conference on

[69] Ian Laird and Dylan D.C. Lu, High Step-up DC/DC Topology and MPPT Algorithm for use with a Thermoelectric Generator, Power Electronics, IEEE Transactions, volume: 28 Issue:7.

[70] R. D. Middlebrook, “Transformerless dc-to-dc converters with large conversion ratios,” in Telecommunications Energy Conference, 1984. INTELEC ’84. International, Nov. 1984, pp. 455 –460.

[71] http://www.renewableenergyworld.com/rea/news/article/2009/09/power-optimizers_

[72] R. Alonso, P. Ibanez and etc. Analysis of Performance of New distributed MPPT Architectures. Industrial Electronics (ISIE), 2010 IEEE International Symposium on

Acknowledgements

This research was carried out at the University of Tokyo, between Apr 2011 and Mar 2014, and was supported by the scholarship of the Monbukagakusho, Japanese Ministry of Education.

I should thank for my supervisor, Dr. Tamaki Ura for welcoming me as a member of this lab and supporting me to develop research in a new field. I am greatly influenced by his attitude towards difficulty which will encourage me to keep calm and positive when suffered to failure. I am very grateful to my co-supervisor, Dr. Shinichi Takagawa, under his guidance, I learned a lot of professional knowledge on mechanical design. In the last year, for this patience and enthusiasm, I have learned how to develop the thesis with reasoned analytical description. I would also like to thank another co-supervisor Dr. Toshihiro Maki, for his help and attention on my research and daily life all the time. Thank you for Dr. Thornton Blair, for his care during the last cruise. I should express a special gratitude to Mr. Yoshiaki Nose, for this support on mechanical design and fabrication, and sacrificed so much time to discuss with me about the research details without impatience. Thank you for his encouragement and generous help whenever I was suffered to troubles. I also wish to thank Ms. Harumi Sugimatsu for her help in daily life and job hunting, Mr. Takashi Sakamaki for his help in experiment. Thank you for Dr. Unnikrishnan.P.V, Sangekar Mehul, Yuya Nishida, Yoshiki Sato, Adrian Bodenmann, Takumi Sato, Takumi Matuda, and Tukasa Sekina, Tomoko Takahashi, for their willingness to help each other, I deeply felt the importance of cooperation in the whole work.

I thank my father Jincai Luan and my mother Huiping Hu, for their faith in me and give me so much freedom to realize my own potential. All the support they have provided me over the years was the greatest gift.